Spring 5-8-2021

Lexicographic Sensitivity Functions for Nonsmooth Models in Mathematical Biology

Matthew D. Ackley
University of Maine, matthew.ackley@maine.edu

LEXICOGRAPHIC SENSITIVITY FUNCTIONS FOR NONSMOOTH MODELS IN MATHEMATICAL BIOLOGY

By

Matthew Ackley

B.A. University of Maine, 2019

A THESIS

Submitted in Partial Fulfillment of the

Requirements for the Degree of

Master of Arts

(in Mathematics)

The Graduate School

The University of Maine

May 2021

Advisory Committee:

Peter Stechlinski, Assistant Professor of Mathematics, Advisor

David Hiebeler, Professor of Mathematics

Brandon Lieberthal, Lecturer of Mathematics

LEXICOGRAPHIC SENSITIVITY FUNCTIONS FOR NONSMOOTH MODELS IN MATHEMATICAL BIOLOGY

By Matthew Ackley

Thesis Advisor: Professor Peter Stechlinski

An Abstract of the Thesis Presented
in Partial Fulfillment of the Requirements for the
Degree of Master of Arts
(in Mathematics)
May 2021

Systems of ordinary differential equations (ODEs) may be used to model a wide variety of real-world phenomena in biology and engineering. Classical sensitivity theory is well-established and concerns itself with quantifying the responsiveness of such models to changes in parameter values. By performing a sensitivity analysis, a variety of insights can be gained into a model (and hence, the real-world system that it represents); in particular, the information gained can uncover a system's most important aspects, for use in design, control or optimization of the system. However, while the results of such analysis are desirable, the approach that classical theory offers is limited to the case of ODE systems whose right-hand side functions are at least once continuously differentiable (C^1). This requirement is restrictive in many real-world systems in which sudden changes in behavior are observed, since a sharp change of this type often translates to a point of nondifferentiability in the model itself. To contend with this issue, recently-developed theory employing a specific class of tools called lexicographic derivatives has been shown to extend classical sensitivity results into a broad subclass of locally Lipschitz continuous ODE systems whose right-hand side functions are referred to as lexicographically smooth. In this thesis, we begin by exploring relevant background theory before presenting

lexicographic sensitivity functions as a useful extension of classical sensitivity functions; after establishing the theory, we apply it to two models in mathematical biology. The first of these concerns a model of glucose-insulin kinetics within the body, in which nondifferentiability arises from a biochemical threshold being crossed within the body; the second models the spread of rioting activity, in which similar nonsmooth behavior is introduced out of a desire to capture a "tipping point" behavior where susceptible individuals suddenly begin to join a riot at a quicker rate after a threshold riot size is crossed. Simulations and lexicographic sensitivity functions are given for each model, and the implications of our results are discussed.

ACKNOWLEDGEMENTS

First and foremost I would like to thank my advisor, Dr. Peter Stechlinski, for his abundance of help and guidance in the creation of this work. Through multiple article publications, presentations, and many hours of meetings, Peter has been an excellent mentor — second to none — and I will truly miss our work together.

I would also like to thank Dr. David Hiebeler and Dr. Brandon Lieberthal for their work as members of my committee and for providing insightful advice and thoughts as this thesis was assembled.

Finally, I would like to thank my family in Rockport, along with my significant other, Sara, for their incredible and incalculable amount of support over the last several years.

Figures and tables appearing in Chapter 4 have been reprinted from the source

> Matthew Ackley and Peter Stechlinski. Lexicographic derivatives of nonsmooth glucose-insulin kinetics under normal and artificial pancreatic responses. *Applied Mathematics and Computation*, 395:125876, 2021. *Copyright © 2021 Elsevier.*

Similarly, figures and tables appearing in Chapter 5 have been reprinted from the source

> Matthew Ackley and Peter Stechlinski. Determining key parameters in riots using lexicographic directional differentiation. *SIAM Journal on Applied Mathematics*, In Production. *Copyright © 2021 Society for Insutrial and Applied Mathematics. Reprinted with permission. All rights reserved.*

The permission of both journals is appreciated.

TABLE OF CONTENTS

LIST OF TABLES

LIST OF FIGURES

LIST OF THEOREMS AND DEFINITIONS

CHAPTER 1
INTRODUCTION

Mathematical models built on a framework of parametric ordinary differential equations (ODEs) enjoy a high degree of adaptability. Said parameters may be calibrated in order to fit the model itself to specific data, for example; however, the choices of parameter values have major implications in the behavior of the model at hand. Broadly, sensitivity theory aims to quantify the change in behavior of a model solution as a result of changes to parameter values. In this thesis, we are most specifically concerned with parametric sensitivity functions, which provide a local measure of model sensitivity via first-order derivative information of solution curves with respect to parameters.

Consider a general parametric initial value problem (IVP) of the form

$$\dot{\boldsymbol{x}}(t, \boldsymbol{p}) = \boldsymbol{f}(t, \boldsymbol{p}, \boldsymbol{x}(t, \boldsymbol{p})),$$
$$\boldsymbol{x}(t_0, \boldsymbol{p}) = \boldsymbol{f}_0(\boldsymbol{p}),$$

with state variables $\boldsymbol{x}$ and parameters $\boldsymbol{p}$. If the participating right-hand side functions $\boldsymbol{f}, \boldsymbol{f}_0$ are at least once continuously differentiable (C^1 or "smooth" for present purposes), then the existence and uniqueness of a solution is guaranteed locally about an initial data point [40]. The requirement of continuous differentiability places this problem in the classical setting and allows the use of well-established theory when, for example, investigating the qualitative model behavior through a sensitivity analysis — in fact, solutions to the IVP inherit the property of being continuously differentiable with respect to parameters [40]. The first-order derivative information which is guaranteed to exist in this setting characterizes the instantaneous rate of change (e.g., "sensitivity") of the model; for this reason, the sensitivity functions in this setting are defined as

$$\mathbf{S}_{\boldsymbol{x}}(t) = \frac{\partial \boldsymbol{x}}{\partial \boldsymbol{p}}(t, \boldsymbol{p}_0),$$

where $\boldsymbol{p}_0$ is a vector of reference parameters [28, 40]. These functions may be solved in closed-form for simple problems, but in practice results are typically given via established and automated numerical methods. Since this information provides predictions about how the model will respond to parameter perturbations, it is particularly useful when pursuing goals such as dynamic control or optimization.

Despite the relative ease of automatic numerical calculation of the classical sensitivity functions, the requirement for $\boldsymbol{f}, \boldsymbol{f}_0$ to be C^1 is often restrictive in problems where switching behavior may arise since the presence of instantaneous change often translates to a point of nondifferentiability in any mathematical models describing the problem. Such an issue arises in both models we examine in this thesis, which concern themselves with modeling glucose-insulin kinetics and the spread of riots, respectively.

Glucose is the most common naturally-occurring simple sugar, and as such plays an active role in the human body due to its prevalence in the average diet. Maintaining a healthy concentration of glucose in the bloodstream is essential; while breaking down glucose provides cellular energy, blood-glucose concentrations which deviate too greatly from the baseline "healthy" level can have drastic consequences on a subject's health. After a sudden influx of glucose to the body (due to, e.g., a meal), it is chiefly the role of insulin (secreted by the pancreas) to aid in returning blood-glucose concentration to the baseline level. Bergman's "minimal model" of glucose-insulin interactions [11] aims to describe the blood-glucose and blood-insulin levels of a healthy individual after glucose is introduced to the body. However, a desire to accurately model insulin input from a healthy pancreas introduces nondifferentiability in the model since the pancreas exhibits switching behavior. Below a threshold blood-glucose concentration, the pancreas remains idle, but it suddenly begins to secrete insulin once this threshold concentration is crossed. To model pancreatic insulin input, Bergman et al. [11] used a max function:

$$u = p_5 t \max(0, G - p_6),$$

where G represents current blood-glucose concentration at time t and p_6 is a parameter describing the threshold concentration. As G crosses the threshold value p_6, the max function changes output, hence introducing nondifferentiability and invalidating any attempts to study qualitative behavior via classical sensitivity theory above.

Furthermore, the body's insulin response to glucose intake may be inhibited by conditions such as type 1 and type 2 diabetes mellitus ("diabetes"). Diabetes is common in general, with over 10% of the American population estimated to be afflicted with some version of the chronic disease and 1.5 million new cases being diagnosed every year [7]. In an effort to extend the minimal model to describe the diabetic case as well, we consider two variations of the model where the concept of "insulin secretion" from the pancreas is replaced by the concept of "insulin infusion" from an external insulin-secreting device. In one variation, insulin is assumed to be infused at an exponentially decaying rate, while the other variation introduces nonsmoothness through abrupt on-and-off features. Again, the nonsmoothness present invalidates any results gained via classical sensitivity theory.

A similar issue arises in a recent model examining the spread of riots published by Bonnasse-Gahot et al. [12]. Rioting activity behaves in a wave-like fashion similar in structure to a wave of disease (i.e., an epidemic). For this reason, the authors of [12] considered riots through the lens of being a "social contagion," and adjusted the general SIR (Susceptible-Infected-Recovered) framework for disease spread [13] to instead describe the spread of rioting behavior. A key feature of riots is the so-called "bandwagon effect," which suggests that the likelihood of an individual joining a riot is proportional to the current number of rioters. However, this effect cannot exist without there being a small population of rioters to begin with — for this reason, the authors of [12] consider a "tipping point" which manifests in the model at hand in the form of a nonsmooth max function. A switch in output from this max function represents a sudden shift from an absence of rioting activity to the beginning of the bandwagon effect (or vice versa), but results in points of nondifferentiability being introduced to the model.

While smoothing approximations have occasionally been used to avoid breaking the C^1 requirement of classical sensitivity theory (see, e.g., [37] for such a treatment of the minimal model), issues arise which are hard to reconcile in general; solutions using this method have inherent numerical error built-in and require subjective user-defined inputs. Furthermore, in large-scale or highly-coupled systems, points of nondifferentiability may be visited frequently, making it difficult to bound or estimate the cumulative error of simulations *a priori*. Other efforts have been made to instead generalize the classical sensitivity functions using nonsmooth analysis. For example, Clarke's set-valued generalized derivative [16] exists at points of nondifferentiability of locally Lipschitz continuous functions. Elements of this generalized derivative characterize local first-derivative information and are useful in dedicated nonsmooth methods, such as those for equation-solving [21, 42] or optimization methods [33, 35]. The Clarke Jacobian itself also satisfies a variety of calculus properties, including a mean value, implicit, and inverse function theorem. It can also be supplied to the aforementioned nonsmooth numerical methods with guaranteed convergence properties; however, the benefits of these properties are hindered in general due to difficulty associated with calculating Clarke Jacobian elements. Any calculus rules associated with the Clarke Jacobian (e.g., the sum or product rules) hold only as inclusions in most settings, invalidating most systematic attempts at calculating such elements.

Only recently have advancements been made in nonsmooth analysis which overcome this issue. So-called lexicographic (L-)derivatives, introduced by Nesterov in [38], are indistinguishable from Clarke Jacobian elements in the aforementioned dedicated nonsmooth numerical methods; furthermore, related objects known as lexicographic directional derivatives [32] provide a systematic, automatable, and accurate method of calculating L-derivatives in general. These objects have been applied in tandem to nonsmooth ODE systems [30] in order to yield generalized sensitivity theory which is applicable to a large class of locally Lipschitz continuous functions referred to as lexicographically smooth [38], including functions which are C^1, piecewise continuously

differentiable (PC^1 in the sense of Scholtes [45]), or convex. This recently-developed theory is numerically implementable even in large-scale problems.

The flexibility of lexicographic sensitivity theory allows its application to both models highlighted above — Bergman's minimal model [11], in which we provide a sensitivity analysis of the original model and several variations tailored for individuals with diabetes, and the model of riot spread introduced in [12], where we examine a municipal-scale model of the 2005 French riots across the entirety of the Île-de-France region. These applications represent the primary original contributions of this thesis, with further original work found in a proof of the lexicographic directional derivative rule for the nonsmooth mid function and in illustrative examples throughout.

The rest of this thesis is structured as follows: in Chapter 2 preliminaries and background theory, including classical sensitivity functions and Clarke's generalized derivative, are discussed. In Chapter 3, we define the class of lexicographically smooth functions and introduce the concept of lexicographic differentiation before introducing recently-developed lexicographic sensitivity functions. We first apply this theory in Chapter 4 after introducing the minimal model of glucose-insulin kinetics, and proceed in Chapter 5 by performing similar analysis on a municipal-scale model of the spread of rioting activity. In Chapter 6, we make concluding remarks and suggest future directions for research.

CHAPTER 2
PRELIMINARIES AND BACKGROUND

In this section we introduce relevant results from nonsmooth analysis and motivate the need for the lexicographic approach in cases where nondifferentiability is present.

2.1 Notation

Throughout this thesis, scalar functions and arguments are denoted as standard-weight lowercase letters; e.g., $f(x)$ is a scalar-valued function which depends on a scalar variable. More generally, vector-valued functions and arguments are denoted as bold lowercase letters; e.g., $\boldsymbol{f}(\boldsymbol{x})$ denotes a vector of outputs $\boldsymbol{f} = (f_1, \ldots, f_m) \in \mathbb{R}^m$ depending on a vector of inputs $\boldsymbol{x} = (x_1, \ldots, x_n) \in \mathbb{R}^n$. Standard-weight uppercase letters (e.g., X) are used to denote sets, while bold uppercase letters (e.g., $\mathbf{X}$) are used to denote real-valued matrices in $\mathbb{R}^{m\times n}$, and well-defined vertical block matrices $\begin{bmatrix}\mathbf{X}\\ \mathbf{Y}\end{bmatrix}$ are represented by the tuple $(\mathbf{X}, \mathbf{Y})$. In particular, the classical Jacobian matrix of a vector-valued continuously differentiable (C^1) function $\boldsymbol{f}$ at $\boldsymbol{x}$ is written $\mathbf{J}\boldsymbol{f}(\boldsymbol{x})$, and is defined as

$$\mathbf{J}\boldsymbol{f}(\boldsymbol{x}) = \begin{bmatrix} \frac{\partial f_1}{\partial x_1}(\boldsymbol{x}) & \ldots & \frac{\partial f_1}{\partial x_n}(\boldsymbol{x}) \\ \vdots & \ddots & \vdots \\ \frac{\partial f_m}{\partial x_1}(\boldsymbol{x}) & \ldots & \frac{\partial f_m}{\partial x_n}(\boldsymbol{x}) \end{bmatrix} \in \mathbb{R}^{m\times n}.$$

Several special generalizations of the classical Jacobian are present throughout this thesis. In the case that $\boldsymbol{f}$ is scalar-valued (i.e., $m = 1$), then we find that $\mathbf{J}f(\boldsymbol{x}) = (\nabla f(\boldsymbol{x}))^{\mathrm{T}}$, where $\nabla f(\boldsymbol{x})$ denotes the gradient of f. If instead we have the case that $\boldsymbol{f}$ is a function of multiple vector-valued inputs $(\boldsymbol{x}, \boldsymbol{y}) \in \mathbb{R}^{n+q}$, then we define

$$\mathbf{J}_{\boldsymbol{x}}\boldsymbol{f}(\boldsymbol{x}, \boldsymbol{y}) = \begin{bmatrix} \frac{\partial f_1}{\partial x_1}(\boldsymbol{x}, \boldsymbol{y}) & \ldots & \frac{\partial f_1}{\partial x_n}(\boldsymbol{x}, \boldsymbol{y}) \\ \vdots & \ddots & \vdots \\ \frac{\partial f_m}{\partial x_1}(\boldsymbol{x}, \boldsymbol{y}) & \ldots & \frac{\partial f_m}{\partial x_n}(\boldsymbol{x}, \boldsymbol{y}) \end{bmatrix} \in \mathbb{R}^{m\times n};$$

$$\mathbf{J}_{\boldsymbol{y}}\boldsymbol{f}(\boldsymbol{x},\boldsymbol{y}) = \begin{bmatrix} \frac{\partial f_1}{\partial y_1}(\boldsymbol{x},\boldsymbol{y}) & \dots & \frac{\partial f_1}{\partial y_q}(\boldsymbol{x},\boldsymbol{y}) \\ \vdots & \ddots & \vdots \\ \frac{\partial f_m}{\partial y_1}(\boldsymbol{x},\boldsymbol{y}) & \dots & \frac{\partial f_m}{\partial y_q}(\boldsymbol{x},\boldsymbol{y}) \end{bmatrix} \in \mathbb{R}^{m\times q}.$$

The Euclidean norm is denoted by $|\cdot|$, and an open n-dimensional Euclidean ball of radius ϵ centered at the point $\boldsymbol{x}_0 \in \mathbb{R}^n$ is referred to as a "neighborhood of $\boldsymbol{x}_0$" and denoted $N_\epsilon(\boldsymbol{x}_0)$; i.e.,

$$N_\epsilon(\boldsymbol{x}_0) = \{\boldsymbol{x} \in \mathbb{R}^n : |\boldsymbol{x} - \boldsymbol{x}_0| < \epsilon\}$$

for some $\epsilon > 0$. The interior of a set $\mathbf{X}$ is denoted as "int($\mathbf{X}$)" and likewise its closure is denoted "cl($\mathbf{X}$)." The convex hull of $\mathbf{X}$ — that is, the smallest convex set containing $\mathbf{X}$ — is denoted "conv($\mathbf{X}$)."

2.2 Classical sensitivity theory of ordinary differential equations

With the goal of quantifying the dependence of ODE-based models to their parameters, we begin by exploring foundational ODE theory. Consider a general initial value problem (IVP) of the form

$$\begin{aligned} \dot{\boldsymbol{x}}(t) &= \boldsymbol{f}(t, \boldsymbol{x}(t)), \\ \boldsymbol{x}(t_0) &= \boldsymbol{x}_0, \end{aligned} \tag{2.1}$$

where $\boldsymbol{x} = (x_1, x_2, \dots, x_n)$ denotes the vector of state variables, t is the independent variable, $\boldsymbol{f} : D_t \times D_x \to \mathbb{R}^n$ is the right-hand side function, where $D_t \subset \mathbb{R}$ and $D_x \subset \mathbb{R}^n$ are open sets, and $t_0 \in D_t$ and $\boldsymbol{x}_0 \in D_x$ are the initial conditions.

Definition 2.1 (Solution of an Initial Value Problem)**.** A *solution* to the IVP (2.1) on the connected set $T \subset D_t$ is some function $\boldsymbol{x}(t)$ satisfying the following properties:

(i) $\boldsymbol{x}(t)$ is differentiable on T;

(ii) $\boldsymbol{x}(t) \in D_x$ for each $t \in T$;

(iii) $\boldsymbol{x}(t_0) = \boldsymbol{x}_0$ with $t_0 \in T$; and

(iv) $\dot{x}(t) = \boldsymbol{f}(t, \boldsymbol{x}(t))$ for each $t \in T$.

In the classical case, the (local) existence and a uniqueness of a solution to the IVP (2.1) is guaranteed; in general, the "classical case" is characterized by the continuous differentiability of the participating right-hand side functions.

Theorem 2.2 (Fundamental Existence-Uniqueness Theorem)**.** *(Adapted from [25].) Suppose that $\boldsymbol{f} : D_t \times D_x \to \mathbb{R}^n$ is C^1 on its domain. Then there exists some $\delta > 0$ such that the initial value problem* (2.1) *has a unique solution $\boldsymbol{x}(t)$ on the interval $[t_0, t_0 + \delta]$.*

Now instead consider a general *parametric* IVP:

$$\begin{aligned} \dot{\boldsymbol{x}}(t, \boldsymbol{p}) &= \boldsymbol{f}(t, \boldsymbol{p}, \boldsymbol{x}(t, \boldsymbol{p})), \\ \boldsymbol{x}(t_0, \boldsymbol{p}) &= \boldsymbol{f}_0(\boldsymbol{p}), \end{aligned} \tag{2.2}$$

where $\boldsymbol{x} = (x_1, x_2, \ldots, x_n)$ continues to denote the vector of state variables and $\boldsymbol{p} = (p_1, p_2, \ldots, p_q)$ now denotes the vector of problem parameters. Furthermore, suppose that $\boldsymbol{f} : D_t \times D_p \times D_x \to \mathbb{R}^m$ and $\boldsymbol{f}_0 : D_p \to D_x$ where $D_t \subset \mathbb{R}$, $D_p \subset \mathbb{R}^q$, and $D_x \subset \mathbb{R}^n$ are open sets and $t_0 \in D_t$, $\boldsymbol{p}^* \in D_p$. The goal of sensitivity theory is to quantify the influence that the model parameters $\boldsymbol{p}$ have on the system; conveniently, in the classical case, the solution of (2.2) inherits the continuous differentiability of the ODE's right-hand side rule.

Assumption 2.3. Suppose that $\boldsymbol{f} : D_t \times D_p \times D_x \to \mathbb{R}^n$ and $\boldsymbol{f}_0 : D_p \to D_x$ are C^1 on their respective domains.

Theorem 2.4 (C^1 Dependence on Parameters)**.** *(Adapted from [40]). Suppose Assumption 2.3 holds. Then there exist $\epsilon, \delta > 0$ such that the initial value problem* (2.2) *has a unique solution $\boldsymbol{x}(t, \boldsymbol{p})$ on $[t_0, t_0 + \delta]$ for each fixed $\boldsymbol{p} \in N_\epsilon(\boldsymbol{p}^*)$, and $\boldsymbol{x}(t, \boldsymbol{p})$ is C^1 with respect to $\boldsymbol{p}$ on $N_\epsilon(\boldsymbol{p}^*)$ for each fixed $t \in [t_0, t_0 + \delta]$.*

Definition 2.5 (Classical Sensitivity Functions)**.** The (classical) *forward-parametric sensitivity functions* associated with a solution $\boldsymbol{x}(t, \boldsymbol{p})$ of the IVP (2.2) on T, if they exist, are

$$\mathbf{S}_{\boldsymbol{x}}(t) = \frac{\partial \boldsymbol{x}}{\partial \boldsymbol{p}}(t, \boldsymbol{p}^*) \in \mathbb{R}^{n \times q}, \tag{2.3}$$

where $\boldsymbol{p}^* \in D_p$ again denotes some chosen reference parameters.

The classical forward-parametric sensitivity functions describe the first-order response of an IVP's solution $\boldsymbol{x}(t, \boldsymbol{p})$ to perturbations in the reference parameters. However, while Theorem 2.2 guarantees the unique existence of a solution to the IVP (2.2) and Theorem 2.4 guarantees C^1 dependence of this solution to parameters $\boldsymbol{p}$ (and hence existence of the sensitivity functions (2.3)), it is often not trivial to produce the sensitivity functions in closed form. Moreover, it is often desirable to calculate sensitivity functions on a non-local time horizon, requiring existence of a solution non-locally instead of relying on the local existence theorem. Therefore, it is often convenient to calculate the sensitivity functions (2.3) numerically via the following result.

Assumption 2.6. Let $t_f > t_0$ and suppose there exists a unique solution of the IVP (2.2) on $[t_0, t_f] \subset D_t$.

Theorem 2.7 (Existence and Calculation of the Classical Sensitivity Functions)**.** *(Adapted from [28].) Suppose that Assumptions 2.3 and 2.6 hold. Then, in addition to the conclusions of Theorem 2.4, the sensitivity functions* (2.3) *exist and are the unique solution of the* sensitivity system

$$\begin{aligned} \dot{\boldsymbol{S}}_{\boldsymbol{x}}(t) &= \boldsymbol{J}_{\boldsymbol{p}} \boldsymbol{f}(t, \boldsymbol{p}^*, \boldsymbol{x}(t, \boldsymbol{p}^*)) + \boldsymbol{J}_{\boldsymbol{x}} \boldsymbol{f}(t, \boldsymbol{p}^*, \boldsymbol{x}(t, \boldsymbol{p}^*)) \boldsymbol{S}_{\boldsymbol{x}}(t), \\ \boldsymbol{S}_{\boldsymbol{x}}(t_0) &= \boldsymbol{J} \boldsymbol{f}_0(\boldsymbol{p}^*), \end{aligned} \tag{2.4}$$

on the time horizon $[t_0, t_f]$.

Example 2.8. Consider the following IVP with parameters $\boldsymbol{p} = (p_1, p_2)$:

$$\begin{aligned} \dot{x}(t, \boldsymbol{p}) &= x(t, \boldsymbol{p}) + p_1, \\ x(0, \boldsymbol{p}) &= p_2. \end{aligned} \tag{2.5}$$

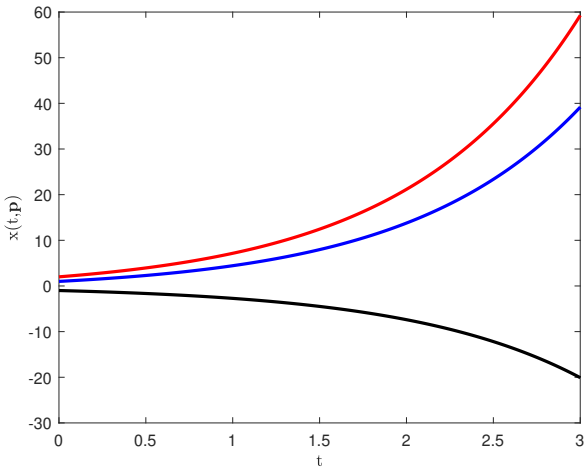

Figure 2.1: Solutions of the system (2.5) with differing choices of reference parameter $\boldsymbol{p}^*$. In black, $\boldsymbol{p}^* = (0, -1)$; in blue, $\boldsymbol{p}^* = (1, 1)$; and in red, $\boldsymbol{p}^* = (1, 2)$.

This ODE is linear and separable and solutions are easily found in closed-form (see Figure 2.1): $x(t, \boldsymbol{p}) = (p_1 + p_2)e^t - p_1$. For different choices of reference parameter $\boldsymbol{p}^* = (p_1^*, p_2^*)$, the long term behavior of solutions to this system varies (see, for example, Figure 2.2). Since solutions are known in closed form, however, given any reference parameter $\boldsymbol{p}^*$, we can calculate the sensitivity functions (2.3) as

$$\mathbf{S}_x(t) = \begin{bmatrix} e^t - 1 & e^t \end{bmatrix}. \tag{2.6}$$

Alternatively, after defining $f(x, \boldsymbol{p}) = x + p_1$ and $f_0(\boldsymbol{p}) = p_2$, we may calculate

$$\begin{aligned} \mathbf{J}_{\boldsymbol{p}} f(\boldsymbol{p}, x(t, \boldsymbol{p}^*)) &= [1 \quad 0], \\ \mathbf{J}_x f(\boldsymbol{p}, x(t, \boldsymbol{p}^*)) &= [1], \\ \mathbf{J} f_0(\boldsymbol{p}^*) &= [0 \quad 1]. \end{aligned}$$

Substitution into the classical sensitivity system (2.4) then yields

$$\begin{aligned} \dot{\mathbf{S}}_x(t) &= [1 \quad 0] + [1]\, \mathbf{S}_x(t), \\ \mathbf{S}_x(0) &= [0 \quad 1]. \end{aligned} \tag{2.7}$$

To solve this system, decompose the vector-valued IVP as

$$\begin{aligned} \dot{S}_x^{p_1}(t) &= 1 + S_x^{p_1}(t), & S_x^{p_1}(0) &= 0, \\ \dot{S}_x^{p_2}(t) &= S_x^{p_2}(t), & S_x^{p_2}(0) &= 1. \end{aligned}$$

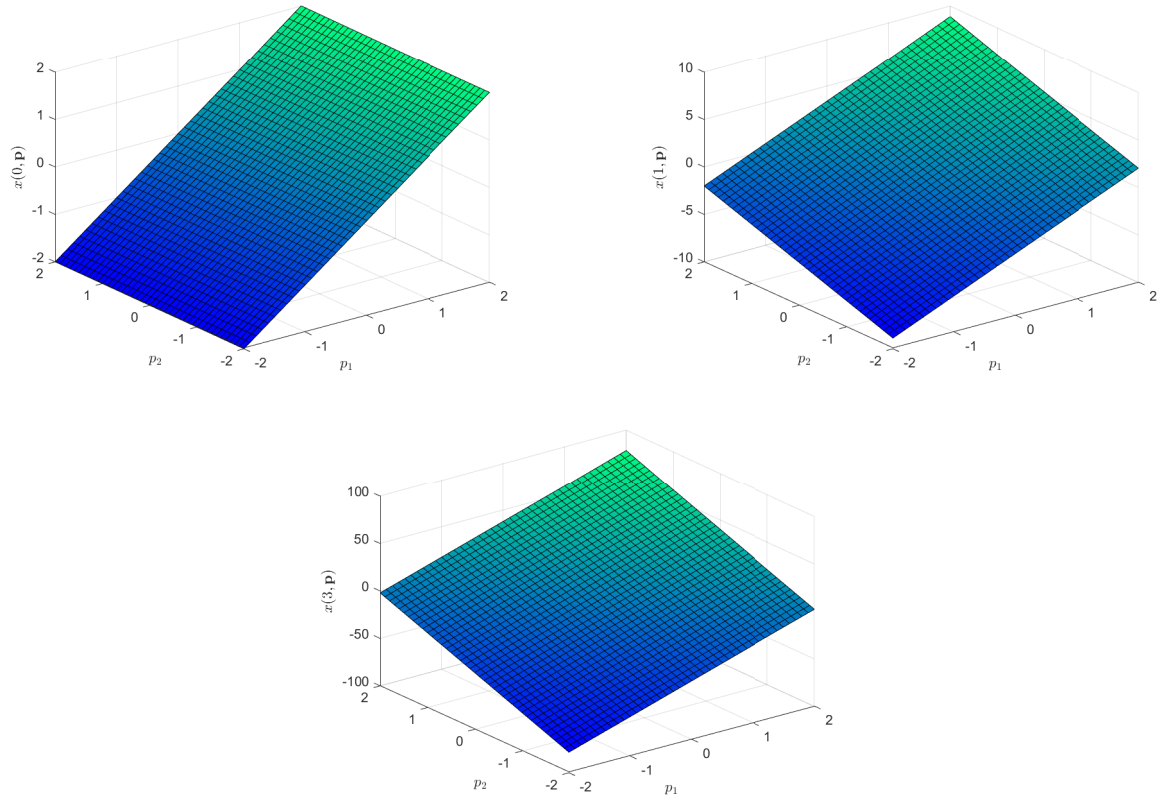

Figure 2.2: Varying behavior in solutions to (2.5) for different choices of $\boldsymbol{p}$ at different fixed times. At top-left, $t = 0$ and solutions take the form of the $x = p_2$ plane. At top-right, $t = 1$ and solutions begin to diverge. At bottom, by $t = 3$, solutions have diverged greatly (note the difference in scale between the figures).

Both systems can be solved independently to find that

$$S_x^{p_1}(t) = e^t - 1, \qquad S_x^{p_2}(t) = e^t.$$

Hence, the solution to the sensitivity system (2.7) recovers the classical sensitivity functions found earlier in Equation (2.6). Fundamentally, these functions describe the first-order response of the solution $\boldsymbol{x}(t, \boldsymbol{p})$ to perturbations in p_1 and p_2. Since $e^t - 1 < e^t$ in general, we find that perturbations in p_2 are more influential in the behavior of the system than similar perturbations in the value of p_1 starting from any reference values $p_1^*, p_2^* \in \mathbb{R}$.

As mentioned in Example 2.8, sensitivity functions are useful in making quantitative comparisons between the effects of different parameters and allow the determination of the

"most influential" parameter at any time within the time horizon. With aims of performing a sensitivity analysis on (i.e., finding the sensitivity functions associated with) the two biological models considered in this thesis, however, we must first note that the C^1 requirement of the right-hand side function $\boldsymbol{f}$ within Assumption 2.3 is broken in each case due to a desire to capture sudden switches in model behavior. Hence, the C^1 dependence of solutions $\boldsymbol{x}(t, \boldsymbol{p})$ to parameters $\boldsymbol{p}$ is *not* guaranteed by Theorem 2.4, and the sensitivity functions (i.e., $\frac{\partial \boldsymbol{x}}{\partial \boldsymbol{p}}$) may not exist as a result. Therefore, in order to characterize parametric sensitivities in the nonsmooth case, we must turn to another method. One approach is using generalized derivative theory; here, we specifically consider Clarke's generalized derivative [16]. Other common approaches to a local sensitivity analysis within the nonsmooth setting include one-at-a-time (OAT) calculations (employing, e.g., directional derivatives) or smoothing approaches. In methods employing an OAT approach, parameters are individually perturbed from their original reference values and the new output is compared with previous solutions to see the effect, though this approach can fail to gain similar insights on parameter interactions which may be present. In methods employing a smoothing approach, a C^1 approximating function is used as a proxy for functions exhibiting nonsmoothness. Shortcomings of this approach in general will be discussed in Chapter 4. Global sensitivity analyses (such as the elementary effects method of Morris [36]) are not the focus of this thesis, nor are established stochastic or variance-based approaches, which have their own set of advantages and shortcomings.

2.3 Clarke's generalized derivative

The field of nonsmooth analysis is broad, and often concerns itself with developing differential calculus rules for functions which are classically nondifferentiable [17]. Such rules are desirable in many of the same applications which employ classical derivatives (e.g., optimization algorithms and numerical solvers for systems of ordinary differential equations), but require special treatment since classical approaches often yield erroneous

conclusions when used in (or adapted for) the nonsmooth case. We proceed by developing the key concepts associated with these specialized rules, which together form the basis of generalized derivative theory. The approach outlined here, based around Clarke's generalized derivative [16], requires that the functions of interest be at least locally Lipschitz continuous.

Definition 2.9 (Lipschitz and Local Lipschitz Continuity)**.** Given an open set $X \subset \mathbb{R}^n$, a function $\boldsymbol{f} : X \to \mathbb{R}^m$ is called Lipschitz continuous on $D \subset X$ if there exists some $L > 0$ such that for all $\boldsymbol{x}, \boldsymbol{y} \in D$,

$$|\boldsymbol{f}(\boldsymbol{x}) - \boldsymbol{f}(\boldsymbol{y})| \leq L|\boldsymbol{x} - \boldsymbol{y}|.$$

The function is called *locally Lipschitz continuous* on X if for each $\boldsymbol{x} \in X$ there exists a neighborhood N around $\boldsymbol{x}$ such that $\boldsymbol{f}$ is Lipschitz continuous on N.

Theorem 2.10 (Rademacher's Theorem)**.** *Given an open set $X \subset \mathbb{R}^n$ and a locally Lipschitz continuous function $f : X \to \mathbb{R}^m$, it must be that f is differentiable almost everywhere. That is, the set of points $Z_f \subset X$ at which f is not differentiable must be of Lebesgue measure zero.*

With this class of functions in mind, we proceed by defining two of the principal objects in generalized derivative theory [16].

Definition 2.11 (Clarke Jacobian)**.** ([16]) Given a locally Lipschitz continuous function $\boldsymbol{f} : X \subset \mathbb{R}^n \to \mathbb{R}^m$, X open, the *Bouligand (B-)subdifferential* of $\boldsymbol{f}$ at $\boldsymbol{x}$ is defined as

$$\partial_B \boldsymbol{f}(\boldsymbol{x}) = \left\{ \mathbf{H} \in \mathbb{R}^{m \times n} : \mathbf{H} = \lim_{k \to \infty} \mathbf{J}\boldsymbol{f}(\boldsymbol{x}_k), \text{where } \{\boldsymbol{x}_k\} \to \boldsymbol{x}, \text{ with } \boldsymbol{x}_k \neq \boldsymbol{x}, \boldsymbol{x}_k \in X \setminus Z_{\boldsymbol{f}} \right\}. \tag{2.8}$$

The *Clarke Jacobian* of $\boldsymbol{f}$ at $\boldsymbol{x}$ is then defined as

$$\partial_C \boldsymbol{f}(\boldsymbol{x}) = \text{conv}(\partial_B \boldsymbol{f}(\boldsymbol{x})).$$

The B-subdifferential (and hence, Clarke Jacobian) of a locally Lipschitz continuous function is necessarily nonempty; furthermore, the B-subdifferential is always a compact

set [16]. Since the B-subdifferential is comprised of the limit of the Jacobian of $\boldsymbol{f}$ evaluated at sequences converging to $\boldsymbol{x}$, it characterizes the behavior of $\boldsymbol{f}$ nearby to $\boldsymbol{x}$; as a result, the B-subdifferential may be roughly conceptualized as a set of "nearby Jacobians" to a point of interest. Motivated by the formulation of the mathematical models explored later in this thesis, we now introduce a subclass of locally Lipschitz functions referred to as *piecewise continuously differentiable*.

Definition 2.12 (Piecewise Differentiable Functions)**.** ([45]) For an open set $X \subset \mathbb{R}^n$, a function $\boldsymbol{f} : X \to \mathbb{R}^m$ is called *piecewise continuously differentiable (PC^1)* at $\boldsymbol{x} \in X$ if there exists (i) some neighborhood $N \subset X$ of $\boldsymbol{x}$ on which $\boldsymbol{f}$ is continuous and (ii) a corresponding finite collection of C^1 selection functions $\mathcal{F}_{\boldsymbol{f}}(\boldsymbol{x}) = \{\boldsymbol{f}_1, \ldots, \boldsymbol{f}_k\}$ (for some $k \in \mathbb{N}$) where each $\boldsymbol{f}_i$ is a C^1 function mapping N to $\mathbb{R}^m$ such that

$$\boldsymbol{f}(\boldsymbol{\eta}) \in \{\boldsymbol{f}_1(\boldsymbol{\eta}), \ldots, \boldsymbol{f}_k(\boldsymbol{\eta})\} \quad \forall \boldsymbol{\eta} \in N.$$

A set of *essentially active indices* of $\boldsymbol{f}$ at $\boldsymbol{x}$ with respect to $\mathcal{F}_{\boldsymbol{f}}(\boldsymbol{x})$ is defined as follows:

$$I^{ess}_{\boldsymbol{f}}(\boldsymbol{x}) = \{i \in \{1, \ldots, k\} : \boldsymbol{x} \in \mathrm{cl}(\mathrm{int}\{\boldsymbol{\eta} \in N : \boldsymbol{f}(\boldsymbol{\eta}) = \boldsymbol{f}_i(\boldsymbol{\eta})\})\}.$$

These indices are used to define the corresponding set of *essentially active selection functions*

$$\mathcal{E}_{\boldsymbol{f}}(\boldsymbol{x}) = \{\boldsymbol{f}_i : i \in I^{ess}_{\boldsymbol{f}}(\boldsymbol{x})\} \subset \mathcal{F}_{\boldsymbol{f}}(\boldsymbol{x}).$$

The function $\boldsymbol{f}$ is called PC^1 on X if it is PC^1 at each $\boldsymbol{x} \in X$.

Functions which are PC^1 are necessarily locally Lipschitz continuous [45] and can be characterized as "nearly-smooth" by virtue of only failing to be continuously differentiable ("smooth") at a set of points whose Lebesgue measure is zero (by the result of Theorem 2.10). The following example demonstrates the process of identifying relevant selection and essentially active selection functions.

Example 2.13. Consider the function $f : \mathbb{R} \to \mathbb{R} : x \mapsto \mathrm{mid}(0, |x| - 1, 1)$, where the mid function returns the median of its three arguments. This function is depicted in Figure 2.3;

notably, it is PC^1 (and hence locally Lipschitz continuous) on its domain, and its set of nondifferentiability is

$$Z_f = \{x : |x| = 1\} \cup \{x : |x| = 2\}.$$

Define the following selection functions:

$$f_1 : x \mapsto 0; \quad f_2 : x \mapsto x - 1; \quad f_3 : x \mapsto -x - 1; \quad f_4 : x \mapsto 1; \quad f_5 : x \mapsto \frac{1}{2}.$$

Then, for $i = 1, 2, 3, 4$, note that the set $\{x \in \mathbb{R} : f(x) = f_i(x)\}$ is an interval and thus has a nonempty interior. However, the set $\{x \in \mathbb{R} : f(x) = f_5(x)\}$ is exactly $\{\frac{-3}{2}, \frac{3}{2}\}$, whose interior is empty. Thus, given any $x^* \in \mathbb{R}$ and $N \subset \mathbb{R}$, the set $I_f^{ess}(x^*)$ will be a subset of the set $\{1, 2, 3, 4\}$ and as a result we have $\mathcal{E}_f(x^*) \subset \{f_1, f_2, f_3, f_4\}$. The selection function f_5 will never be essentially active since for any such combination of $x^* \in \mathbb{R}$, $N \subset \mathbb{R}$, we will have

$$\mathrm{cl}(\mathrm{int}\{\eta \in N : f(\eta) = f_5(\eta)\}) \subset \mathrm{cl}\Big(\mathrm{int}\Big\{\frac{-3}{2}, \frac{3}{2}\Big\}\Big) = \mathrm{cl}(\emptyset) = \emptyset.$$

Broadly, global satisfaction of the PC^1 criteria implies that the function at hand may be constructed in a piecewise fashion where the result is both continuous and is composed of finitely many essentially active C^1 "pieces." Furthermore, given a PC^1 function $\boldsymbol{f} : X \subset \mathbb{R}^n \to \mathbb{R}^m$, X open, the B-subdifferential (2.8) simplifies as

$$\partial_B \boldsymbol{f}(\boldsymbol{x}) = \{\mathbf{J}\boldsymbol{f}_i(\boldsymbol{x}) : \boldsymbol{f}_i \in \mathcal{E}_{\boldsymbol{f}}(\boldsymbol{x})\}.$$

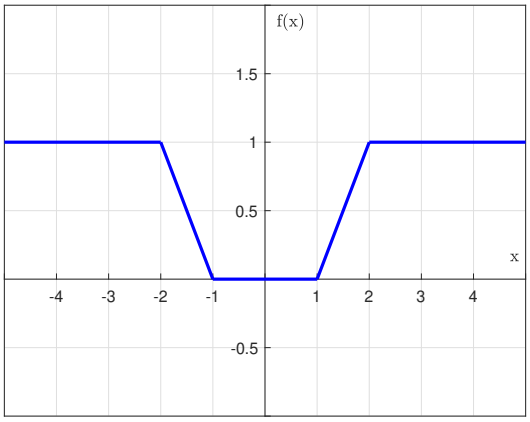

Figure 2.3: A graphical representation of the function $f(x) = \mathrm{mid}(0, |x|-1, 1)$ from Examples 2.13 and 2.14.

Using this simplified relationship, it is easy to check that the Clarke Jacobian recovers the classical Jacobian in the case of functions which are C^1, since for any relevant $\boldsymbol{x}^*$ the set $\mathcal{E}_{\boldsymbol{f}}(\boldsymbol{x}^*)$ will be a singleton and consequently

$$\partial_C \boldsymbol{f}(\boldsymbol{x}^*) = \partial_B \boldsymbol{f}(\boldsymbol{x}^*) = \{\mathbf{J}\boldsymbol{f}(\boldsymbol{x}^*)\} \tag{2.9}$$

in this case.

Example 2.14. Recall the function and corresponding selection functions introduced in Example 2.13:

$$f(x) = \text{mid}(0, |x| - 1, 1).$$

As noted previously, this function exhibits nonsmoothness at the point where $x = 1$. Letting $N = \left(\frac{1}{2}, \frac{3}{2}\right)$, note that $\mathcal{E}_f(1) = \{0, x - 1\} = \{f_1, f_2\}$ is an appropriate set of essentially active selection functions, which can be seen by examining the behavior of the function to the immediate left and right of $x = 1$ in Figure 2.3. Therefore, the B-subdifferential of this function at $x^* = 1$ is calculated as

$$\partial_B f(1) = \{0, 1\},$$

while the Clarke Jacobian is calculated as the convex interval

$$\partial_C f(1) = [0, 1].$$

To summarize, the Clarke Jacobian is motivated by a desire to at least describe the nearby first-order derivative behavior of a function at points where the function itself is nondifferentiable. This object and methods based around it benefit from several key advantages. First and perhaps most obviously, in the context of functions which are at least locally Lipschitz continuous (e.g., PC^1), the Clarke Jacobian is defined at points where the classical Jacobian is undefined. Secondly, the Clarke Jacobian possesses theoretical properties which allow for its use in dedicated numerical methods [16]. Important theoretical results include a mean value theorem, inverse function theorem, and

an implicit function theorem; numerically, elements of the Clarke Jacobian are able to be utilized in dedicated nonsmooth methods for equation-solving (e.g., [21, 42]) and optimization (e.g., [33, 35]).

And yet, despite the great advantages offered by the Clarke Jacobian, its drawbacks can be debilitating to methods employing it in many circumstances. The common theme in these shortcomings is difficulty in the computation of Clarke Jacobian elements for complex functions, even despite the aforementioned theoretical and numerical tools [8]. Here, we will examine two of these through constructive examples.

Example 2.15. Consider the trio of functions

$$f(x) = \text{mid}(0, x, 1); \qquad g(x) = \text{mid}(0, x, x-1); \qquad h(x) = f(x) + g(x) = x,$$

displayed in Figure 2.4. Notice that f and g are both PC^1 while their sum, h, is in fact C^1. We can find essentially active selection functions at $x = 0$, for example, easily:

$$\mathcal{E}_f(0) = \{0, x\}; \qquad \mathcal{E}_g(0) = \{0, x\}; \qquad \mathcal{E}_h(0) = \{x\}.$$

Direct calculation of the respective B-subdifferentials reveals that $\partial_B f(0) = \partial_B g(0) = \{0, 1\}$, and consequently $\partial_C f(0) = \partial_C g(0) = [0, 1]$. With regards to the function h, however, we find that $\partial_B h(0) = \{1\} = \partial_C h(0)$. Notice here that $0 \in \partial_C f(0), \partial_C g(0)$, yet $(0 + 0) \notin \partial_C (f + g)(0) = \partial_C h(0)$. Therefore, we find that any

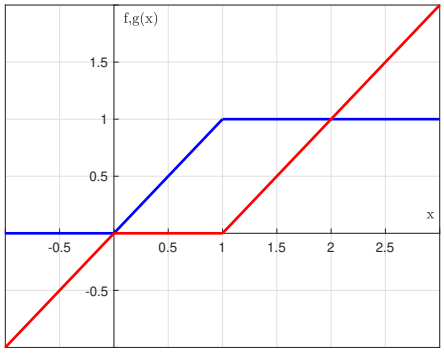

(a) Functions f (blue) and g (red).

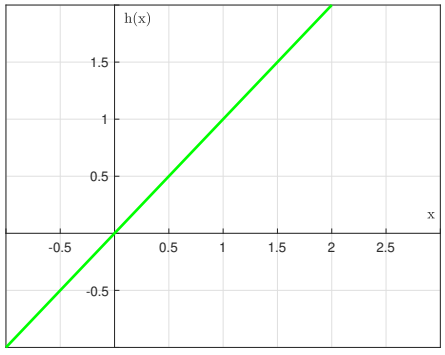

(b) Function h (i.e., $f + g$).

Figure 2.4: Depictions of the functions associated with Example 2.15.

attempt to find elements of the Clarke Jacobian of the function h using a rule of sums is strictly inclusive in this case: that is, $\partial_C h(0) \subsetneq \partial_C f(0) + \partial_C g(0)$.

A similar result occurs at $x = 1$: $\mathcal{E}_f(1) = \{x, 1\}$, $\mathcal{E}_g(1) = \{0, x-1\}$, $\mathcal{E}_h(1) = \{x\}$ implies $\partial_C f(1) = \partial_C g(1) = [0, 1]$ and $\partial_C h(1) = \{1\}$, so we conclude $\partial_C h(1) \subsetneq \partial_C f(1) + \partial_C g(1)$ in this case as well.

Examples like this one provide an illuminating view of how Clarke Jacobian computation can be hindered even in simple circumstances. Despite the prevalence of the "sharp" (i.e., equality-based) rule of sums in classical derivative theory, we find that the analogous rule holds only as an inclusion in the case of Clarke Jacobians. Indeed, any calculus rules associated with the Clarke Jacobian are only inclusions in general, making the systematic calculation of Clarke Jacobian elements difficult. The use of the Clarke Jacobian can cause failure even in dedicated numerical methods, such as nonsmooth extensions of classical automatic differentiation (AD) [23], as a result of the inability of these rules to obey sharp equality in general.

In order to explore a different attempt at calculating Clarke Jacobian elements, we now turn to directional derivatives.

Definition 2.16 (Directional Derivative)**.** Given an open set $X \subset \mathbb{R}^n$, a function $\boldsymbol{f} : X \to \mathbb{R}^m$, and some $\boldsymbol{x} \in X$, the (one-sided) *directional derivative* of $\boldsymbol{f}$ at $\boldsymbol{x}$ in the direction $\boldsymbol{d} \in \mathbb{R}^n$ is given by

$$\boldsymbol{f}'(\boldsymbol{x}; \mathbf{d}) = \lim_{\alpha \to 0^+} \frac{\boldsymbol{f}(\boldsymbol{x} + \alpha \boldsymbol{d}) - \boldsymbol{f}(\boldsymbol{x})}{\alpha},$$

if it exists. We call $\boldsymbol{f}$ *directionally differentiable at* $\boldsymbol{x}$ if $\boldsymbol{f}'(\boldsymbol{x}; \mathbf{d})$ exists for all $\mathbf{d} \in \mathbb{R}^n$, and furthermore we say that $\boldsymbol{f}$ is *directionally differentiable on* X if it is directionally differentiable at all possible $\boldsymbol{x} \in X$.

The class of directionally differentiable functions includes — but is broader than — the class of C^1 functions. For example, functions which are only PC^1 are also necessarily

directionally differentiable on their domain [45]; therefore, in the case of functions which are only PC^1, directional derivatives offer the advantage of being defined even at points of classical nondifferentiability. As an example, the PC^1 function $f(x) = |x|$ is not differentiable at $x = 0$, yet for any chosen direction $d \in \mathbb{R}$, we find that the directional derivative is defined and in particular

$$f'(0;d) = \begin{cases} d & \text{if } d \geq 0, \\ -d & \text{if } d < 0. \end{cases}$$

If $\mathbf{f}$ does happen to be C^1 then the directional derivative and classical Jacobian are related in the following way:

$$\boldsymbol{f}'(\boldsymbol{x};\mathbf{d}) = \mathbf{J}\boldsymbol{f}(\boldsymbol{x})\mathbf{d}. \tag{2.10}$$

Due to this relationship, directional derivatives in the unit coordinate directions may be appended in the C^1 setting to calculate the Jacobian of a given function at a point of interest since in this case, letting $\mathbf{e}_i$ be the i^{th} unit coordinate vector, we find

$$\begin{aligned} [\boldsymbol{f}'(\boldsymbol{x};\mathbf{e}_1) \quad \boldsymbol{f}'(\boldsymbol{x};\mathbf{e}_2) \quad \cdots \quad \boldsymbol{f}'(\boldsymbol{x};\mathbf{e}_n)] &= [\mathbf{J}\boldsymbol{f}(\boldsymbol{x})\mathbf{e}_1 \quad \mathbf{J}\boldsymbol{f}(\boldsymbol{x})\mathbf{e}_2 \quad \cdots \quad \mathbf{J}\boldsymbol{f}(\boldsymbol{x})\mathbf{e}_n] \\ &= \mathbf{J}\boldsymbol{f}(\boldsymbol{x})\,[\mathbf{e}_1 \quad \mathbf{e}_2 \quad \cdots \quad \mathbf{e}_n] \\ &= \mathbf{J}\boldsymbol{f}(\boldsymbol{x})\mathbf{I} \\ &= \mathbf{J}\boldsymbol{f}(\boldsymbol{x}), \end{aligned}$$

as expected. However, the analogous approach in the PC^1 setting fails to reliably produce an element of Clarke's generalized Jacobian as desired.

Example 2.17. (***Part a.***) Consider the C^1 mapping $f : \mathbb{R}^2 \to \mathbb{R} : (x_1, x_2) \mapsto x_1^2 - x_2^2$, which forms a saddle when visualized in $\mathbb{R}^3$ as seen in Figure 2.5. The Jacobian of this function is easily computed directly:

$$\mathbf{J}f(\boldsymbol{x}) = \begin{bmatrix} \frac{\partial f}{\partial x_1}(\boldsymbol{x}) & \frac{\partial f}{\partial x_2}(\boldsymbol{x}) \end{bmatrix} = \begin{bmatrix} 2x_1 & -2x_2 \end{bmatrix}.$$

Consider instead the directional derivative in the unit coordinate directions. Begin by letting $\mathbf{d}_1 = (1, 0)$ (i.e., the unit x_1 direction). Then,

$$\begin{aligned} f'(\boldsymbol{x}, \mathbf{d}_1) &= \lim_{\alpha \to 0^+} \frac{f(\boldsymbol{x} + \alpha(1,0)) - f(\boldsymbol{x})}{\alpha} \\ &= \lim_{\alpha \to 0^+} \frac{f(x_1 + \alpha, x_2) - f(x_1, x_2)}{\alpha} \\ &= \lim_{\alpha \to 0^+} \frac{[(x_1 + \alpha)^2 - x_2^2] - (x_1^2 - x_2^2)}{\alpha} \\ &= \lim_{\alpha \to 0^+} \frac{2x_1\alpha + \alpha^2}{\alpha} \\ &= 2x_1. \end{aligned}$$

Similar analysis with a choice of $\mathbf{d}_2 = (0, 1)$ (i.e., the unit x_2 direction) yields

$$f'(\boldsymbol{x}, \mathbf{d}_2) = -2x_2.$$

Now, note that the Jacobian can be recovered by assembling these two unit-coordinate directional derivatives in a matrix:

$$\begin{bmatrix} f'(\boldsymbol{x}, \mathbf{d}_1) & f'(\boldsymbol{x}, \mathbf{d}_2) \end{bmatrix} = \begin{bmatrix} 2x_1 & -2x_2 \end{bmatrix} = \mathbf{J}f(\boldsymbol{x}),$$

as required, independent of the choice of $\boldsymbol{x}$.

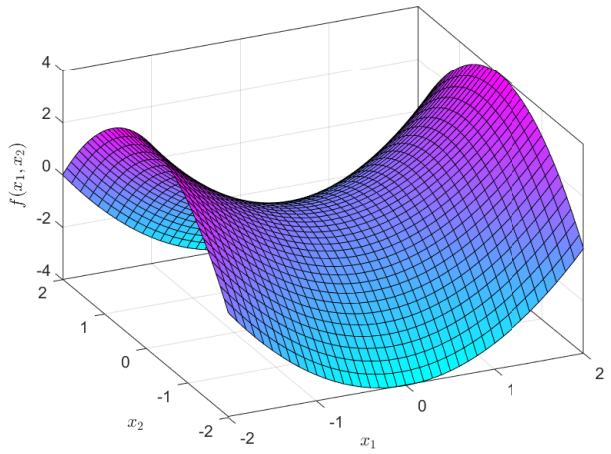

Figure 2.5: Function f, explored in Example 2.17, Part a.

(***Part b.***) Now instead consider the related PC^1 mapping

$$g : \mathbb{R}^2 \to \mathbb{R} : (x_1, x_2) \mapsto \left| x_1^2 - x_2^2 \right|$$

(depicted in Figure 2.6a), which is nondifferentiable along the set

$$Z_g = \{(x_1, x_2) : x_1 = x_2\} \cup \{(x_1, x_2) : x_1 = -x_2\}.$$

This mapping has essentially active selection functions

$$\mathcal{E}_g(\boldsymbol{x}) \subset \{x_1^2 - x_2^2, -(x_1^2 - x_2^2)\} = \{g_1(\boldsymbol{x}), g_2(\boldsymbol{x})\}.$$

At the point $(1, 1) \in Z_g$, for example, we find that $\partial_B g(1, 1) = \{[2 \quad -2], [-2 \quad 2]\}$. In this case, the Clarke Jacobian evaluates as

$$\partial_C g(1, 1) = \operatorname{conv}\left(\partial_B g(1, 1)\right) = \left\{ \begin{bmatrix} 2\lambda & -2\lambda \end{bmatrix} : \lambda \in [-1, 1] \right\}.$$

Figure 2.6b illustrates the difficulty of attempting to recover an element of the Clarke Jacobian using the directional derivative approach. In the unit coordinate direction $(1, 0)$, our function g behaves as the C^1 essentially active selection function g_1. Calculating the

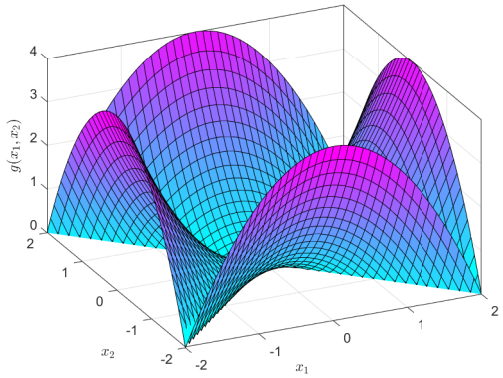

(a) Function g.

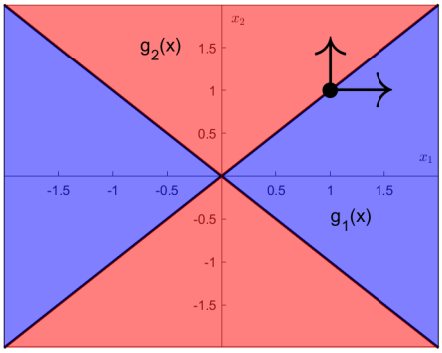

(b) A view of the domain of g. In the blue regions, g mimics the behavior of selection function g_1; in red regions it instead mimics selection function g_2. At $(1, 1)$, unit coordinate vectors probe into different regions.

Figure 2.6: A depiction of the function explored in Example 2.17, Part b.

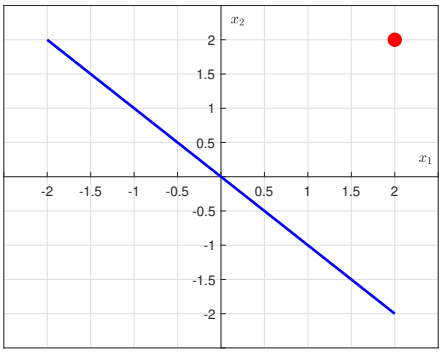

Figure 2.7: In blue, a graphical depiction of $\partial_C g(1,1)$ calculated in Part b. of Example 2.17 with the Clarke Jacobian elements in $\mathbb{R}^{1\times 2}$ interpreted as an ordered pair. The object constructed by assembling unit coordinate directional derivatives lies outside this set in red.

directional derivative, we find that

$$g'((1,1);(1,0)) = g_1'((1,1);(1,0)) = 2.$$

Meanwhile, in the unit coordinate direction $(0,1)$, our function g behaves as the C^1 essentially active selection function g_2; calculating the appropriate directional derivative here yields

$$g'((1,1);(0,1)) = 2,$$

as well. Thus, following a similar procedure as in Part a. above, we find that

$$\begin{bmatrix} g'((1,1);(1,0)) & g'((1,1);(0,1)) \end{bmatrix} = [2 \quad 2] \notin \partial_C g(1,1).$$

The location of this object in relation to the Clarke Jacobian is depicted in Figure 2.7. Ultimately, assembling the unit coordinate directional derivatives as is allowed in the C^1 environment fails to yield even a generalized Jacobian object here.

Though this approach centered around directional derivatives may fail when applied directly to the PC^1 setting, we will shortly see their utility elsewhere. As a result of the weaknesses outlined above, Clarke Jacobian elements are, plainly, difficult to calculate in the case of complex or composite functions — and certainly in the setting of nonsmooth dynamic models, which are the focus of this thesis. Yet, we have noted that these objects are still desirable for the purposes of dedicated nonsmooth methods for equation-solving,

for example. Ultimately, we seek an automatable and tractable method of calculating these computationally relevant Clarke Jacobian elements. Recent developments by Khan and Barton [32] in the topic of lexicographic differentiation pioneered by Nesterov [38] provide a practically implementable such method.

CHAPTER 3
LEXICOGRAPHIC SENSITIVITY FUNCTIONS FOR NONSMOOTH ORDINARY DIFFERENTIAL EQUATIONS

Motivated by the shortcomings of trying to calculate Clarke Jacobian elements in a straightforward and systematic way, we introduce the lexicographic derivative in this chapter as an attractive alternative. This object possesses many traits which are desirable in the search for computationally relevant generalized derivative (e.g., Clarke Jacobian) elements including a sharp (equality-based) collection of calculus rules. Furthermore, these objects can be extended into the theory of nonsmooth ordinary differential equations to yield sensitivity theory analogous to the classical theory introduced in Section 2.2. We start, however, with the relevant class of functions which allow this approach.

3.1 Lexicographically smooth functions and the lexicographic derivative

Lexicographic differentiation, first introduced by Nesterov in [38], is applicable to a broad class of sufficiently-smooth functions referred to as "lexicographically smooth."

Definition 3.1 (Lexicographically Smooth Functions)**.** ([38]) Given an open set $X \subset \mathbb{R}^n$ and a locally Lipschitz continuous function $\boldsymbol{f} : X \to \mathbb{R}^m$, $\boldsymbol{f}$ is called *lexicographically smooth* (*L-smooth*) at $\boldsymbol{x} \in X$ if it is directionally differentiable at $\boldsymbol{x}$ and if for any $k \in \mathbb{N}$ and $\mathbf{M} = [\mathbf{m}_1 \quad \mathbf{m}_2 \quad \dots \quad \mathbf{m}_k] \in \mathbb{R}^{n\times k}$ the following functions are well-defined:

$$
\begin{aligned}
&\boldsymbol{f}^{(0)}_{\boldsymbol{x},\mathbf{M}} : \mathbb{R}^n \to \mathbb{R}^m : \mathbf{d} \mapsto \boldsymbol{f}'(\boldsymbol{x};\mathbf{d}),\\
&\boldsymbol{f}^{(1)}_{\boldsymbol{x},\mathbf{M}} : \mathbb{R}^n \to \mathbb{R}^m : \mathbf{d} \mapsto [\boldsymbol{f}^{(0)}_{\boldsymbol{x},\mathbf{M}}]'(\mathbf{m}_1;\mathbf{d}),\\
&\boldsymbol{f}^{(2)}_{\boldsymbol{x},\mathbf{M}} : \mathbb{R}^n \to \mathbb{R}^m : \mathbf{d} \mapsto [\boldsymbol{f}^{(1)}_{\boldsymbol{x},\mathbf{M}}]'(\mathbf{m}_2;\mathbf{d}),\\
&\vdots\\
&\boldsymbol{f}^{(k)}_{\boldsymbol{x},\mathbf{M}} : \mathbb{R}^n \to \mathbb{R}^m : \mathbf{d} \mapsto [\boldsymbol{f}^{(k-1)}_{\boldsymbol{x},\mathbf{M}}]'(\mathbf{m}_k;\mathbf{d}).
\end{aligned}
$$

The function $\boldsymbol{f}$ is then called *L-smooth on* X if it is L-smooth at each point $\boldsymbol{x} \in X$.

Any function which is PC^1, C^1, convex, or a composition or integral of such functions is necessarily L-smooth [32, 38]. Notably, the solution of any L-smooth system of ordinary differential equations also inherits L-smoothness with respect to parameters [30]. In addition, notice the reappearance of the directional derivative in these mappings; indeed, the process above actually defines a chain of recursive directional derivatives. As with classical directional derivatives, the mapping furnished at each step fundamentally depends on the directions being "probed" (see, e.g., Example 2.17), which are represented by the columns of the matrix $\mathbf{M}$ — for this reason, $\mathbf{M}$ is referred to as a *directions matrix*. If we impose the additional constraint that $\mathbf{M}$ is full row rank (i.e., that the rows of $\mathbf{M}$ are linearly independent), we gain the following result.

Proposition 3.2. *([38]) Given an open set $X \subset \mathbb{R}^n$, an L-smooth function $\boldsymbol{f} : X \to \mathbb{R}^m$, and a full row rank matrix $\boldsymbol{M} \in \mathbb{R}^{n\times k}$, the final mapping in the recursive directional derivative process in Definition 3.1 (i.e., $\boldsymbol{f}^{(k)}_{\boldsymbol{x},\boldsymbol{M}}$) is linear.*

Roughly, the above result can be understood as follows: for any L-smooth function $\boldsymbol{f}$, the domain over which $\boldsymbol{f}$ is nondifferentiable must be a set of Lebesgue measure zero by Theorem 2.10. Thus, since $\mathbf{M}$ represents a collection of "probing" directions in the n-dimensional domain space of $\boldsymbol{f}$, the requirement of being full row rank guarantees that this final recursive mapping probes away from any nonsmoothness which may be present. This concept will be illustrated and expanded on in the following section (Example 3.8); more immediately, the linearity of $\boldsymbol{f}^{(k)}_{\boldsymbol{x},\mathbf{M}}$ guaranteed by this proposition implies it is also C^1, and we are now prepared to introduce the lexicographic derivative.

Definition 3.3 (Lexicographic Derivative)**.** ([38]) Given an open set $X \subset \mathbb{R}^n$, an L-smooth function $\boldsymbol{f} : X \to \mathbb{R}^m$, and a full row rank matrix $\mathbf{M} \in \mathbb{R}^{n\times k}$, the *lexicographic (L-)derivative* of $\boldsymbol{f}$ at $\boldsymbol{x}$ is

$$\mathbf{J}_L \boldsymbol{f}(\boldsymbol{x}; \mathbf{M}) = \mathbf{J}\boldsymbol{f}^{(k)}_{\boldsymbol{x};\mathbf{M}}(\mathbf{0}_n) \in \mathbb{R}^{m\times n}.$$

This object can be understood as the classical Jacobian of the necessarily linear mapping $\boldsymbol{f}^{(k)}_{\boldsymbol{x};\mathbf{M}}$ evaluated at $\mathbf{0}_n$ by convention (as the Jacobian of a linear function is constant). However, as we have already noted, the mapping $\boldsymbol{f}^{(k)}_{\boldsymbol{x};\mathbf{M}}$ (and hence the L-derivative) is fundamentally influenced by the entries of $\mathbf{M}$. Thus, it is feasible that different acceptable choices of $\mathbf{M}$ yield different L-derivatives in general.

Definition 3.4 (Lexicographic Subdifferential)**.** ([38]) Given an L-smooth function $\boldsymbol{f} : \mathbb{R}^n \to \mathbb{R}^m$, the *lexicographic (L-)subdifferential* of $\boldsymbol{f}$ at $\boldsymbol{x}$ is given by

$$\partial_L \boldsymbol{f}(\boldsymbol{x}) = \{\mathbf{J}_L \boldsymbol{f}(\boldsymbol{x}; \mathbf{M}) : k \in \mathbb{N}, \mathbf{M} \in \mathbb{R}^{n\times k}, \mathbf{M} \text{ has full row rank}\},$$

and represents the set of all possible L-derivatives.

This subdifferential is necessarily nonempty and moreover is a non-singleton set when evaluated at a point in the function's domain of nondifferentiability. In general, elements of the L-subdifferential are closely related to elements of the Clarke Jacobian.

Proposition 3.5. *([30, 32]) Given an open set $X \subset \mathbb{R}^n$ and an L-smooth function $\boldsymbol{f} : X \to \mathbb{R}^m$, L-derivatives of $\boldsymbol{f}$ are indistinguishable from Clarke Jacobian elements in matrix-vector products; i.e.,*

$$\{\boldsymbol{A}\boldsymbol{d} : \boldsymbol{A} \in \partial_L \boldsymbol{f}(\boldsymbol{x}), \boldsymbol{d} \in \mathbb{R}^n\} \subset \{\boldsymbol{A}\boldsymbol{d} : \boldsymbol{A} \in \partial_C \boldsymbol{f}(\boldsymbol{x}), \boldsymbol{d} \in \mathbb{R}^n\}.$$

If $\boldsymbol{f}$ satisfies the stronger requirement of being PC^1, then we find that

$$\partial_L \boldsymbol{f}(\boldsymbol{x}) \subset \partial_B \boldsymbol{f}(\boldsymbol{x}) \subset \partial_C \boldsymbol{f}(\boldsymbol{x}).$$

As we have discussed previously, Clarke Jacobian elements are useful tools in dedicated nonsmooth methods. Such methods, however, typically only employ generalized derivatives in the context of matrix-vector products or scalar-valued functions, implying any single L-derivative or element of the Clarke Jacobian is sufficient for convergence whenever such an outcome is possible. Lexicographic derivatives are therefore highly computationally relevant and desirable in, e.g., numerical methods; unlike the Clarke Jacobian, however,

L-derivatives possess a closely-related tool which allows accurate and automatable calculation.

3.2 Computation of lexicographic derivatives

Recall the recursive chain of directional derivatives used to define the concept of L-smoothness in Definition 3.1. We have defined the L-derivative as the Jacobian of the final (linear) mapping produced by this process, and seek an automatable method of calculating this object in general. Khan and Barton have presented such a method in [32], which is constructed from the intermediate directional derivatives of the recursive process.

Definition 3.6 (Lexicographic Directional Derivative)**.** ([32]) Given an open set $X \subset \mathbb{R}^n$, a function $\boldsymbol{f} : X \to \mathbb{R}^m$ which is L-smooth at $\boldsymbol{x} \in X$, and a matrix $\mathbf{M} = [\mathbf{m}_1 \quad \mathbf{m}_2 \quad \dots \quad \mathbf{m}_k] \in \mathbb{R}^{n \times k}$, the *lexicographic directional (LD-)derivative* of $\boldsymbol{f}$ at $\boldsymbol{x}$ in the directions given by $\mathbf{M}$ is

$$\boldsymbol{f}'(\boldsymbol{x}; \mathbf{M}) = \left[\boldsymbol{f}^{(0)}_{\boldsymbol{x},\mathbf{M}}(\mathbf{m}_1) \quad \boldsymbol{f}^{(1)}_{\boldsymbol{x},\mathbf{M}}(\mathbf{m}_2) \quad \dots \quad \boldsymbol{f}^{(k-1)}_{\boldsymbol{x},\mathbf{M}}(\mathbf{m}_k) \right].$$

LD-derivatives generalize the classical directional derivative in order to provide first-order generalized derivative information about $\boldsymbol{f}$ near $\boldsymbol{x}$ using the series of directions specified by the columns of $\mathbf{M}$. In the case where $k = 1$, note that $\mathbf{M}$ is in fact a column vector and $\boldsymbol{f}'(\boldsymbol{x}; \mathbf{M}) = \boldsymbol{f}^{(0)}_{\boldsymbol{x},\mathbf{M}}(\mathbf{m}_1) = \boldsymbol{f}'(\boldsymbol{x}; \mathbf{m}_1)$; hence, if $k = 1$ then the LD-derivative recovers the classical directional derivative. Furthermore, a general relationship between LD- and L-derivatives (analogous to Equation (2.10)) is found in the L-smooth case.

Theorem 3.7 (Relation of LD- and L-Derivatives)**.** *([32]) Given an open set $X \subset \mathbb{R}^n$, a function $\boldsymbol{f} : X \to \mathbb{R}^m$ which is L-smooth at $x \in X$, and a full row rank matrix $\boldsymbol{M} = \left[\boldsymbol{m}_1 \quad \boldsymbol{m}_2 \quad \dots \quad \boldsymbol{m}_k \right] \in \mathbb{R}^{n \times k}$, then*

$$\boldsymbol{f}'(\boldsymbol{x}; \boldsymbol{M}) = \boldsymbol{J}_L \boldsymbol{f}(\boldsymbol{x}; \boldsymbol{M}) \boldsymbol{M},$$

or equivalently,

$$\boldsymbol{J}_L \boldsymbol{f}(\boldsymbol{x}; \boldsymbol{M}) = \boldsymbol{f}'(\boldsymbol{x}; \boldsymbol{M}) \boldsymbol{M}^{-1}.$$

This theorem establishes the LD-derivative as a desirable object since a corresponding L-derivative can be easily calculated using one whenever the directions matrix is full row rank (and hence right-invertible). Often, it is convenient to choose $\mathbf{M} = \mathbf{I}_n$ (i.e., the n by n identity matrix) since in this case $\mathbf{M}^{-1} = \mathbf{M}$; as a result, any LD-derivative furnished with this choice is also an L-derivative. Separately, if $\boldsymbol{f}$ satisfies the stronger requirement of being C^1, we find that the theorem specializes as

$$\boldsymbol{f}'(\boldsymbol{x}; \mathbf{M}) = \mathbf{J}\boldsymbol{f}(\boldsymbol{x})\mathbf{M} \tag{3.1}$$

by Proposition 3.5 applied in conjunction with the relation in Equation (2.9).

Example 3.8. Recall the PC^1 (and hence L-smooth) function explored in Example 2.17, Part b:

$$g : \mathbb{R}^2 \to \mathbb{R} : (x_1, x_2) \mapsto \left| x_1^2 - x_2^2 \right|,$$

which has the set of nondifferentiability

$$Z_g = \{(x_1, x_2) : x_1 = x_2\} \cup \{(x_1, x_2) : x_1 = -x_2\}$$

and essentially active selection functions

$$\mathcal{E}_g(\boldsymbol{x}) \subset \{x_1^2 - x_2^2, -(x_1^2 - x_2^2)\} = \{g_1(\boldsymbol{x}), g_2(\boldsymbol{x})\}.$$

Consider the point $\boldsymbol{x}_0 = (1, 1) \in Z_g$ and the full row rank directions matrix $\mathbf{M} = \mathbf{I}_2 \in \mathbb{R}^{2\times 2}$. We aim to find an L-derivative of this function by first finding an LD-derivative; as Definition 3.6 would suggest, we first need to calculate the first two recursive directional derivatives of $\boldsymbol{g}$.

The first directional derivative of $\boldsymbol{g}$ at $\boldsymbol{x}_0$ is calculated as

$$\begin{aligned}
\boldsymbol{f}^{(0)}_{\boldsymbol{x}_0,\mathbf{M}}(d_1, d_2) &= \lim_{\alpha\to 0^+} \frac{\boldsymbol{g}(\boldsymbol{x}_0 + \alpha(d_1, d_2)) - \boldsymbol{g}(\boldsymbol{x}_0)}{\alpha} \\
&= \lim_{\alpha\to 0^+} \frac{|(1 + \alpha d_1)^2 - (1 + \alpha d_2)^2| - |1^2 - 1^2|}{\alpha} \\
&= \lim_{\alpha\to 0^+} \frac{|1 + 2\alpha d_1 + \alpha^2 d_1^2 - 1 - 2\alpha d_2 - \alpha^2 d_2^2|}{\alpha}
\end{aligned}$$

$$
\begin{aligned}
&= \lim_{\alpha \to 0^+} \frac{|2\alpha d_1 + \alpha^2 d_1^2 - 2\alpha d_2 - \alpha^2 d_2^2|}{\alpha} \\
&= \lim_{\alpha \to 0^+} |2d_1 + \alpha d_1^2 - 2d_2 - \alpha d_2^2| \\
&= |2d_1 - 2d_2|,
\end{aligned}
$$

where the penultimate equality holds by virtue of α being greater than zero (by definition). In the direction $(1, 0)$ given by the first column $\mathbf{m}_1$ of the directions matrix $\mathbf{M}$, we find that

$$
\boldsymbol{f}^{(0)}_{\boldsymbol{x}_0, \mathbf{M}}(\mathbf{m}_1) = 2.
$$

The next directional derivative mapping has the effect of being "smoothed," as $\boldsymbol{f}^{(0)}_{\boldsymbol{x}_0, \mathbf{M}}(d_1, d_2)$ is smooth in the direction $(1, 0)$ (see Figure 3.1a) and the directional derivative process is applied recursively. In effect,

$$
\begin{aligned}
\boldsymbol{f}^{(1)}_{\boldsymbol{x}_0, \mathbf{M}}(d_1, d_2) &= [\boldsymbol{f}^{(0)}_{\boldsymbol{x}_0, \mathbf{M}}]'(\boldsymbol{m}_1; (d_1, d_2)) \\
&= \lim_{\alpha \to 0^+} \frac{|2(1 + \alpha d_1) - 2(0 + \alpha d_2)| - |2 - 0|}{\alpha} \\
&= \lim_{\alpha \to 0^+} \frac{|2 + 2\alpha d_1 - 2\alpha d_2| - 2}{\alpha}.
\end{aligned}
$$

Now since $\alpha \to 0^+$, the number 2 is the dominating term within the argument of the absolute value function and a positive result is yielded in the limit. Hence,

$$
\begin{aligned}
\boldsymbol{f}^{(1)}_{\boldsymbol{x}_0, \mathbf{M}}(d_1, d_2) &= \lim_{\alpha \to 0^+} \frac{2 + 2\alpha d_1 - 2\alpha d_2 - 2}{\alpha} \\
&= 2d_1 - 2d_2.
\end{aligned}
$$

With this information, we may calculate

$$
\boldsymbol{f}^{(1)}_{\boldsymbol{x}_0, \mathbf{M}}(\mathbf{m}_2) = -2,
$$

where $\mathbf{m}_2 = (0, 1)$ is the second column of the directions matrix $\mathbf{M}$ here. All together, we may assemble the LD-derivative of $\boldsymbol{f}$ at $\boldsymbol{x}_0$ in directions given by $\mathbf{M}$:

$$
\boldsymbol{f}'(\boldsymbol{x}_0; \mathbf{M}) = \begin{bmatrix} \boldsymbol{f}^{(0)}_{\boldsymbol{x}, \mathbf{M}}(\mathbf{m}_1) & \boldsymbol{f}^{(1)}_{\boldsymbol{x}, \mathbf{M}}(\mathbf{m}_2) \end{bmatrix} = \begin{bmatrix} 2 & -2 \end{bmatrix}.
$$

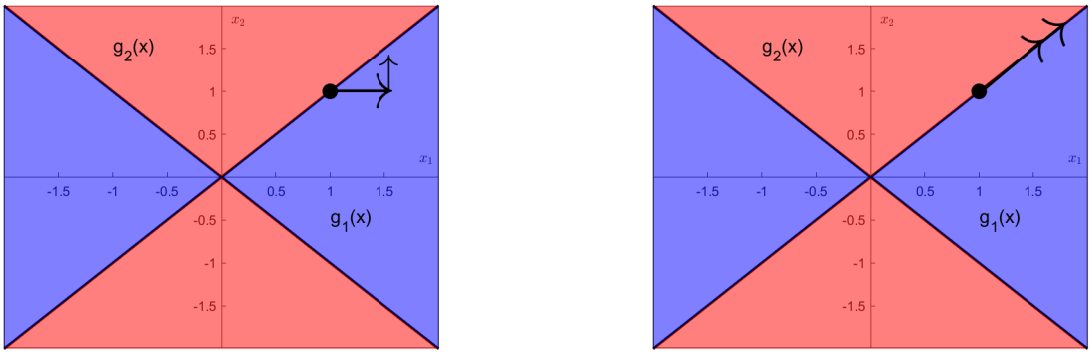

(a) (b)

Figure 3.1: A conceptual view of the probing processes defined by directions matrices $\mathbf{M} = \mathbf{I}_2$ and $\begin{bmatrix} 1 & 1 \\ 1 & 1 \end{bmatrix}$, respectively.

Finally, from the LD-derivative, we may use the inverse of $\mathbf{M} = \mathbf{I}$ to furnish an L-derivative:

$$\mathbf{J}_L \boldsymbol{f}(\boldsymbol{x}_0; \mathbf{M}) = \begin{bmatrix} 2 & -2 \end{bmatrix} \mathbf{I}^{-1} = \begin{bmatrix} 2 & -2 \end{bmatrix} \in \partial_C \boldsymbol{f}(\boldsymbol{x}_0).$$

This L-derivative is indeed an element of the Clarke Jacobian since $\boldsymbol{g}$ itself is PC^1, as Proposition 3.5 would suggest.

Notice, however, that a poor choice of directions matrix need not furnish an L-derivative. Consider the same computation with a choice of $\mathbf{M} = \begin{bmatrix} 1 & 1 \\ 1 & 1 \end{bmatrix}$, which is not full row rank. The first directional derivative is again calculated as

$$\boldsymbol{f}'_{\boldsymbol{x}_0, \mathbf{M}}(d_1, d_2) = |2d_1 - 2d_2|.$$

However, this mapping exhibits nonsmoothness in the direction $(1, 1)$ given by the first column of the directions matrix. Thus, we probe along the line of nondifferentiability $x_1 = x_2$, and the "smoothing" effect exhibited before does not occur (Figure 3.1b). Thus,

the next directional derivative evaluates as the same function:

$$\begin{aligned}
\boldsymbol{f}^{(1)}_{\boldsymbol{x}_0,\mathbf{M}}(d_1,d_2) &= [\boldsymbol{f}^{(0)}_{\boldsymbol{x}_0,\mathbf{M}}]'(\boldsymbol{m}_1;(d_1,d_2)) \\
&= \lim_{\alpha\to 0^+} \frac{|2(1+\alpha d_1)-2(1+\alpha d_2)|-|2-2|}{\alpha} \\
&= \lim_{\alpha\to 0^+} \frac{|2\alpha d_1 - 2\alpha d_2|}{\alpha} \\
&= |2d_1 - 2d_2|.
\end{aligned}$$

Again, no further information is gained by probing in the direction $(1,1)$ given by the second column of our directions matrix, as we fail to probe away from the set of nondifferentiability and directional derivatives remain nonsmooth. Therefore, we may not use the information supplied by this probing matrix to furnish an L-derivative.

Keeping our original goal in mind — namely, the automatable calculation of generalized derivative elements — we now note that LD-derivatives satisfy a long list of attractive sharp calculus rules. These rules do indeed allow automatable LD-derivative computation, and subsequent utilization of Theorem 3.7 in turn yields an L-derivative (i.e., a generalized derivative object lying in or near the Clarke Jacobian).

Proposition 3.9. *([32]) Consider some open sets $X \subset \mathbb{R}^n$, $Y \subset \mathbb{R}^q$ and functions $\boldsymbol{f}, \boldsymbol{g} : X \to \mathbb{R}^m$, $\boldsymbol{h} : Y \to X$ which are L-smooth on X and Y, respectively. Given any directions matrix $\boldsymbol{M} \in \mathbb{R}^{n\times k}$, the following calculus rules for LD-derivatives are satisfied:*

$$\begin{aligned}
\boldsymbol{f}'(\boldsymbol{x};\boldsymbol{M}) &= (f_1'(\boldsymbol{x};\boldsymbol{M}), f_2'(\boldsymbol{x};\boldsymbol{M}), \ldots, f_n'(\boldsymbol{x};\boldsymbol{M})), \\
[\boldsymbol{f}+\boldsymbol{g}]'(\boldsymbol{x};\boldsymbol{M}) &= \boldsymbol{f}'(\boldsymbol{x};\boldsymbol{M}) + \boldsymbol{g}'(\boldsymbol{x};\boldsymbol{M}), \\
[fg]'(\boldsymbol{x};\boldsymbol{M}) &= g(\boldsymbol{x})f'(\boldsymbol{x};\boldsymbol{M}) + f(\boldsymbol{x})g'(\boldsymbol{x};\boldsymbol{M}), \\
[\boldsymbol{f}\circ\boldsymbol{h}]'(\boldsymbol{x},\boldsymbol{M}) &= \boldsymbol{f}'(\boldsymbol{g}(\boldsymbol{x});\boldsymbol{g}'(\boldsymbol{x};\boldsymbol{M})).
\end{aligned}$$

The sharp calculus rules outlined above allow for practical use in numerical methods; for example, dedicated nonsmooth automatic differentiation methods employing the LD-derivative have already been developed [29, 32]. These calculus rules may also be used

to develop of a library of LD-derivative rules for common elemental nonsmooth functions. An example of such a function is the maximum function, which can be extended to matrix-valued inputs by using so-called lexicographic ordering to compare the matrices at hand.

Definition 3.10 (Lexicographic Ordering)**.** For any two vectors $\boldsymbol{a}, \boldsymbol{b} \in \mathbb{R}^k$, we say that $\boldsymbol{a}$ is *lexicographically less than* $\boldsymbol{b}$ if $a_i < b_i$ for the first index $i \in \{1, 2, \ldots, k\}$ such that $a_i \neq b_i$ and write $\boldsymbol{a} \prec \boldsymbol{b}$. We instead say $\boldsymbol{a}$ is *lexicographically greater than* $\boldsymbol{b}$ if $a_i > b_i$ for the first index $i \in \{1, 2, \ldots, k\}$ such that $a_i \neq b_i$ and write $\boldsymbol{a} \succ \boldsymbol{b}$. The relational operators $\preceq$ and $\succeq$ are used similarly whenever equality of $\boldsymbol{a}$ and $\boldsymbol{b}$ is possible.

Remark 3.11. The term "lexicographic" is used to describe this style of ordering due to the conventional hierarchy of the elements of a vector (e.g., there is a "first element," then a "second element," etc.). The vectors at hand (whether column or row vectors) are compared element-wise with the highest level of importance given to the first elements in the vectors; comparison moves to the second elements only if the first comparison resulted in a tie and so on. As an example,

$$[4 \quad 1 \quad 3] \prec [4 \quad 7 \quad 0],$$

but

$$[4 \quad 1 \quad 3] \succ [4 \quad 0 \quad 7].$$

This compares to alphabetical ordering; within a lexicon (the collection of words comprising a language), a similar approach is used letter-wise in order to alphabetize a list of distinct words.

We are now equipped to extend the classical scalar-valued "max" function to a matrix-valued analog. This new function, the "lexicographic maximum," takes in matrices of identical dimension and compares them row-by-row. In each comparison, the row which is lexicographically greatest is selected, and the result is a matrix consisting of these

selected rows; e.g.,

$$\mathbf{lmax}\left(\begin{bmatrix}1 & 2 & 3\\ 4 & 5 & 6\end{bmatrix}, \begin{bmatrix}0 & 5 & 9\\ 4 & 7 & 9\end{bmatrix}\right) = \begin{bmatrix}1 & 2 & 3\\ 4 & 7 & 9\end{bmatrix}.$$

The "shifted lexicographic maximum" function is defined as the left shift of the **lmax** function:

$$\mathbf{slmax}\left(\begin{bmatrix}1 & 2 & 3\\ 4 & 5 & 6\end{bmatrix}, \begin{bmatrix}0 & 5 & 9\\ 4 & 7 & 9\end{bmatrix}\right) = \begin{bmatrix}2 & 3\\ 7 & 9\end{bmatrix}.$$

Proposition 3.12. *([47]) Let $X \subset \mathbb{R}^n$ and $Y \subset \mathbb{R}^m$ be open sets and $\boldsymbol{f} : X \times Y \to \mathbb{R}^v$ and $\boldsymbol{g} : X \times Y \to \mathbb{R}^v$ be C^1 at $(\boldsymbol{x}, \boldsymbol{y}) \in X \times Y$. Given directions matrix $\boldsymbol{M} = (\boldsymbol{X}, \boldsymbol{Y}) \in \mathbb{R}^{(n+m)\times k}$,*

$$\begin{aligned}&[\boldsymbol{max} \circ (\boldsymbol{f}, \boldsymbol{g})]'(\boldsymbol{x}, \boldsymbol{y}; (\boldsymbol{X}, \boldsymbol{Y}))\\ &= \boldsymbol{slmax}\left(\begin{bmatrix}\boldsymbol{f}(\boldsymbol{x}, \boldsymbol{y}) & \boldsymbol{J_x f} \cdot \boldsymbol{X} + \boldsymbol{J_y f} \cdot \boldsymbol{Y}\end{bmatrix}, \begin{bmatrix}\boldsymbol{g}(\boldsymbol{x}, \boldsymbol{y}) & \boldsymbol{J_x g} \cdot \boldsymbol{X} + \boldsymbol{J_y g} \cdot \boldsymbol{Y}\end{bmatrix}\right) \in \mathbb{R}^{v\times k},\end{aligned} \tag{3.2}$$

where the partial Jacobian matrices are evaluated at $(\boldsymbol{x}, \boldsymbol{y})$.

The **slmin** function is defined similarly as the LD-derivative of the lexicographic minimum function of two vector-valued arguments. An analogous rule for the lexicographic mid function can be derived.

The lexicographic mid function returns the (row-by-row) median of its three matrix-valued arguments; e.g.,

$$\mathbf{lmid}\left(\begin{bmatrix}1 & 2 & 3\\ 4 & 5 & 6\end{bmatrix}, \begin{bmatrix}0 & 5 & 9\\ 4 & 7 & 9\end{bmatrix}, \begin{bmatrix}6 & 2 & 5\\ 4 & 7 & 3\end{bmatrix}\right) = \begin{bmatrix}1 & 2 & 3\\ 4 & 7 & 3\end{bmatrix}.$$

We continue by constructing the lexicographic mid function as a composition of the matrix-valued max and min functions[1] .

Lemma 3.13. *For any $\boldsymbol{A}, \boldsymbol{B}, \boldsymbol{C} \in \mathbb{R}^{n\times m}$, it holds that*

$$\boldsymbol{lmid}(\boldsymbol{A}, \boldsymbol{B}, \boldsymbol{C}) = \boldsymbol{lmax}\Big(\boldsymbol{lmin}(\boldsymbol{A}, \boldsymbol{B}), \boldsymbol{lmin}\Big(\boldsymbol{lmax}(\boldsymbol{A}, \boldsymbol{B}), \boldsymbol{C}\Big)\Big).$$

[1]This lemma and its proof correct an error in Lemma 2.1 in [1].

Moreover,

$$\boldsymbol{slmid}(\boldsymbol{A}, \boldsymbol{B}, \boldsymbol{C}) = \boldsymbol{slmax}\Big(\boldsymbol{lmin}(\boldsymbol{A}, \boldsymbol{B}), \boldsymbol{lmin}\Big(\boldsymbol{lmax}(\boldsymbol{A}, \boldsymbol{B}), \boldsymbol{C}\Big)\Big).$$

Proof. Since the lexicographic functions operate row-wise, we proceed by showing the identities hold for an arbitrary row of $\mathbf{A}, \mathbf{B}, \mathbf{C}$; denote these rows $\boldsymbol{a}, \boldsymbol{b}, \boldsymbol{c}$, respectively. It is straightforward to simply consider the six possible cases.

1. If $\boldsymbol{a} \preceq \boldsymbol{b} \preceq \boldsymbol{c}$, then

   $$\mathbf{lmax}\Big(\mathbf{lmin}(\boldsymbol{a}, \boldsymbol{b}), \mathbf{lmin}\Big(\mathbf{lmax}(\boldsymbol{a}, \boldsymbol{b}), \boldsymbol{c}\Big)\Big) = \mathbf{lmax}\Big(\boldsymbol{a}, \mathbf{lmin}(\boldsymbol{b}, \boldsymbol{c})\Big) = \mathbf{lmax}(\boldsymbol{a}, \boldsymbol{b}) = \boldsymbol{b},$$

   and thus this composition returns the lexicographic median of the vectors as expected.

2. If instead $\boldsymbol{a} \preceq \boldsymbol{c} \preceq \boldsymbol{b}$, then

   $$\mathbf{lmax}\Big(\mathbf{lmin}(\boldsymbol{a}, \boldsymbol{b}), \mathbf{lmin}\Big(\mathbf{lmax}(\boldsymbol{a}, \boldsymbol{b}), \boldsymbol{c}\Big)\Big) = \mathbf{lmax}\Big(\boldsymbol{a}, \mathbf{lmin}(\boldsymbol{b}, \boldsymbol{c})\Big) = \mathbf{lmax}(\boldsymbol{a}, \boldsymbol{c}) = \boldsymbol{c},$$

   as expected;

3. if $\boldsymbol{b} \preceq \boldsymbol{a} \preceq \boldsymbol{c}$, then

   $$\mathbf{lmax}\Big(\mathbf{lmin}(\boldsymbol{a}, \boldsymbol{b}), \mathbf{lmin}\Big(\mathbf{lmax}(\boldsymbol{a}, \boldsymbol{b}), \boldsymbol{c}\Big)\Big) = \mathbf{lmax}\Big(\boldsymbol{b}, \mathbf{lmin}(\boldsymbol{a}, \boldsymbol{c})\Big) = \mathbf{lmax}(\boldsymbol{b}, \boldsymbol{a}) = \boldsymbol{a},$$

   as expected;

4. if $\boldsymbol{b} \preceq \boldsymbol{c} \preceq \boldsymbol{a}$, then

   $$\mathbf{lmax}\Big(\mathbf{lmin}(\boldsymbol{a}, \boldsymbol{b}), \mathbf{lmin}\Big(\mathbf{lmax}(\boldsymbol{a}, \boldsymbol{b}), \boldsymbol{c}\Big)\Big) = \mathbf{lmax}\Big(\boldsymbol{b}, \mathbf{lmin}(\boldsymbol{a}, \boldsymbol{c})\Big) = \mathbf{lmax}(\boldsymbol{b}, \boldsymbol{c}) = \boldsymbol{c},$$

   as expected;

5. if $\boldsymbol{c} \preceq \boldsymbol{a} \preceq \boldsymbol{b}$, then

   $$\mathbf{lmax}\Big(\mathbf{lmin}(\boldsymbol{a}, \boldsymbol{b}), \mathbf{lmin}\Big(\mathbf{lmax}(\boldsymbol{a}, \boldsymbol{b}), \boldsymbol{c}\Big)\Big) = \mathbf{lmax}\Big(\boldsymbol{a}, \mathbf{lmin}(\boldsymbol{b}, \boldsymbol{c})\Big) = \mathbf{lmax}(\boldsymbol{a}, \boldsymbol{c}) = \boldsymbol{a},$$

   as expected;

6. and finally, if $\boldsymbol{c} \preceq \boldsymbol{b} \preceq \boldsymbol{a}$, then

$$\mathbf{lmax}\Big(\mathbf{lmin}(\boldsymbol{a},\boldsymbol{b}),\mathbf{lmin}\Big(\mathbf{lmax}(\boldsymbol{a},\boldsymbol{b}),\boldsymbol{c}\Big)\Big) = \mathbf{lmax}\Big(\boldsymbol{b},\mathbf{lmin}(\boldsymbol{a},\boldsymbol{c})\Big) = \mathbf{lmax}(\boldsymbol{b},\boldsymbol{c}) = \boldsymbol{b},$$

as expected.

Since the composition at hand returns the lexicographic median in each possible case, the first statement of the lemma holds in general. The lemma's second conclusion follows immediately after a left-shift of both sides. □

Proposition 3.14. *Let $X \subset \mathbb{R}^n$, $Y \subset \mathbb{R}^m$, and $Z \subset \mathbb{R}^p$ be open sets and functions $\boldsymbol{f} : X \times Y \times Z \to \mathbb{R}^v$, $\boldsymbol{g} : X \times Y \times Z \to \mathbb{R}^v$, and $\boldsymbol{h} : X \times Y \times Z \to \mathbb{R}^v$ be C^1 at $(\boldsymbol{x},\boldsymbol{y},\boldsymbol{z}) \in X \times Y \times Z$. Given the choice of directions matrix $\boldsymbol{M} = (\boldsymbol{X}, \boldsymbol{Y}, \boldsymbol{Z}) \in \mathbb{R}^{(n+m+p)\times k}$,*

$$\begin{aligned}[\boldsymbol{mid} \circ (\boldsymbol{f},\boldsymbol{g},\boldsymbol{h})]'(\boldsymbol{x},\boldsymbol{y},\boldsymbol{z};(\boldsymbol{X},\boldsymbol{Y},\boldsymbol{Z})) \\ = \boldsymbol{slmid}\Bigg(&\begin{bmatrix}\boldsymbol{f}(\boldsymbol{x},\boldsymbol{y},\boldsymbol{z}) & \boldsymbol{J_x f}\cdot\boldsymbol{X} + \boldsymbol{J_y f}\cdot\boldsymbol{Y} + \boldsymbol{J_z f}\cdot\boldsymbol{Z}\end{bmatrix}, \\ &\begin{bmatrix}\boldsymbol{g}(\boldsymbol{x},\boldsymbol{y},\boldsymbol{z}) & \boldsymbol{J_x g}\cdot\boldsymbol{X} + \boldsymbol{J_y g}\cdot\boldsymbol{Y} + \boldsymbol{J_z g}\cdot\boldsymbol{Z}\end{bmatrix}, \\ &\begin{bmatrix}\boldsymbol{h}(\boldsymbol{x},\boldsymbol{y},\boldsymbol{z}) & \boldsymbol{J_x h}\cdot\boldsymbol{X} + \boldsymbol{J_y h}\cdot\boldsymbol{Y} + \boldsymbol{J_z h}\cdot\boldsymbol{Z}\end{bmatrix}\Bigg) \in \mathbb{R}^{v\times k},\end{aligned}$$

with partial Jacobian matrices evaluated at $(\boldsymbol{x},\boldsymbol{y},\boldsymbol{z})$.

Proof. We start by employing Lemma 3.13 with a choice of $\mathbf{A} = \boldsymbol{f}(\boldsymbol{x},\boldsymbol{y},\boldsymbol{z}) \in \mathbb{R}^{v\times 1}$, $\mathbf{B} = \boldsymbol{g}(\boldsymbol{x},\boldsymbol{y},\boldsymbol{z}) \in \mathbb{R}^{v\times 1}$, and $\mathbf{C} = \boldsymbol{h}(\boldsymbol{x},\boldsymbol{y},\boldsymbol{z}) \in \mathbb{R}^{v\times 1}$. Since each argument is a column vector, the result of Lemma 3.13 simplifies as

$$[\mathbf{mid} \circ (\boldsymbol{f},\boldsymbol{g},\boldsymbol{h})](\boldsymbol{x},\boldsymbol{y},\boldsymbol{z}) = \mathbf{max}\Big(\mathbf{min}(\boldsymbol{f},\boldsymbol{g}),\mathbf{min}\Big(\mathbf{max}(\boldsymbol{f},\boldsymbol{g}),\boldsymbol{h}\Big)\Big),$$

with $\boldsymbol{f},\boldsymbol{g},\boldsymbol{h}$ each evaluated at $(\boldsymbol{x},\boldsymbol{y},\boldsymbol{z})$. (The arguments of $\boldsymbol{f},\boldsymbol{g},\boldsymbol{h}$ are omitted as needed throughout this proof; however, these functions are always evaluated at $(\boldsymbol{x},\boldsymbol{y},\boldsymbol{z})$.) Define

the mappings

$$\begin{aligned}
\Psi &: \mathbf{X} \times \mathbf{Y} \times \mathbf{Z} \to \mathbb{R}^v : (\boldsymbol{x}, \boldsymbol{y}, \boldsymbol{z}) \mapsto \mathbf{min}(\boldsymbol{f}(\boldsymbol{x}, \boldsymbol{y}, \boldsymbol{z}), \boldsymbol{g}(\boldsymbol{x}, \boldsymbol{y}, \boldsymbol{z})), \\
\zeta &: \mathbf{X} \times \mathbf{Y} \times \mathbf{Z} \to \mathbb{R}^v : (\boldsymbol{x}, \boldsymbol{y}, \boldsymbol{z}) \mapsto \mathbf{max}(\boldsymbol{f}(\boldsymbol{x}, \boldsymbol{y}, \boldsymbol{z}), \boldsymbol{g}(\boldsymbol{x}, \boldsymbol{y}, \boldsymbol{z})), \\
\lambda &: \mathbf{X} \times \mathbf{Y} \times \mathbf{Z} \to \mathbb{R}^v : (\boldsymbol{x}, \boldsymbol{y}, \boldsymbol{z}) \mapsto \mathbf{min}(\zeta(\boldsymbol{x}, \boldsymbol{y}, \boldsymbol{z}), \boldsymbol{h}(\boldsymbol{x}, \boldsymbol{y}, \boldsymbol{z})), \\
\Gamma &: \mathbf{X} \times \mathbf{Y} \times \mathbf{Z} \to \mathbb{R}^{2v} : (\boldsymbol{x}, \boldsymbol{y}, \boldsymbol{z}) \mapsto (\Psi(\boldsymbol{x}, \boldsymbol{y}, \boldsymbol{z}), \lambda(\boldsymbol{x}, \boldsymbol{y}, \boldsymbol{z})).
\end{aligned}$$

Then, by the LD-derivative chain rule described in Proposition 3.9,

$$\begin{aligned}
[\mathbf{mid} \circ (\boldsymbol{f}, \boldsymbol{g}, \boldsymbol{h})]'(\boldsymbol{x}, \boldsymbol{y}, \boldsymbol{z}; (\mathbf{X}, \mathbf{Y}, \mathbf{Z})) &= [\mathbf{max} \circ (\Psi, \lambda)]'(\boldsymbol{x}, \boldsymbol{y}, \boldsymbol{z}; (\mathbf{X}, \mathbf{Y}, \mathbf{Z})), \\
&= \mathbf{max}'(\Gamma(\boldsymbol{x}, \boldsymbol{y}, \boldsymbol{z}), \Gamma'(\boldsymbol{x}, \boldsymbol{y}, \boldsymbol{z}; (\mathbf{X}, \mathbf{Y}, \mathbf{Z})).
\end{aligned} \tag{3.3}$$

We note that the LD-derivative mapping $\Gamma'(\boldsymbol{x}, \boldsymbol{y}, \boldsymbol{z}; (\mathbf{X}, \mathbf{Y}, \mathbf{Z}))$ can be found component-wise based on the first rule outlined in Proposition 3.9:

$$\begin{aligned}
\Gamma'(\boldsymbol{x}, \boldsymbol{y}, \boldsymbol{z}; (\mathbf{X}, \mathbf{Y}, \mathbf{Z})) &= \begin{bmatrix} \Psi'(\boldsymbol{x}, \boldsymbol{y}, \boldsymbol{z}; (\mathbf{X}, \mathbf{Y}, \mathbf{Z})) \\ \lambda'(\boldsymbol{x}, \boldsymbol{y}, \boldsymbol{z}; (\mathbf{X}, \mathbf{Y}, \mathbf{Z})) \end{bmatrix}, \\
&= \begin{bmatrix} [\mathbf{min} \circ (\boldsymbol{f}, \boldsymbol{g})]'(\boldsymbol{x}, \boldsymbol{y}, \boldsymbol{z}; (\mathbf{X}, \mathbf{Y}, \mathbf{Z})) \\ \lambda'(\boldsymbol{x}, \boldsymbol{y}, \boldsymbol{z}; (\mathbf{X}, \mathbf{Y}, \mathbf{Z})) \end{bmatrix}, \\
&= \begin{bmatrix} \mathbf{slmin}\left(\begin{bmatrix} \boldsymbol{f} & \mathbf{J}\boldsymbol{f} \cdot \begin{bmatrix} \boldsymbol{X} \\ \boldsymbol{Y} \\ \boldsymbol{Z} \end{bmatrix} \end{bmatrix}, \begin{bmatrix} \boldsymbol{g} & \mathbf{J}\boldsymbol{g} \cdot \begin{bmatrix} \boldsymbol{X} \\ \boldsymbol{Y} \\ \boldsymbol{Z} \end{bmatrix} \end{bmatrix} \right) \\ \lambda'(\boldsymbol{x}, \boldsymbol{y}, \boldsymbol{z}; (\mathbf{X}, \mathbf{Y}, \mathbf{Z})) \end{bmatrix}, \\
&= \begin{bmatrix} \mathbf{slmin}\left(\begin{bmatrix} \boldsymbol{f} & \mathbf{J}\boldsymbol{f} \cdot \mathbf{M} \end{bmatrix}, \begin{bmatrix} \boldsymbol{g} & \mathbf{J}\boldsymbol{g} \cdot \mathbf{M} \end{bmatrix} \right) \\ \lambda'(\boldsymbol{x}, \boldsymbol{y}, \boldsymbol{z}; (\mathbf{X}, \mathbf{Y}, \mathbf{Z})) \end{bmatrix}.
\end{aligned} \tag{3.4}$$

Now notice that using a similar process, we have

$$\begin{aligned}
\lambda'(\boldsymbol{x}, \boldsymbol{y}, \boldsymbol{z}; (\mathbf{X}, \mathbf{Y}, \mathbf{Z})) &= [\mathbf{min} \circ (\zeta, \boldsymbol{h})]'(\boldsymbol{x}, \boldsymbol{y}, \boldsymbol{z}; (\mathbf{X}, \mathbf{Y}, \mathbf{Z})), \\
&= \mathbf{min}'\left(\begin{bmatrix} \zeta(\boldsymbol{x}, \boldsymbol{y}, \boldsymbol{z}) \\ \boldsymbol{h}(\boldsymbol{x}, \boldsymbol{y}, \boldsymbol{z}) \end{bmatrix}; \begin{bmatrix} \zeta'(\boldsymbol{x}, \boldsymbol{y}, \boldsymbol{z}; (\mathbf{X}, \mathbf{Y}, \mathbf{Z})) \\ \boldsymbol{h}'(\boldsymbol{x}, \boldsymbol{y}, \boldsymbol{z}; (\mathbf{X}, \mathbf{Y}, \mathbf{Z})) \end{bmatrix} \right)
\end{aligned}$$

by a second application of the LD-derivative chain rule, where

$$\begin{aligned}\begin{bmatrix}\zeta'(\boldsymbol{x},\boldsymbol{y},\boldsymbol{z};(\mathbf{X},\mathbf{Y},\mathbf{Z}))\\ \boldsymbol{h}'(\boldsymbol{x},\boldsymbol{y},\boldsymbol{z};(\mathbf{X},\mathbf{Y},\mathbf{Z}))\end{bmatrix} &= \begin{bmatrix}[\mathbf{max}\circ(\boldsymbol{f},\boldsymbol{g})]'(\boldsymbol{x},\boldsymbol{y},\boldsymbol{z};(\mathbf{X},\mathbf{Y},\mathbf{Z}))\\ \mathbf{J}\boldsymbol{h}\cdot\begin{bmatrix}\boldsymbol{X}\\ \boldsymbol{Y}\\ \boldsymbol{Z}\end{bmatrix}\end{bmatrix},\\ &= \begin{bmatrix}\mathbf{slmax}\left(\begin{bmatrix}\boldsymbol{f} & \mathbf{J}\boldsymbol{f}\cdot\begin{bmatrix}\boldsymbol{X}\\ \boldsymbol{Y}\\ \boldsymbol{Z}\end{bmatrix}\end{bmatrix},\begin{bmatrix}\boldsymbol{g} & \mathbf{J}\boldsymbol{g}\cdot\begin{bmatrix}\boldsymbol{X}\\ \boldsymbol{Y}\\ \boldsymbol{Z}\end{bmatrix}\end{bmatrix}\right)\\ \mathbf{J}\boldsymbol{h}\cdot\begin{bmatrix}\boldsymbol{X}\\ \boldsymbol{Y}\\ \boldsymbol{Z}\end{bmatrix}\end{bmatrix},\\ &= \begin{bmatrix}\mathbf{slmax}\left(\begin{bmatrix}\boldsymbol{f} & \mathbf{J}\boldsymbol{f}\cdot\mathbf{M}\end{bmatrix},\begin{bmatrix}\boldsymbol{g} & \mathbf{J}\boldsymbol{g}\cdot\mathbf{M}\end{bmatrix}\right)\\ \mathbf{J}\boldsymbol{h}\cdot\mathbf{M}\end{bmatrix}\end{aligned}$$

after component-wise calculation. Thus,

$$\begin{aligned}&\lambda'(\boldsymbol{x},\boldsymbol{y},\boldsymbol{z};(\mathbf{X},\mathbf{Y},\mathbf{Z})) = [\mathbf{min}\circ(\zeta,\boldsymbol{h})]'(\boldsymbol{x},\boldsymbol{y},\boldsymbol{z};(\mathbf{X},\mathbf{Y},\mathbf{Z})),\\ &\quad= \mathbf{min}'\left(\begin{bmatrix}[\mathbf{max}\circ(\boldsymbol{f},\boldsymbol{g})](\boldsymbol{x},\boldsymbol{y},\boldsymbol{z})\\ \boldsymbol{h}(\boldsymbol{x},\boldsymbol{y},\boldsymbol{z})\end{bmatrix};\begin{bmatrix}\mathbf{slmax}\left(\begin{bmatrix}\boldsymbol{f} & \mathbf{J}\boldsymbol{f}\cdot\mathbf{M}\end{bmatrix},\begin{bmatrix}\boldsymbol{g} & \mathbf{J}\boldsymbol{g}\cdot\mathbf{M}\end{bmatrix}\right)\\ \mathbf{J}\boldsymbol{h}\cdot\mathbf{M}\end{bmatrix}\right),\\ &\quad= \mathbf{slmin}\left(\begin{bmatrix}[\mathbf{max}\circ(\boldsymbol{f},\boldsymbol{g})] & \mathbf{slmax}\left(\begin{bmatrix}\boldsymbol{f} & \mathbf{J}\boldsymbol{f}\cdot\mathbf{M}\end{bmatrix},\begin{bmatrix}\boldsymbol{g} & \mathbf{J}\boldsymbol{g}\cdot\mathbf{M}\end{bmatrix}\right)\end{bmatrix},\begin{bmatrix}\boldsymbol{h} & \mathbf{J}\boldsymbol{h}\cdot\mathbf{M}\end{bmatrix}\right),\\ &\quad= \mathbf{slmin}\left(\mathbf{lmax}\left(\begin{bmatrix}\boldsymbol{f} & \mathbf{J}\boldsymbol{f}\cdot\mathbf{M}\end{bmatrix},\begin{bmatrix}\boldsymbol{g} & \mathbf{J}\boldsymbol{g}\cdot\mathbf{M}\end{bmatrix}\right),\begin{bmatrix}\boldsymbol{h} & \mathbf{J}\boldsymbol{h}\cdot\mathbf{M}\end{bmatrix}\right).\end{aligned}$$

Now substitution of this result into Equation (3.4) gives

$$\Gamma'(\boldsymbol{x},\boldsymbol{y},\boldsymbol{z};(\mathbf{X},\mathbf{Y},\mathbf{Z})) = \begin{bmatrix}\mathbf{slmin}\left(\begin{bmatrix}\boldsymbol{f} & \mathbf{J}\boldsymbol{f}\cdot\mathbf{M}\end{bmatrix},\begin{bmatrix}\boldsymbol{g} & \mathbf{J}\boldsymbol{g}\cdot\mathbf{M}\end{bmatrix}\right)\\ \mathbf{slmin}\left(\mathbf{lmax}\left(\begin{bmatrix}\boldsymbol{f} & \mathbf{J}\boldsymbol{f}\cdot\mathbf{M}\end{bmatrix},\begin{bmatrix}\boldsymbol{g} & \mathbf{J}\boldsymbol{g}\cdot\mathbf{M}\end{bmatrix}\right),\begin{bmatrix}\boldsymbol{h} & \mathbf{J}\boldsymbol{h}\cdot\mathbf{M}\end{bmatrix}\right)\end{bmatrix},$$

and subsequent substitution to Equation (3.3) yields

$$[\mathbf{mid}\circ(\boldsymbol{f},\boldsymbol{g},\boldsymbol{h})]'(\boldsymbol{x},\boldsymbol{y},\boldsymbol{z};(\mathbf{X},\mathbf{Y},\mathbf{Z})) = \mathbf{max}'(\Gamma(\boldsymbol{x},\boldsymbol{y},\boldsymbol{z}),\Gamma'(\boldsymbol{x},\boldsymbol{y},\boldsymbol{z};(\mathbf{X},\mathbf{Y},\mathbf{Z})),$$

$$\begin{aligned}&= \mathbf{slmax}\left(\begin{bmatrix}[\mathbf{min}\circ(\boldsymbol{f},\boldsymbol{g})]\\ \mathbf{min}\circ([\mathbf{max}\circ(\boldsymbol{f},\boldsymbol{g})],\boldsymbol{h}])\end{bmatrix};\begin{bmatrix}\mathbf{slmin}\left(\begin{bmatrix}\boldsymbol{f} & \mathbf{J}\boldsymbol{f}\cdot\mathbf{M}\end{bmatrix},\begin{bmatrix}\boldsymbol{g} & \mathbf{J}\boldsymbol{g}\cdot\mathbf{M}\end{bmatrix}\right)\\ \mathbf{slmin}\left(\mathbf{lmax}\left(\begin{bmatrix}\boldsymbol{f} & \mathbf{J}\boldsymbol{f}\cdot\mathbf{M}\end{bmatrix},\begin{bmatrix}\boldsymbol{g} & \mathbf{J}\boldsymbol{g}\cdot\mathbf{M}\end{bmatrix}\right),\begin{bmatrix}\boldsymbol{h} & \mathbf{J}\boldsymbol{h}\cdot\mathbf{M}\end{bmatrix}\right)\end{bmatrix}\right),\\ &= \mathbf{slmax}\left(\left[\mathbf{lmin}\left(\begin{bmatrix}\boldsymbol{f} & \mathbf{J}\boldsymbol{f}\cdot\mathbf{M}\end{bmatrix},\begin{bmatrix}\boldsymbol{g} & \mathbf{J}\boldsymbol{g}\cdot\mathbf{M}\end{bmatrix}\right),\mathbf{lmin}\left(\mathbf{lmax}\left(\begin{bmatrix}\boldsymbol{f} & \mathbf{J}\boldsymbol{f}\cdot\mathbf{M}\end{bmatrix},\begin{bmatrix}\boldsymbol{g} & \mathbf{J}\boldsymbol{g}\cdot\mathbf{M}\end{bmatrix}\right),\begin{bmatrix}\boldsymbol{h} & \mathbf{J}\boldsymbol{h}\cdot\mathbf{M}\end{bmatrix}\right)\right]\right).\end{aligned}$$

Lastly, by Lemma 3.13 with matrices $\mathbf{A} = [\boldsymbol{f}(\boldsymbol{x},\boldsymbol{y},\boldsymbol{z}) \quad \mathbf{J}\boldsymbol{f}\cdot\mathbf{M}]$, $\mathbf{B} = [\boldsymbol{g}(\boldsymbol{x},\boldsymbol{y},\boldsymbol{z}) \quad \mathbf{J}\boldsymbol{g}\cdot\mathbf{M}]$ and $\mathbf{C} = [\boldsymbol{h}(\boldsymbol{x},\boldsymbol{y},\boldsymbol{z}) \quad \mathbf{J}\boldsymbol{h}\cdot\mathbf{M}]$,

$$\begin{aligned}
&[\mathbf{mid}\circ(\boldsymbol{f},\boldsymbol{g},\boldsymbol{h})]'(\boldsymbol{x},\boldsymbol{y},\boldsymbol{z};(\mathbf{X},\mathbf{Y},\mathbf{Z}))\\
&= \mathbf{slmid}\left(\left[\boldsymbol{f}(\boldsymbol{x},\boldsymbol{y},\boldsymbol{z}) \quad \mathbf{J}_{\boldsymbol{x}}\boldsymbol{f}\cdot\mathbf{X}+\mathbf{J}_{\boldsymbol{y}}\boldsymbol{f}\cdot\mathbf{Y}+\mathbf{J}_{\boldsymbol{z}}\boldsymbol{f}\cdot\mathbf{Z}\right],\right.\\
&\qquad\left[\boldsymbol{g}(\boldsymbol{x},\boldsymbol{y},\boldsymbol{z}) \quad \mathbf{J}_{\boldsymbol{x}}\boldsymbol{g}\cdot\mathbf{X}+\mathbf{J}_{\boldsymbol{y}}\boldsymbol{g}\cdot\mathbf{Y}+\mathbf{J}_{\boldsymbol{z}}\boldsymbol{g}\cdot\mathbf{Z}\right],\\
&\qquad\left.\left[\boldsymbol{h}(\boldsymbol{x},\boldsymbol{y},\boldsymbol{z}) \quad \mathbf{J}_{\boldsymbol{x}}\boldsymbol{h}\cdot\mathbf{X}+\mathbf{J}_{\boldsymbol{y}}\boldsymbol{h}\cdot\mathbf{Y}+\mathbf{J}_{\boldsymbol{z}}\boldsymbol{h}\cdot\mathbf{Z}\right]\right),
\end{aligned}$$

where the omitted arguments of Jacobian and partial Jacobian matrices are $(\boldsymbol{x},\boldsymbol{y},\boldsymbol{z})$. □

3.3 Generalized sensitivity analysis of nonsmooth ordinary differential equations

We now move to the applications of lexicographic theory in nonsmooth differential equations. A lexicographic approach to systems of ODEs whose right-hand-side functions are only L-smooth has yielded sensitivity theory [30] analogous to the classical case discussed in Section 2.2.

Recall the general form of a parametric IVP:

$$\begin{aligned}
\dot{\boldsymbol{x}}(t,\boldsymbol{p}) &= \boldsymbol{f}(t,\boldsymbol{p},\boldsymbol{x}(t,\boldsymbol{p})),\\
\boldsymbol{x}(t_0,\boldsymbol{p}) &= \boldsymbol{f}_0(\boldsymbol{p}),
\end{aligned} \tag{3.5}$$

where $\boldsymbol{x} = (x_1, x_2, \ldots, x_n)$ denotes the vector of state variables, $\boldsymbol{p} = (p_1, p_2, \ldots, p_q)$ denotes the vector of problem parameters, $\boldsymbol{f} : D_t \times D_p \times D_x \to \mathbb{R}^m$, and $\boldsymbol{f}_0 : D_p \to D_x$, where $D_t \subset \mathbb{R}$, $D_p \subset \mathbb{R}^q$, and $D_x \subset \mathbb{R}^n$ are open sets and $t_0 \in D_t$, $\boldsymbol{p}^* \in D_p$. Rather than the continuous differentiability of $\boldsymbol{f}$, $\boldsymbol{f}_0$ required in classical theory, we proceed with the following assumptions.

Assumption 3.15. Suppose that $\boldsymbol{f} : D_t \times D_p \times D_x \to \mathbb{R}^m$ and $\boldsymbol{f}_0 : D_p \to D_x$ are L-smooth on their respective domains.

The result of Theorem 2.2 (i.e., existence and uniqueness of a solution) extends to those IVPs whose right-hand side functions $\boldsymbol{f}$, $\boldsymbol{f}_0$ are only locally Lipschitz continuous (see, e.g., [25]), and thus includes the case where they are L-smooth on their respective domains. However, the C^1 dependence of solutions $\boldsymbol{x}(t, \boldsymbol{p})$ with respect to $\boldsymbol{p}$ is no longer guaranteed, inviting the application of lexicographic theory instead.

Theorem 3.16 (L-Smooth Dependence on Parameters)**.** *(Adapted from [30]). Suppose Assumption 3.15 holds. Then there exist $\epsilon, \delta > 0$ such that the initial value problem* (3.5) *has a unique solution $\boldsymbol{x}(t, \boldsymbol{p})$ on $[t_0, t_0 + \delta]$ for each fixed $\boldsymbol{p} \in N_\epsilon(\boldsymbol{p}^*)$, and $\boldsymbol{x}(t, \boldsymbol{p})$ is L-smooth with respect to $\boldsymbol{p}$ on $N_\epsilon(\boldsymbol{p}^*)$ for each fixed $t \in [t_0, t_0 + \delta]$.*

Roughly, the result of this theorem implies that solutions to L-smooth ODEs inherit the property of being L-smooth with respect to parameters, motivating the definition of the objects which form the foundation of this thesis.

Definition 3.17 (Lexicographic Sensitivity Functions)**.** The *lexicographic (forward-parametric) sensitivity functions* associated with a solution $\boldsymbol{x}(t, \boldsymbol{p})$ of the IVP (3.5) on T, if they exist, are

$$\mathbf{S}_{\boldsymbol{x}}(t) = \mathbf{J}_L[\boldsymbol{x}(t, \boldsymbol{p})](\boldsymbol{p}^*; \mathbf{M}) \in \mathbb{R}^{n \times q}, \tag{3.6}$$

where $\boldsymbol{p}^* \in \mathbb{R}^q$ denotes some chosen reference parameters and $\mathbf{M} \in \mathbb{R}^{n \times k}$ is full row rank.

As noted in Section 3.1, lexicographic derivatives characterize generalized first-order derivative information around a point of interest; therefore, we may use them in place of the classical sensitivity functions when nondifferentiability is present in the right-hand side of (3.5). In general, we may calculate the lexicographic sensitivity functions using corresponding LD-derivative objects.

Definition 3.18 (LD-Sensitivity Functions)**.** The *LD-sensitivity functions* associated with a solution $\boldsymbol{x}(t, \boldsymbol{p})$ of the IVP (3.5) on T, if they exist, are

$$\mathbf{X}(t) = [\boldsymbol{x}(t, \boldsymbol{p})]'(\boldsymbol{p}^*; \mathbf{M}) \in \mathbb{R}^{n \times k} \tag{3.7}$$

where $\boldsymbol{p}^* \in \mathbb{R}^q$ denotes some chosen reference parameters.

The LD-sensitivity functions are at least absolutely continuous when they exist [30].

Definition 3.19 (Absolute Continuity)**.** Given a connected set $X \subset \mathbb{R}$, a function $\boldsymbol{f} : X \to \mathbb{R}^m$ is called *absolutely continuous* on X if for every compact subinterval $\bar{X} \subset X$ and every $\epsilon > 0$ there exists some $\delta > 0$ such that for each finite sequence of pairwise disjoint subintervals $\{[a_i, b_i] : i = 1, \ldots, q, q \in \mathbb{N}\}$ of $\bar{X}$ satisfying $\sum_{i=1}^{q}(b_i - a_i) < \delta$ then $\sum_{i=1}^{q} |\boldsymbol{f}(b_i) - \boldsymbol{f}(a_i)| < \epsilon$.

Assumption 3.20. Let $t_f > t_0$ and suppose there exists a unique solution of the IVP (3.5) on $[t_0, t_f] \subset D_t$.

Theorem 3.21 (Existence and Calculation of the LD-Sensitivity Functions)**.** *(Adapted from [30].) Suppose that Assumptions 3.15 and 3.20 hold. Given any matrix $\boldsymbol{M} \in \mathbb{R}^{n\times k}$, the LD-sensitivity functions* (3.7) *exist, are absolutely continuous, and are the unique solution of the* LD-sensitivity system

$$\begin{aligned} \dot{\boldsymbol{X}}(t) &= [\boldsymbol{f}_t]'(\boldsymbol{p}^*, \boldsymbol{x}(t, \boldsymbol{p}^*); (\boldsymbol{M}, \boldsymbol{X}(t))), \\ \boldsymbol{X}(t_0) &= \boldsymbol{f}_0'(\boldsymbol{p}^*; \boldsymbol{M}). \end{aligned} \tag{3.8}$$

on the time horizon $[t_0, t_f]$ where $\boldsymbol{f}_t : (\boldsymbol{p}, \boldsymbol{x}) \mapsto \boldsymbol{f}(t, \boldsymbol{p}, \boldsymbol{x})$.

If **M** satisfies the stronger condition of being full row rank, then we may use Theorem 3.7 to generate an L-derivative object (for fixed t on the relevant horizon) instead.

Theorem 3.22 (Existence and Calculation of the Lexicographic Sensitivity Functions)**.** *(Adapted from [30].) Suppose Assumption 3.15 holds and suppose that $\boldsymbol{M} \in \mathbb{R}^{n\times k}$ is full row rank. Then, in addition to the conclusions of Theorem 3.16, the LD-sensitivity functions* (3.7) *and lexicographic sensitivity functions* (3.6) *exist; furthermore, for some fixed t on the time horizon $[t_0, t_f]$, the lexicographic sensitivity functions* (3.6) *may be calculated as*

$$\boldsymbol{S}_{\boldsymbol{x}}(t) = \boldsymbol{X}(t)\boldsymbol{M}^{-1} \in \mathbb{R}^{n\times q}.$$

We emphasize that lexicographic derivatives are Jacobian-like in nature and lie in or near the Clarke Jacobian when participating functions are at least L-smooth (recall Proposition 3.5); therefore, they characterize local first-order sensitivity information much in the way that classical sensitivity functions do. Furthermore, if we find that $\boldsymbol{f}$, $\boldsymbol{f}_0$ are in fact C^1 on their domains and the choice of $\mathbf{M} = \mathbf{I}_n$ is made, then the classical sensitivity functions are recovered since

$$\mathbf{J}_L[\boldsymbol{x}(t,\boldsymbol{p})](\boldsymbol{p}^*;\mathbf{I}) = \mathbf{X}(t)\mathbf{I}^{-1} = [\boldsymbol{x}(t,\boldsymbol{p})]'(\boldsymbol{p}^*;\mathbf{I}) = \mathbf{J}_{\boldsymbol{p}}\boldsymbol{x}(t,\boldsymbol{p}^*) = \frac{\partial \boldsymbol{x}}{\partial \boldsymbol{p}}(t,\boldsymbol{p}^*)$$

in that case by Equation 3.1.

Example 3.23. Consider the following nonsmooth IVP with parameters $\boldsymbol{p} = (p_1, p_2)$:

$$\begin{aligned} \dot{x}(t,\boldsymbol{p}) &= |x(t,\boldsymbol{p})| + p_1, \\ x(0,\boldsymbol{p}) &= p_2. \end{aligned} \tag{3.9}$$

Notice that this is the same system given in Example 2.8 with the exception that the term $x(t,\boldsymbol{p})$ appearing on the right-hand side is now composed with the absolute value function. Sample solutions to this system are given in Figure 3.2, while differences in the long term behavior of the system for different choices of $\boldsymbol{p}$ are depicted in Figure 3.3.

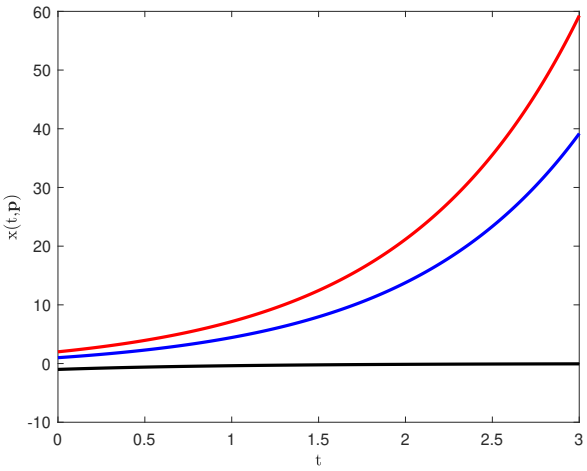

Figure 3.2: Solutions of the system (3.9) with differing choices of reference parameter $\boldsymbol{p}^*$. In black, $\boldsymbol{p}^* = (0,-1)$; in blue, $\boldsymbol{p}^* = (1,1)$; and in red, $\boldsymbol{p}^* = (1,2)$.

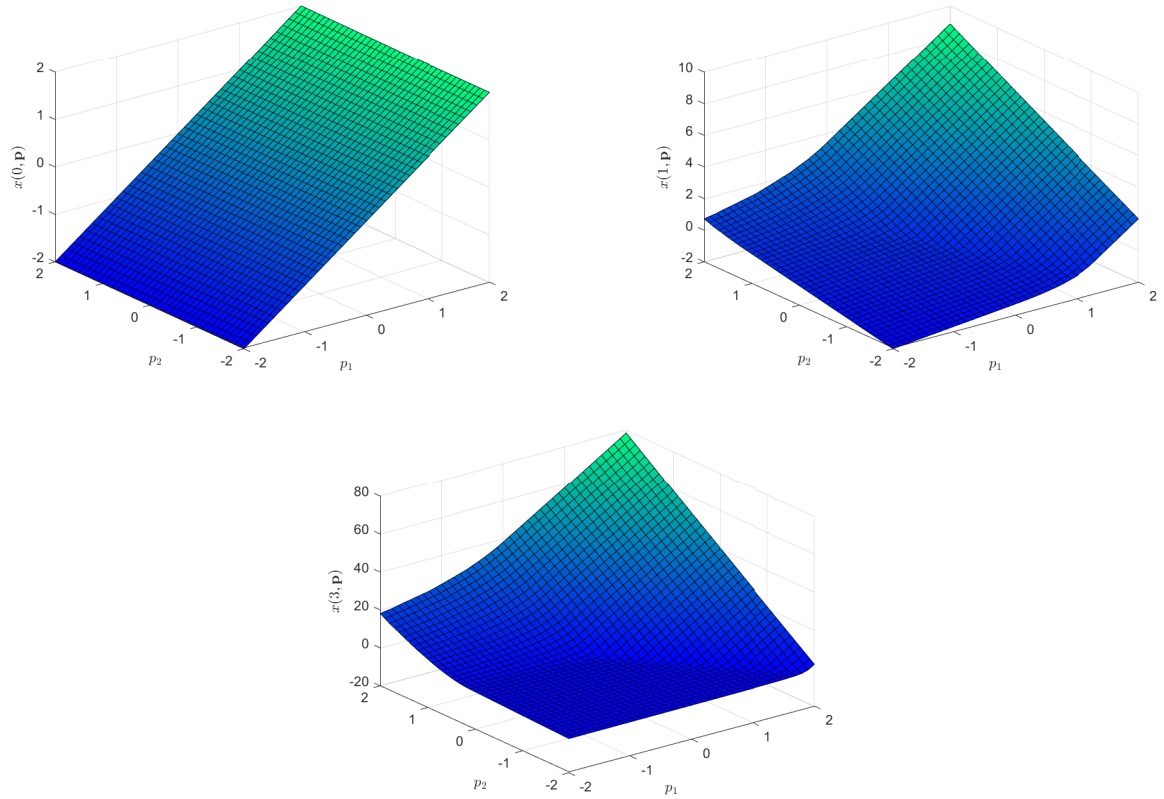

Figure 3.3: Varying behavior in solutions to (3.9) for different choices of $\boldsymbol{p}$ at different fixed times. At top-left, $t = 0$ and solutions take the form of the $x = p_2$ plane. At top-right, $t = 1$ and solutions begin to diverge, with a nonsmooth crease apparent near the origin. At bottom, by $t = 3$, solutions have diverged greatly and the crease is more prominent.

Given directions matrix $\mathbf{M} = [M_1 \; M_2 \; \cdots \; M_k] \in \mathbb{R}^{1\times k}$, the LD-derivative of the absolute value function is [8, 32]:

$$\text{abs}'(x;\mathbf{M}) = \text{fsign}(x, M_1, \ldots, M_k)\mathbf{M} \in \mathbb{R}^{1\times k}, \tag{3.10}$$

where the fsign function returns the sign of its first non-zero entry (or zero otherwise).

Given this rule, we can calculate the LD-sensitivity system (i.e., Equation (3.8)) corresponding to the L-smooth IVP (3.9) as

$$\begin{aligned}
\dot{X}^{p_1}(t) &= \text{fsign}\left(0, X^{p_1}(t), X^{p_2}(t)\right) X^{p_1}(t) + P_{1,1}, \quad X^{p_1}(0) = P_{2,1}, \\
\dot{X}^{p_2}(t) &= \text{fsign}\left(0, X^{p_1}(t), X^{p_2}(t)\right) X^{p_2}(t) + P_{1,2}, \quad X^{p_2}(0) = P_{2,2},
\end{aligned} \tag{3.11}$$

where the directions matrix is given by

$$\mathbf{M} = \begin{bmatrix} \mathbf{P}_1 \\ \mathbf{P}_2 \end{bmatrix} = \begin{bmatrix} P_{1,1} & P_{1,2} \\ P_{2,1} & P_{2,2} \end{bmatrix} \in \mathbb{R}^{2\times 2}.$$

If we choose $\mathbf{M} = \mathbf{I}_2$, then the system takes the form

$$\begin{aligned} \dot{X}^{p_1}(t) &= \text{fsign}\left(0, X^{p_1}(t), X^{p_2}(t)\right) X^{p_1}(t) + 1, & X^{p_1}(0) &= 0, \\ \dot{X}^{p_2}(t) &= \text{fsign}\left(0, X^{p_1}(t), X^{p_2}(t)\right) X^{p_2}(t), & X^{p_2}(0) &= 1. \end{aligned}$$

Note that by inspection the unique solution to this system may be expressed as

$$\mathbf{X}(t) = \begin{bmatrix} X^{p_1}(t) & X^{p_2}(t) \end{bmatrix} = \begin{bmatrix} e^t - 1 & e^t \end{bmatrix}.$$

Recall Theorem 3.22. After right-multiplication of the inverse of the directions matrix, the lexicographic sensitivity functions (i.e., Equation (3.6)) are furnished:

$$\mathbf{S}_x(t) = \mathbf{J}_L[x(t,\boldsymbol{p})](\boldsymbol{p}^*;\mathbf{I}_2) = \mathbf{X}(t)\mathbf{I}_2^{-1} = \begin{bmatrix} e^t - 1 & e^t \end{bmatrix},$$

which is computationally relevant sensitivity information. Indeed, this choice of directions matrix actually recovers the result from Example (2.8).

A unique trait of lexicographic sensitivity theory as opposed to classical theory, however, is that different lexicographic sensitivity functions (i.e., L-derivatives) may be furnished under different choices of directions matrix $\mathbf{M}$. Say, for example, that we instead chose $\mathbf{M} = \left[\begin{smallmatrix} 0 & -1 \\ -1 & 0 \end{smallmatrix}\right]$. In that case, Equation (3.11) simplifies to the system

$$\begin{aligned} \dot{X}^{p_1}(t) &= \text{fsign}\left(0, X^{p_1}(t), X^{p_2}(t)\right) X^{p_1}(t), & X^{p_1}(0) &= -1, \\ \dot{X}^{p_2}(t) &= \text{fsign}\left(0, X^{p_1}(t), X^{p_2}(t)\right) X^{p_2}(t) - 1, & X^{p_2}(0) &= 0, \end{aligned}$$

which admits the unique solution $\mathbf{X}(t) = \begin{bmatrix} X^{p_1}(t) & X^{p_1}(t) \end{bmatrix} = \begin{bmatrix} -e^{-t} & e^{-t} - 1 \end{bmatrix}$. As before, we may furnish the corresponding lexicographic sensitivity functions by right-multiplication of $\mathbf{M}^{-1}$ (which, in this case, is identical to $\mathbf{M}$):

$$\mathbf{S}_x(t) = \mathbf{J}_L[x(t,\cdot)]\left(\boldsymbol{p}^*; \begin{bmatrix} 0 & -1 \\ -1 & 0 \end{bmatrix}\right) = \mathbf{X}(t) \begin{bmatrix} 0 & -1 \\ -1 & 0 \end{bmatrix}^{-1} = \begin{bmatrix} -e^{-t} + 1 & e^{-t} \end{bmatrix}.$$

Both classical and lexicographic sensitivity functions may also be normalized in order to more easily compare the predicted effects of different parameters; examples and applications of such normalization are discussed in Chapters 4 and 5.

CHAPTER 4
QUANTIFYING PARAMETRIC SENSITIVITIES OF A NONSMOOTH MODEL OF GLUCOSE-INSULIN INTERPLAY

The contents, figures, and tables appearing in this chapter are based on [1]. Within this chapter, we demonstrate the utility of the lexicographic sensitivity functions explored in Section 3.3 on a commonly-referenced nonsmooth model describing the dynamic interaction between glucose and insulin in the body.

4.1 Model background

Glucose is a type of carbohydrate, and is in fact the most abundant monosaccharide (i.e., "simple sugar") found in nature [20]. The human body uses glucose as its primary source of energy production [15], with a non-trivial baseline concentration being circulated through the bloodstream at all times (i.e., "blood sugar") and reserves of the saccharide being stored in muscle and adipose (fat) cells throughout the body. The ability of the body to maintain its healthy baseline concentration of glucose, or return to such a concentration after a sudden influx, is referred to as glucose homeostasis.

In the ideal case, the body employs two key hormones in the quest of maintaining homeostasis: glucagon, which is produced and released by pancreatic alpha (α-)cells to stimulate glucose release from cell reserves, and insulin, which is produced and released by pancreatic beta (β-)cells to stimulate glucose uptake from the bloodstream into cell reserves. Over time, as blood-glucose concentration varies naturally due to use, decay, and influx from food digestion, these two hormones cooperate to minimize deviation from the baseline concentration.

The failure of the body to maintain homeostasis can have serious consequences. If glucose concentration in the bloodstream drops too low (hypoglycemia), subjects may experience serious symptoms such as fainting, vomiting, slurred speech, confusion, or heart

palpitations; in extreme cases, the brain is effectively starved of energy, causing brain death [6]. If instead blood glucose remains too high (hyperglycemia), subjects may experience symptoms such as blurred vision, fatigue, and excessive thirst, though more serious complications can occur if levels remain elevated long-term [5]. As a result of these potential issues, homeostasis is an essential physiological process. Moving forward, we primarily concern ourselves with the body's ability to return to homeostasis after a glucose influx (e.g., a meal), and as a result turn our attention to glucose-insulin kinetics in particular.

There are two common bodily failures which cause an inadequate insulin response to an influx of glucose, referred to as type 1 and type 2 diabetes mellitus ("diabetes"). Type 1 diabetes is an autoimmune disease typically identified in early life which results in the destruction of the pancreatic β-cells; consequently, the body is unable to secrete its own insulin. The exact cause of the disease is unknown [3]. Type 2 diabetes often manifests later in life and the risk factors associated with it are better understood; essentially, the body is unable to absorb a sufficient amount of glucose from the bloodstream (often due to a developed insensitivity to insulin or insufficient insulin production). Both types are presently incurable, though well-timed insulin injections can induce homeostasis in the short-term and alleviate symptoms [3].

The Intravenous Glucose Tolerance Test (IVGTT) was first used in 1941 as a standardized method of measuring glucose and insulin interactions in the body [34]. Test subjects fast for one night, and then are injected with a bolus of glucose whose size is proportional to the subjects' weight. Intravenous blood samples are taken periodically over a predetermined time horizon (most generally, 1-3 hours; see, e.g., [11, 19, 49]) so glucose and insulin concentrations in the subjects' bloodstream may be measured. Due to its relative simplicity, the test remains a feasible option in the modern day, with advantages such as decreased variance in results over similar tests such as the Oral Glucose Tolerance Test (where oral glucose intake invites error from gastrointestinal factors which may vary

subject-to-subject). Furthermore, a subject's results may be compared to others' at the population level to predict or detect patterns associated with diabetes.

The "minimal model" of the IVGTT was developed out of a desire to replicate the typical results of an IVGTT test subject with as few parameters as possible. The model was first published in 1979 by Bergman et al. [11], and was shown to be the most accurate of several variations studied. One year later, the model was improved and published under the same name in [49]. While the model is minimalistic in nature (as the name would suggest), it has been shown to yield a reasonable approximation of the biology at hand and has been studied extensively [48].

In its original formulation, meant to model a healthy (non-diabetic) individual, nonsmoothness arises from a desire to model the natural pancreatic process: below a threshold blood-glucose concentration, pancreatic $\beta-$cells remain inactive, but they suddenly begin secreting insulin once the biochemical threshold is crossed. A max function is used to model this switch in behavior, and points of nondifferentiability are introduced as a result. A slight variation on the minimal model employed by many other authors is also studied here to give insight into the case where the subject is afflicted with type 1 diabetes [9, 14, 22]. In the case of a healthy individual, glucose is introduced to the bloodstream from the intestine at a negligible rate due to the required fast; if the subject is instead diabetic, the rate of this exogenous introduction of glucose becomes non-negligible. The model variation studied here incorporates an additional exponential term to describe this difference. Furthermore, the failures in the insulin subsystem of type 1 diabetics mean that pancreatic insulin secretion is practically nonexistent in this case [14]. Therefore, a model input is considered which describes insulin secretion from an external (wearable) device. Two different profiles are explored in detail here: one following a nonsmooth sigmoidal pattern with abrupt on and off features, and another which describes secretion at a progressively (exponentially) decreasing rate.

We will proceed by introducing the model itself and describing its physical interpretation. Since the presence of nonsmoothness in this model invalidates the classical approach, we will then turn to the lexicographic theory outlined in Section 3.3 in order to perform a sensitivity analysis of the system and describe its qualitative dependence on parameters.

4.2 Model formulation for healthy subjects

The minimal model itself is an ODE system containing ten problem parameters. The state variables described by the model are $G(t)$, the glucose concentration in a subject's bloodstream in units (mg/dL), $I(t)$, the insulin concentration in a subject's bloodstream in (μU/mL), and $X(t)$, which describes the net effect of insulin on glucose disappearance with units (1/min). These variables are related as follows [11]:

$$\begin{aligned} \dot{G} &= -p_2(G - p_9) - GX, & G(0) &= p_1, \\ \dot{X} &= -p_3X + p_4(I - p_{10}), & X(0) &= 0, \\ \dot{I} &= u - p_7(I - p_{10}), & I(0) &= p_8 + p_{10}, \end{aligned} \tag{4.1}$$

where the arguments of the independent variable t are suppressed for readability and the present right-hand side functions are notably PC^1 (and hence L-smooth). The physical interpretation and reference value p_i^* of each model parameter is given in Table 4.1, sourced from [1]. It should be noted that reference values for each parameter can vary widely from subject to subject; the values selected for our simulations were originally meant to model an "average" person and were sourced from [4, 19]. These choices were also previously shown to give reasonable results in a study done by Munir [37].

Parameters			
p_i	*Units*	*Description* [37]	p_i^* [4, 19]
p_1	mg/dL	"Theoretical glucose concentration in plasma at time $t = 0$;" i.e., post-injection glucose concentration	291.2
p_2	min^{-1}	"Rate constant of insulin-independent glucose uptake in muscles and adipose tissue"	0.0317
p_3	min^{-1}	"Rate constant for decrease in tissue glucose uptake ability"	0.0123
p_4	$\text{min}^{-2}(\mu\text{U/mL})^{-1}$	"Rate constant for the insulin-dependent increase in glucose uptake ability in tissue per unit of insulin concentration above p_{10}"	4.92×10^{-6}
p_5	$\left(\frac{\mu\text{U}}{\text{mL}*\text{min}^2}\right)\frac{1}{(\text{mg/dL})}$	"Rate constant for insulin secretion by the pancreatic β-cells after the glucose injection and with glucose concentration above threshold value p_6"	0.0039
p_6	mg/dL	"Threshold value of glucose in plasma above which the pancreatic β-cells secrete insulin"	79.0353
p_7	min^{-1}	"First order decay rate for insulin in plasma"	0.2659
p_8	μU/mL	"$p_8 + p_{10}$ is the theoretical insulin concentration in plasma at time $t = 0$"	357.8
p_9	mg/dL	"Baseline pre-injection level of glucose"	60
p_{10}	μU/mL	"Baseline pre-injection level of insulin"	7

Table 4.1: Parameters in (4.1) are labeled and described above. Note that p_i^* represents a reference parameter [1].

While X plays an important internal role in modeling the interactivity of glucose and insulin, we will proceed in our analysis with most emphasis placed on the state variables G and I, which possess a more obvious physical interpretation in general. Indeed, even the individual terms present in the equations for $\dot{G}$, $\dot{I}$ are easily interpreted in a biological manner: for example, since p_9 represents the basal (pre-injection) glucose concentration, $(G - p_9)$ represents the amount of excess glucose in a subject's bloodstream at time t. Since p_2 describes the constant rate at which glucose is removed from the bloodstream from insulin-independent means, we may then conclude that the term $-p_2(G - p_9)$ represents the rate at which excess glucose is removed from the bloodstream by means outside of insulin itself. The term GX, on the other hand, represents the rate at which glucose is removed from the bloodstream as a direct result of insulin interaction.

On the right-hand side of the equation for $\dot{I}$, we notice similarly that the term $-p_7(I - p_{10})$ represents the rate at which excess insulin decays (or is removed) from the bloodstream. The term u, which also appears, is a model input representing the rate at which insulin is introduced to the bloodstream. In the case of a healthy individual, insulin is produced and secreted by the pancreas in response to elevated glucose levels; to model this scenario, Bergman et al. [11] originally proposed

$$u = u_1 = p_5 t \max(0, G - p_6). \tag{4.2}$$

The max function appears here in order to model the switching behavior exhibited by insulin-producing pancreatic beta cells. When blood-glucose concentration in the body remains below the threshold value p_6, we find that $\max(0, G - p_6) = 0$ and the pancreas is idle; once this biochemical threshold is reached, the max function switches output to model the pancreas beginning to release insulin.

Simulations of the state variables G and I using reference parameters $\boldsymbol{p}^* \in \mathbb{R}^{10}$ (from Table 4.1) are given in Figure 4.1. Note that glucose and insulin concentration levels do indeed stabilize at their basal values (i.e., p_9 and p_{10}, respectively). Furthermore, the insulin concentration simulated here mirrors the real-life behavior of the pancreas, which

occurs in two phases. The first phase is characterized by a large initial secretion, seen in the spike at $t = 0$ min; the second phase is smaller in scale and can be seen as the brief plateau which follows. However, despite these features of the insulin subsystem, we also note that glucose concentration tends back to its basal value in a seemingly smooth, controlled manner — indicative that the body's steady return to glucose homeostasis is successful in this case. Finally, we note that the point where G intersects the value p_6^* represents the time at which the max function in (4.2) switches output (and hence causes a point of nondifferentiability). With our choice of $\boldsymbol{p}^*$, this switch occurs at roughly $t = 55.2$ min.

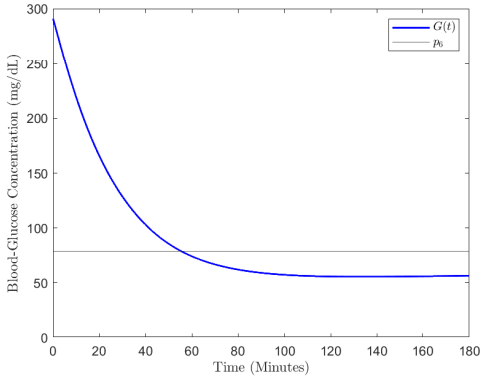

(a) The intersection of $G(t)$ and p_6 occurs at $t = 55.2$ min and indicates the time at which the max function switches outputs.

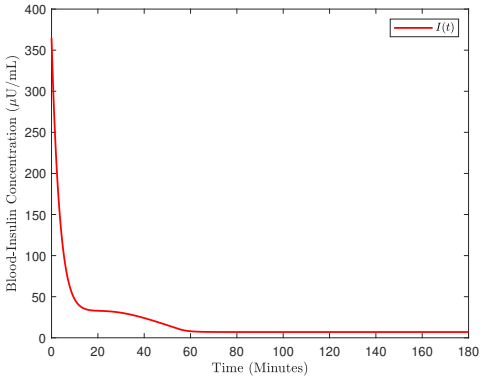

(b) Numerical simulation of $I(t)$.

Figure 4.1: Glucose and insulin concentrations attained over the course of three hours, respectively, using $u = u_1$ (Equation (4.2)) and $\boldsymbol{p} = \boldsymbol{p}^*$ [1].

We again emphasize the main goal of this section: to characterize the sensitivity of these biologically-based state variables to their parameters. The presence of the nonsmoothness discussed here, however, invalidates any classical attempt at characterizing the sensitivity of the system to its parameters. Assuming a solution to the IVP in Equation (4.1) exists over a time horizon of three hours, we proceed by deriving the nonsmooth sensitivity system (3.8) for a generic model input u.

Theorem 4.1 (Lexicographic Sensitivity System of the Minimal Model)**.** *Given some L-smooth model input u and reference parameter $\boldsymbol{p}^*$, assume the corresponding reference*

solution (G, X, I) *exists on the time horizon* $[t_0, t_f] = [0, 180]$. *Suppose* $\boldsymbol{M} \in \mathbb{R}^{10\times 10}$ *is a full row rank directions matrix. Then the lexicographic (forward parametric) sensitivity functions are given by*

$$\begin{bmatrix} \boldsymbol{S}_G(t) \\ \boldsymbol{S}_X(t) \\ \boldsymbol{S}_I(t) \end{bmatrix} = \begin{bmatrix} \boldsymbol{X}_G(t)\boldsymbol{M}^{-1} \\ \boldsymbol{X}_X(t)\boldsymbol{M}^{-1} \\ \boldsymbol{X}_I(t)\boldsymbol{M}^{-1} \end{bmatrix} = \begin{bmatrix} [G(t;\cdot)]'(\boldsymbol{p}^*;\boldsymbol{M})\boldsymbol{M}^{-1} \\ [X(t;\cdot)]'(\boldsymbol{p}^*;\boldsymbol{M})\boldsymbol{M}^{-1} \\ [I(t;\cdot)]'(\boldsymbol{p}^*;\boldsymbol{M})\boldsymbol{M}^{-1} \end{bmatrix}, \tag{4.3}$$

where, letting $\boldsymbol{M}_{(i)}$ *represent the* i^{th} *row of* $\boldsymbol{M}$, *the LD-derivatives* $(\boldsymbol{X}_G, \boldsymbol{X}_X, \boldsymbol{X}_I)$ *are the unique solution of the LD-sensitivity system*

$$\begin{aligned} \dot{\boldsymbol{X}}_G(t) &= -(G(t) - p_9^*)\boldsymbol{M}_{(2)} + p_2^*\boldsymbol{M}_{(9)} - (p_2^* + X(t))\boldsymbol{X}_G(t) - G(t)\boldsymbol{X}_X(t), \\ \dot{\boldsymbol{X}}_X(t) &= -X(t)\boldsymbol{M}_{(3)} + (I(t) - p_{10}^*)\boldsymbol{M}_{(4)} - p_4^*\boldsymbol{M}_{(10)} - p_3^*\boldsymbol{X}_X(t) + p_4^*\boldsymbol{X}_I(t), \\ \dot{\boldsymbol{X}}_I(t) &= [u(t;\cdot)]'(\boldsymbol{p}^*;\boldsymbol{M}) - (I(t) - p_{10}^*)\boldsymbol{M}_{(7)} + p_7^*\boldsymbol{M}_{(10)} - p_7^*\boldsymbol{X}_I(t) \end{aligned} \tag{4.4}$$

on the time horizon $[t_0, t_f] = [0, 180]$ *with initial conditions*

$$\begin{bmatrix} \boldsymbol{X}_G(0) \\ \boldsymbol{X}_X(0) \\ \boldsymbol{X}_I(0) \end{bmatrix} = \begin{bmatrix} \boldsymbol{M}_{(1)} \\ \boldsymbol{0} \\ \boldsymbol{M}_{(8)} + \boldsymbol{M}_{(10)} \end{bmatrix}. \tag{4.5}$$

Furthermore, if $u = u_1 = p_5 tmax(0, G - p_6)$, *then*

$$[u_1(t;\cdot)]'(\boldsymbol{p}^*;\boldsymbol{M}) = tmax(0, G(t) - p_6^*)\boldsymbol{M}_{(5)} + p_5^* t\boldsymbol{slmax}\left(\boldsymbol{0}_{1\times 11}, \begin{bmatrix} (G(t) - p_6^*) & \boldsymbol{X_G}(t) - \boldsymbol{M}_{(6)} \end{bmatrix}\right).$$

Proof. Recall that the right-hand side function of (4.1) is given by

$$\boldsymbol{f}(t, \boldsymbol{p}, G, X, I) = \begin{bmatrix} f_1(t, \boldsymbol{p}, G, X, I) \\ f_2(t, \boldsymbol{p}, G, X, I) \\ f_3(t, \boldsymbol{p}, G, X, I) \end{bmatrix} = \begin{bmatrix} -p_2(G - p_9) - GX \\ -p_3 X + p_4(I - p_{10}) \\ u - p_7(I - p_{10}) \end{bmatrix}. \tag{4.6}$$

Given any full row rank directions matrix $\mathbf{M} \in \mathbb{R}^{10\times 10}$, we aim to find the LD-derivative of the right-hand side function $\boldsymbol{f}$ from (4.6) to apply Theorem 3.21, where the LD-sensitivity

system (3.8) is given by

$$\begin{bmatrix} \dot{\mathbf{X}}_G(t) \\ \dot{\mathbf{X}}_X(t) \\ \dot{\mathbf{X}}_I(t) \end{bmatrix} = [\boldsymbol{f}_t]' \left(\begin{bmatrix} \boldsymbol{p}^* \\ G(t) \\ X(t) \\ I(t) \end{bmatrix}; \begin{bmatrix} \mathbf{M} \\ \mathbf{X}_G(t) \\ \mathbf{X}_X(t) \\ \mathbf{X}_I(t) \end{bmatrix} \right) \tag{4.7}$$

where $\boldsymbol{f}_t : (\boldsymbol{p}, G, X, I) \mapsto \boldsymbol{f}(t, \boldsymbol{p}, G, X, I)$.

The LD-derivative in (4.7) may be calculated component-wise by Proposition 3.9. Since the first two components f_1 and f_2 are smooth on their domains, Equation (3.1) implies that for any fixed t we have

$$\begin{aligned} &[f_{1_t}]'(\boldsymbol{p}^*, G(t), X(t), I(t); (\mathbf{M}, \mathbf{X}_G(t), \mathbf{X}_X(t), \mathbf{X}_I(t))) \\ &= \frac{\partial f_1}{\partial \boldsymbol{p}}\mathbf{M} + \frac{\partial f_1}{\partial G}\mathbf{X}_G(t) + \frac{\partial f_1}{\partial X}\mathbf{X}_X(t) + \frac{\partial f_1}{\partial I}\mathbf{X}_I(t), \\ &= -(G(t) - p_9^*)\mathbf{M}_{(2)} + p_2^*\mathbf{M}_{(9)} - (p_2^* + X(t))\mathbf{X}_G(t) - G(t)\mathbf{X}_X(t), \end{aligned}$$

where the partial derivatives are evaluated at reference solutions (G, X, I), and similarly,

$$\begin{aligned} &[f_{2_t}]'(\boldsymbol{p}^*, G(t), X(t), I(t); (\mathbf{M}, \mathbf{X}_G(t), \mathbf{X}_X(t), \mathbf{X}_I(t))) \\ &= \frac{\partial f_2}{\partial \boldsymbol{p}}\mathbf{M} + \frac{\partial f_2}{\partial G}\mathbf{X}_G(t) + \frac{\partial f_2}{\partial X}\mathbf{X}_X(t) + \frac{\partial f_2}{\partial I}\mathbf{X}_I(t), \\ &= -X(t)\mathbf{M}_{(3)} + (I(t) - p_{10}^*)\mathbf{M}_{(4)} - p_4^*\mathbf{M}_{(10)} - p_3^*\mathbf{X}_X(t) + p_4^*\mathbf{X}_I(t). \end{aligned}$$

Lastly, we find that

$$\begin{aligned} &[f_{3_t}]'(\boldsymbol{p}^*, G(t), X(t), I(t); (\mathbf{M}, \mathbf{X}_G(t), \mathbf{X}_X(t), \mathbf{X}_I(t))) \\ &= [u(t;\cdot)]'(\boldsymbol{p}^*; \mathbf{M}) - (I(t) - p_{10}^*)\mathbf{M}_{(7)} + p_7^*\mathbf{M}_{(10)} - p_7^*\mathbf{X}_I(t). \end{aligned}$$

Condensing our results so far, we have that the LD-sensitivity system (4.7) is given by the following system of ODEs:

$$\begin{aligned} \dot{\mathbf{X}}_G(t) &= -(G(t) - p_9^*)\mathbf{M}_{(2)} + p_2^*\mathbf{M}_{(9)} - (p_2^* + X(t))\mathbf{X}_G(t) - G(t)\mathbf{X}_X(t), \\ \dot{\mathbf{X}}_X(t) &= -X(t)\mathbf{M}_{(3)} + (I(t) - p_{10}^*)\mathbf{M}_{(4)} - p_4^*\mathbf{M}_{(10)} - p_3^*\mathbf{X}_X(t) + p_4^*\mathbf{X}_I(t), \\ \dot{\mathbf{X}}_I(t) &= [u(t;\cdot)]'(\boldsymbol{p}^*; \mathbf{M}) - (I(t) - p_{10}^*)\mathbf{M}_{(7)} + p_7^*\mathbf{M}_{(10)} - p_7^*\mathbf{X}_I(t). \end{aligned} \tag{4.8}$$

Furthermore, since $\mathbf{f}_0 : \boldsymbol{p} \mapsto (p_1, 0, p_8 + p_{10})$ is itself a C^1 function, the initial conditions for this sensitivity system are given by

$$\begin{bmatrix} \mathbf{X}_G(0) \\ \mathbf{X}_X(0) \\ \mathbf{X}_I(0) \end{bmatrix} = [\boldsymbol{f}_0]'(\boldsymbol{p}^*; \mathbf{M}) = \mathbf{J}\boldsymbol{f}_0(\boldsymbol{p}^*)\mathbf{M} = \begin{bmatrix} \mathbf{M}_{(1)} \\ \mathbf{0} \\ \mathbf{M}_{(8)} + \mathbf{M}_{(10)} \end{bmatrix}. \tag{4.9}$$

The form of the lexicographic sensitivity functions (4.3) follows directly from an application of Theorem 3.22 to the solutions of (4.8) with initial conditions (4.9).

Separately, our choice of $u = u_1 = p_5 t \max(0, G - p_6)$ (i.e., Equation (4.2), motivated by a healthy individual's pancreatic response) is PC^1 and hence L-smooth, allowing the use of LD-derivative calculus rules from Proposition 3.9. Let $u_1 = \alpha_t \rho$, where in particular

$$\rho : \mathbb{R}^{10} \times \mathbb{R}^3 \to \mathbb{R} : (\boldsymbol{p}, G, X, I) \mapsto \max(0, G - p_6),$$
$$\alpha_t : \mathbb{R}^{10} \times \mathbb{R}^3 \to \mathbb{R} : (\boldsymbol{p}, G, X, I) \mapsto p_5 t.$$

Then,

$$\rho'(\boldsymbol{p}, G, X, I; (\mathbf{M}, \mathbf{X}_G, \mathbf{X}_X, \mathbf{X}_I)) = \mathbf{slmax}\left(\begin{bmatrix} 0 & \mathbf{0}_{1\times 10} \end{bmatrix}, \begin{bmatrix} (G - p_6) & \mathbf{X_G} - \mathbf{M}_{(6)} \end{bmatrix}\right),$$
$$= \begin{cases} \mathbf{0}_{1\times 10}, & \text{if } G > p_6 \text{ or } G = p_6, \mathbf{X}_G \succeq \mathbf{M}_{(6)}, \\ \mathbf{X_G} - \mathbf{M}_{(6)}, & \text{otherwise,} \end{cases}$$

where we recall that the relational operator $\succeq$ is evaluated using lexicographic ordering. Separately,

$$\alpha_t'(\boldsymbol{p}, G, X, I; (\mathbf{M}, \mathbf{X}_G, \mathbf{X}_X, \mathbf{X}_I)) = \mathbf{J}\alpha_t(\boldsymbol{p}, (G, X, I)) \begin{bmatrix} \mathbf{M} \\ \mathbf{X}_G \\ \mathbf{X}_X \\ \mathbf{X}_I \end{bmatrix} = t\mathbf{M}_{(5)}.$$

Putting these pieces together via the lexicographic product rule, we find that

$$[u_1(t;\cdot)]'(\boldsymbol{p}^*; \mathbf{M}) = t\max(0, G(t) - p_6^*)\mathbf{M}_{(5)} + p_5^* t \mathbf{slmax}\left(\mathbf{0}_{1\times 11}, \begin{bmatrix} (G(t) - p_6^*) & \mathbf{X}_G(t) - \mathbf{M}_{(6)} \end{bmatrix}\right),$$

as we required. □

Thanks to the library of common LD-derivative rules outlined in Chapter 3 and the tractability of lexicographic sensitivity theory in general, we find that the ODE system in Theorem 4.1 can be solved by standard numerical methods. Here, in order to simultaneously solve the LD-sensitivity system (4.4), initial conditions (4.5), and minimal model itself (4.1) with reference parameter $\boldsymbol{p}^*$ as required, equations were implemented in the ode45 solver of MATLAB on the time horizon $[t_0, t_f] = [0, 180]$. The ode45 solver is a common, versatile solver built around the fourth-order Runge-Kutta method; here, apart from defining an explicit function for the shifted lexicographic maximum (**slmax**), no special treatment is necessary to find solutions. We emphasize that this process furnishes the LD-sensitivity functions $(\mathbf{X}_G, \mathbf{X}_X, \mathbf{X}_I)$, and subsequent right-multiplication by $\mathbf{M}^{-1}$ for each fixed time t on the time horizon yields the lexicographic sensitivity functions $(\mathbf{S}_G, \mathbf{S}_X, \mathbf{S}_I)$ found in Equation (4.3).

Initially, we selected $\mathbf{M} = \mathbf{I}_{10}$ as the directions matrix; however, since local sensitivities in the L-smooth case are characterized by L-derivatives, we recall that different choices for the directions matrix $\mathbf{M}$ may ultimately yield different elements of the L-subdifferential. To begin exploring this possibility, we also simulated results with the matrices furnished by nine successive circular right-shifts of the identity matrix, which was easily implemented due to the freedom of choice for full row rank $\mathbf{M}$ granted by Theorem 4.1. By virtue of being built around the concept of lexicographic ordering, lexicographic differentiation gives inherent preference to the first column of $\mathbf{M}$, and only considers subsequent columns in the case of ties. Therefore, the ten choices of $\mathbf{M}$ outlined above represent granting lexicographic "favor" to each unit coordinate direction in parameter space. Beyond these choices, we also performed the simulation with 1,000 different randomized (full row rank) directions matrices. In each and every case, however, simulation results were identical to those furnished by the choice of $\mathbf{M} = \mathbf{I}_{10}$ within a small degree of numerical error.

Since the reference values of the parameters $\boldsymbol{p}^*$ differ from each other largely (by up to five orders of magnitude), we provide the *relative* sensitivity functions here, which scale the

lexicographic sensitivity functions by both the reference solution and parameter for the purpose of more direct comparison: i.e.,

$$\begin{aligned}\widehat{\mathbf{S}}_G(t) &= \mathbf{S}_G(t) \odot \frac{(\boldsymbol{p}^*)^{\mathrm{T}}}{G(t)};\\ \widehat{\mathbf{S}}_I(t) &= \mathbf{S}_I(t) \odot \frac{(\boldsymbol{p}^*)^{\mathrm{T}}}{I(t)},\end{aligned} \tag{4.10}$$

where $\odot$ denotes the Hadamard (element-wise) product of the two vectors. The relative sensitivity functions $\widehat{\mathbf{S}}_G$ and $\widehat{\mathbf{S}}_I$ are given in Figures 4.2a and 4.2b, respectively. A vertical line appears at $t = 55.2$ min in each figure to represent the time at which the max function within (4.2) changes output.

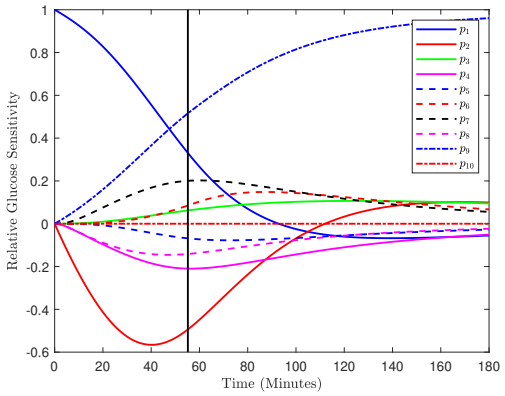

(a) Relative sensitivities of glucose concentration in the bloodstream with $\mathbf{M} = \mathbf{I}$.

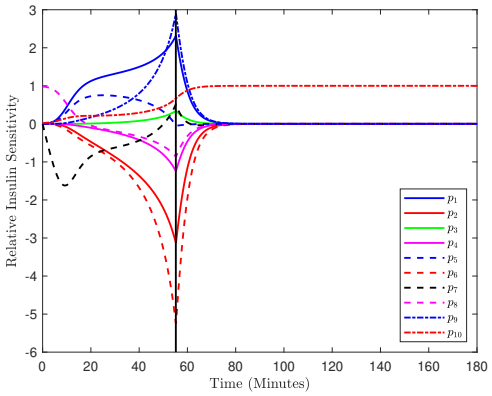

(b) Relative sensitivities of insulin concentration in the bloodstream with $\mathbf{M} = \mathbf{I}$.

Figure 4.2: Numerical solutions of the lexicographic sensitivity system (4.3) scaled according to (4.10) [1].

The numerical sensitivity solutions depicted in Figure 4.2 provide several insights to the model which we highlight here, and we begin by examining the sensitivities of state variable G. Parameter p_1 represents the (higher-than-basal) blood-glucose concentration of a subject who has just received the initial injection; therefore, it would make sense that this parameter is most influential to blood-glucose concentration G as a whole at the beginning of the time horizon, with decreasing importance as time goes on and glucose is removed from the bloodstream. Indeed, Figure 4.2a supports this idea. Similarly, recall that parameter p_2 represents the constant rate at which glucose is absorbed due to

insulin-independent means; G predictably becomes highly sensitive to this parameter, but its influence decreases as glucose approaches its basal concentration once more starting at approximately $t = 40$ min (see Figure 4.1a). Furthermore, the sensitivity of G to this parameter is negative, implying that an increase in the reference value p_2^* would have the predicted effect of decreasing the reference solution G across the time horizon; this also makes intuitive sense, as an increase in glucose uptake would result in less glucose remaining in the bloodstream. Finally, we note that parameter p_9 actually possesses increasing influence over time. This can be explained by the physical interpretation of p_9 as the baseline blood-glucose concentration: since this is the concentration the body is aiming to return to over time, its exact value becomes more important as G itself approaches. Overall, parameters p_1, p_2, and p_9 can clearly be seen as the most influential to G on average, since other parameters play at most moderate roles over the relevant time horizon.

With respect to blood-insulin concentrations I, our simulations in Figure 4.2b suggest that the greatest overall sensitivity is observed with respect to the threshold parameter p_6 appearing in Equation (4.2). The fact that the magnitude of this sensitivity is greatest nearby to the switching time $t = 55.2$ min is unsurprising: since p_6 itself has direct influence on when the max function appearing in Equation (4.2) switches output, the system becomes more sensitive to small perturbations in this parameter as the switching time is approached. Away from this time, perturbations simply carry less importance. Outside of p_6, insulin sensitivity to other parameters tends follow a more homogeneous pattern than those of glucose in general. It is clear that the nonsmoothness introduced by the switching of the max function is translated into these sensitivities and captured by the L-derivative, but it is of special note that the nonsmoothness is not limited to the threshold parameter p_6 and is instead echoed throughout the dynamic system. This can be seen through the clear sharp peak in sensitivity exhibited by nearly every parameter at the switching time $t = 55.2$ min, with the notable exception to this remark being parameter p_{10}. As the

baseline concentration of glucose, the value of p_{10} becomes gradually more influential over time as I stabilizes (similarly to parameter p_9 in the case of glucose, discussed above).

4.3 Variations for modeling subjects with type 1 diabetes

Two main issues arise when extending the minimal model to subjects with type 1 diabetes ("diabetes" for the remainder of this section except where otherwise noted). First, we find that individuals with diabetes often have a non-negligible amount of glucose entering their bloodstream from digestive processes, even after a night of fasting (in healthy individuals, on the other hand, the body handles this input more efficiently and it becomes unimportant). An exponential term employed by many other authors (e.g., [9, 14, 22]) is added to the right-hand side of $\dot{G}$ to represent this change and two more model parameters are introduced as a result, yielding the adjusted model

$$\begin{aligned} \dot{G} &= -p_2(G - p_9) - GX + p_{11}\exp(-p_{12}t), & G(0) &= p_1, \\ \dot{X} &= -p_3X + p_4(I - p_{10}), & X(0) &= 0, \\ \dot{I} &= u - p_7(I - p_{10}), & I(0) &= p_8 + p_{10}. \end{aligned} \tag{4.11}$$

Descriptions of these new parameters are found in Table 4.2. The second main issue regards the virtual nonexistence of any endogenous (pancreatic) insulin secretion. This invalidates the choice of u_1 (hereafter, Input Method 1) used before, which was motivated by "normal" pancreatic behavior. Consequently, we consider the model input u to now describe insulin infusion from an external, wearable device, such as an insulin pump. Since such pumps are not typically able to dynamically measure blood-glucose concentrations, the two predetermined insulin infusion patterns for u studied here (hereafter, Input Methods 2 and 3) do not incorporate the state variable G.

Both input methods repurpose the parameters p_5 and p_6 originally appearing in Input Method 1. Input Method 2 utilizes a mid function in addition to a third parameter, γ (which is unique to this input method, and hence raises the total number of model parameters in this setting to 13 — i.e., $\boldsymbol{p} = (p_1, p_2, \ldots, p_{12}, \gamma)$). The resulting infusion

profile is best described as nonsmooth, decreasing, and sigmoidal in nature; switching times indicate when a sharp change in insulin infusion behavior occurs. From $t = 0$ min to $t = p_5$ min, insulin infusion occurs at constant rate γ; at $t = p_5$ min, the infusion rate decays linearly until infusion ceases completely at time $t = p_6$ min. On the other hand, Input Method 3 employs only parameters p_5 and p_6, and is meant to describe continuous insulin infusion at an exponentially decreasing rate. This model formulation means that all participating right-hand side functions in the minimal model (4.1) are smooth (i.e., C^1).

The precise formulation of each input method, along with parameter interpretations and reference parameter values in each case, are found in Table 4.3. The reference parameters for Input Methods 2 and 3 were chosen such that the total amount of insulin infused to the body mimics that secreted by a healthy subject's pancreatic $\beta-$cells over the same time horizon. As a result, we find that even with these different choices for the model input u, the corresponding reference solutions G and I very closely resemble those illustrated in Figure 4.1 in each case; in fact, at the scale of this figure, all three reference solutions overlap with little deviation. For ease of comparison between the three different choices for u, Figure 4.3 depicts the dynamic rate at which insulin is released alongside the total insulin introduced to the body over time for each of the three input methods.

Parameters			
p_i	*Units*	*Description*	p_i^* [22]
p_{11}	mg/(dL*min)	Positive constant; initial rate of the bodily introduction of glucose sourced from meals	0.5
p_{12}	Unitless	Positive constant describing the steepness of the drop-off in the rate of bodily introduction of glucose sourced from meals	0.05

Table 4.2: The parameters introduced to the minimal model when formulated to represent a diabetic patient. Note that p_i^* represents a reference parameter [1].

We now proceed with the sensitivity analysis of our two variations on the minimal model. In each case, the LD-sensitivity system derived closely mirrors the system found previously in Theorem 4.1, though we again emphasize the relevant differences. Recall that

Input Method	u	p_i	*Units*	*Description*	p_i^*
1	$p_5 t \max(0, G - p_6)$	p_5	$\left(\frac{\mu U}{mL*min}\right) \frac{1}{(mg/dL)}$	See Table 4.1	0.0039
		p_6	mg/dL	See Table 4.1	79.0353
2	$\text{mid}\left(0, \frac{\gamma(t-p_6)}{p_5-p_6}, \gamma\right)$	γ	μU/(mL*min)	Initial rate of external insulin infusion	5.9
		p_5	min	Time at which insulin infusion rate begins to decline	20
		p_6	min	Time at which external insulin infusion ceases	60
3	$p_5 \exp(-p_6 t)$	p_5	μU/(mL*min)	Initial rate of external insulin infusion	10
		p_6	Unitless	Positive constant which describes the rate of decrease of external insulin infusion	0.0423

Table 4.3: The different considerations of the insulin infusion term u [1].

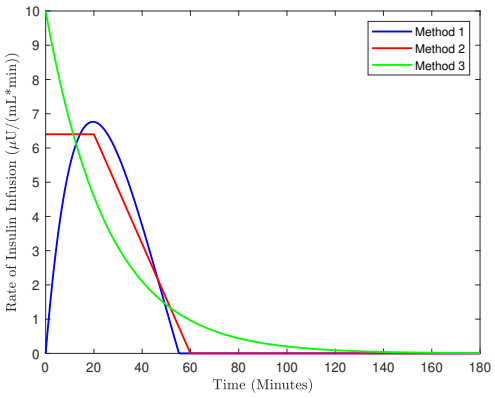

(a) The rate of insulin infusion associated with all three input methods.

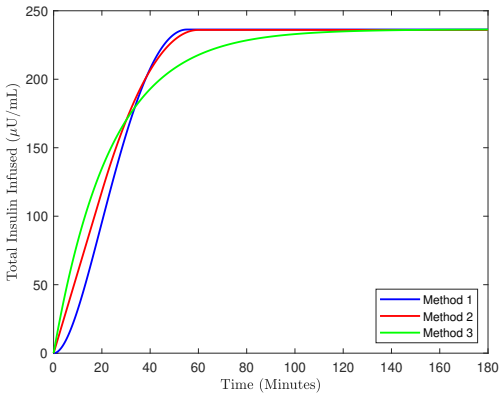

(b) The cumulative amount of insulin infusion over the time horizon via each input method. Each choice yields a total infusion of approximately 236.3 μU/mL.

Figure 4.3: Comparison of total insulin infusion over the time horizon based on different choices of u with reference parameters from Table 4.3 [1].

the adjustments incorporated in the right-hand side function for $\dot{G}$ in Equation 4.11 cause a slight adjustment in the formulation of $\mathbf{X}_G$ which was derived in Theorem 4.1. Secondly,

the original minimal model (4.1) contained ten parameters, prompting the directions matrix $\mathbf{M}$ to be full row rank and an element of $\mathbb{R}^{10\times 10}$; these new input methods require adjustment. In Input Method 2, there are thirteen parameters $\boldsymbol{p} = (p_1, p_2, \ldots, p_{12}, \gamma)$ in total, so $\mathbf{M} \in \mathbb{R}^{13\times 13}$ with $\mathbf{M}_{(13)}$ representing the probing directions for γ. In Input Method 3, twelve parameters $\boldsymbol{p} = (p_1, \ldots, p_{12})$ are present, and so $\mathbf{M} \in \mathbb{R}^{12\times 12}$ in this case.

Under the same assumptions associated with Theorem 4.1, the lexicographic sensitivity functions associated with Input Method 2 are as follows.

Theorem 4.2 (Lexicographic Sensitivity System of the Adjusted Minimal Model with Input Method 2)**.** *Let* $u = u_2 = mid\left(0, \frac{\gamma(t-p_6)}{p_5-p_6}, \gamma\right)$ *and let* $\boldsymbol{p}^*$ *be a reference parameter. Assume that a corresponding reference solution* (G, X, I) *exists on the time horizon* $[t_0, t_f] = [0, 180]$*. Letting* $\boldsymbol{M} \in \mathbb{R}^{13\times 13}$ *be a full row rank directions matrix, the lexicographic forward-parametric sensitivity functions of the adjusted minimal model are given by Equation* (4.3) *where the LD-derivatives appearing on the right-hand side are the unique solution of the system*

$$\begin{aligned}
\dot{\boldsymbol{X}}_G(t) &= -(G(t) - p_9^*)\boldsymbol{M}_{(2)} + p_2^*\boldsymbol{M}_{(9)} + \exp(-p_{12}^* t)[\boldsymbol{M}_{(11)} - p_{11}^* t\boldsymbol{M}_{(12)}] \\
&\quad - (p_2^* + X(t))\boldsymbol{X}_G(t) - G(t)\boldsymbol{X}_X(t), \\
\dot{\boldsymbol{X}}_X(t) &= -X(t)\boldsymbol{M}_{(3)} + (I(t) - p_{10}^*)\boldsymbol{M}_{(4)} - p_4^*\boldsymbol{M}_{(10)} - p_3^*\boldsymbol{X}_X(t) + p_4^*\boldsymbol{X}_I(t), \\
\dot{\boldsymbol{X}}_I(t) &= [u(t;\cdot)]'(\boldsymbol{p}^*;\boldsymbol{M}) - (I(t) - p_{10}^*)\boldsymbol{M}_{(7)} + p_7^*\boldsymbol{M}_{(10)} - p_7^*\boldsymbol{X}_I(t)
\end{aligned} \tag{4.12}$$

on $[t_0, t_f] = [0, 180]$*, with initial conditions in Equation* (4.5)*, and where* $[u(t;\cdot)]'(\boldsymbol{p}^*;\boldsymbol{M})$ *is calculated as*

$$\begin{aligned}
&[u_2(t;\cdot)]'(\boldsymbol{p}^*;\boldsymbol{M}) \\
&= \boldsymbol{slmid}\left(\boldsymbol{0}_{1\times 14}, \begin{bmatrix} \frac{\gamma^*(t-p_6^*)}{p_5^*-p_6^*} & \frac{t-p_6^*}{p_5^*-p_6^*}\boldsymbol{M}_{(13)} - \frac{\gamma^*(t-p_6^*)}{(p_5^*-p_6^*)^2}\boldsymbol{M}_{(5)} + \frac{\gamma^*(t-p_5^*)}{(p_5^*-p_6^*)^2}\boldsymbol{M}_{(6)} \end{bmatrix}, \begin{bmatrix} \gamma^* & \boldsymbol{M}_{(13)} \end{bmatrix}\right).
\end{aligned}$$

Proof. The proof mirrors that of Theorem 4.1, with the main difference that

$$\begin{aligned}
&[f_{1_t}]'(\boldsymbol{p}^*, G(t), X(t), I(t); (\mathbf{M}, \mathbf{X}_G(t), \mathbf{X}_X(t), \mathbf{X}_I(t))) \\
&= \frac{\partial f_1}{\partial \boldsymbol{p}}\mathbf{M} + \frac{\partial f_1}{\partial G}\mathbf{X}_G(t) + \frac{\partial f_1}{\partial X}\mathbf{X}_X(t) + \frac{\partial f_1}{\partial I}\mathbf{X}_I(t), \\
&= -(G(t) - p_9^*)\mathbf{M}_{(2)} + p_2^*\mathbf{M}_{(9)} + \exp(-p_{12}^* t)[\mathbf{M}_{(11)} - p_{11}^* t\mathbf{M}_{(12)}] \\
&\quad - (p_2^* + X(t))\mathbf{X}_G(t) - G(t)\mathbf{X}_X(t).
\end{aligned}$$

The formulation of $[u_2(t;\cdot)]'(\mathbf{p}^*;\mathbf{M})$ follows directly from an application of Proposition 3.14 where $\mathbf{M}_{(i)}$ continues to denote the i^{th} row of $\mathbf{M}$, $(\boldsymbol{x}, \boldsymbol{y}, \boldsymbol{z}) = \boldsymbol{p}^*$, and $(\boldsymbol{f}, \boldsymbol{g}, \boldsymbol{h}) = (0, \frac{\gamma(t-p_6)}{p_5-p_6}, \gamma)$, since

$$\begin{aligned}
&\mathbf{J}_{\boldsymbol{p}}\boldsymbol{f} = \mathbf{0}_{1\times 13}, \\
&\mathbf{J}_{\boldsymbol{p}}\boldsymbol{g} = \begin{bmatrix} 0 & 0 & 0 & 0 & -\frac{\gamma(t-p_6)}{(p_5-p_6)^2} & \frac{\gamma(t-p_5)}{(p_5-p_6)^2} & 0 & 0 & 0 & 0 & 0 & 0 & \frac{t-p_6}{p_5-p_6} \end{bmatrix}, \\
&\mathbf{J}_{\boldsymbol{p}}\boldsymbol{h} = \begin{bmatrix} \mathbf{0}_{1\times 12} & 1 \end{bmatrix}.
\end{aligned}$$

□

Again under the same assumptions as Theorem 4.1, the lexicographic sensitivity functions associated with Input Method 3 are given as follows.

Theorem 4.3 (Lexicographic Sensitivity System of the Adjusted Minimal Model with Input Method 3)**.** *Let $u = u_3 = p_5 exp(-p_6 t)$ and let $\boldsymbol{p}^*$ be a reference parameter. Assume that a corresponding reference solution (G, X, I) exists on the time horizon $[t_0, t_f] = [0, 180]$. Letting $\boldsymbol{M} \in \mathbb{R}^{12\times 12}$ be a full row rank directions matrix, the lexicographic forward-parametric sensitivity functions of the adjusted minimal model are given by Equation* (4.3) *where the LD-derivatives appearing on the right-hand side are the unique solution of Equation* (4.12) *on $[t_0, t_f] = [0, 180]$ with initial conditions given in Equation* (4.5) *and where $[u(t;\cdot)]'(\boldsymbol{p}^*;\boldsymbol{M})$ is calculated as*

$$[u_3(t;\cdot)]'(\boldsymbol{p}^*;\boldsymbol{M}) = \exp(-p_6^* t)\boldsymbol{M}_{(5)} - p_5^* t\exp(-p_6^* t)\boldsymbol{M}_{(6)}.$$

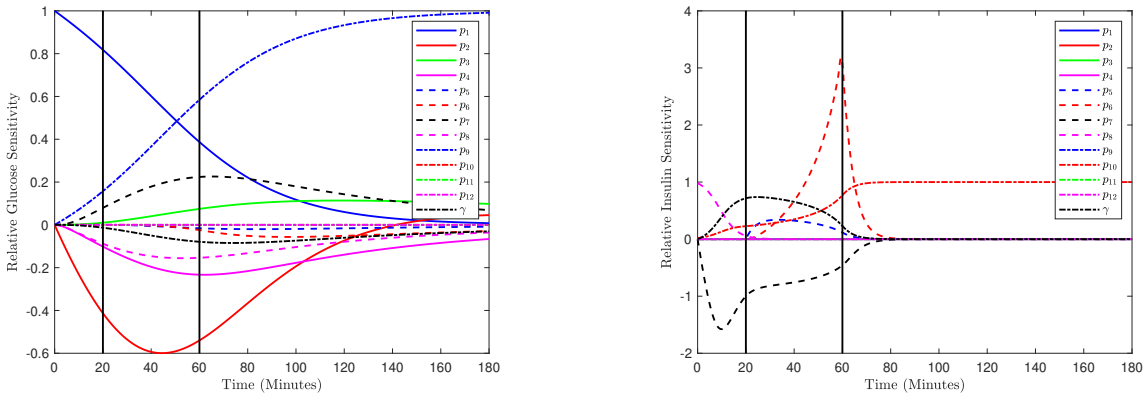

(a) (b)

Figure 4.4: With a choice of Input Method 2: in 4.4a, the relative sensitivities of glucose to parameters, and in 4.4b, the relative sensitivities of insulin to parameters [1].

Proof. The proof of the formulation of the LD-sensitivity system is identical to that of Theorem 4.2. The formulation of $[u_3(t;\cdot)]'(\mathbf{p}^*;\mathbf{M})$ requires the product and chain rules along with Equation (3.1), and yields

$$\begin{aligned}
[u_3(t;\cdot)]'(\mathbf{p}^*;\mathbf{M}) &= [p_5\exp(-p_6t)]'(\mathbf{p}^*;\mathbf{M}),\\
&= p_5^*[\exp(-p_6t)]'(\mathbf{p}^*;\mathbf{M}) + \exp(-p_6^*t)[p_5]'(\mathbf{p}^*;\mathbf{M}),\\
&= p_5^*\exp(-p_6^*t)(-\mathbf{M}_{(6)}t) + \exp(-p_6^*t)\mathbf{M}_{(5)},\\
&= \exp(-p_6^*t)\mathbf{M}_{(5)} - p_5^*t\exp(-p_6^*t)\mathbf{M}_{(6)},
\end{aligned}$$

as we aimed to show. □

Our choice of Input Method 2, which is nonsmooth, required a hard-coded implementation of the mid and **slmid** functions and also invited further analysis with different choices of directions matrix $\mathbf{M}$ (similar to the analysis done in the previous section). In each case, however, the same L-derivative was again recovered within a small degree of numerical error. Since the choice of u associated with Input Method 3 is in fact C^1, the lexicographic sensitivity functions are guaranteed to recover the classical sensitivity functions with every choice of full row rank $\mathbf{M}$. The relative sensitivity functions furnished by the choice of Input Method 2 and 3 are presented in Figures 4.4 and 4.5, respectively.

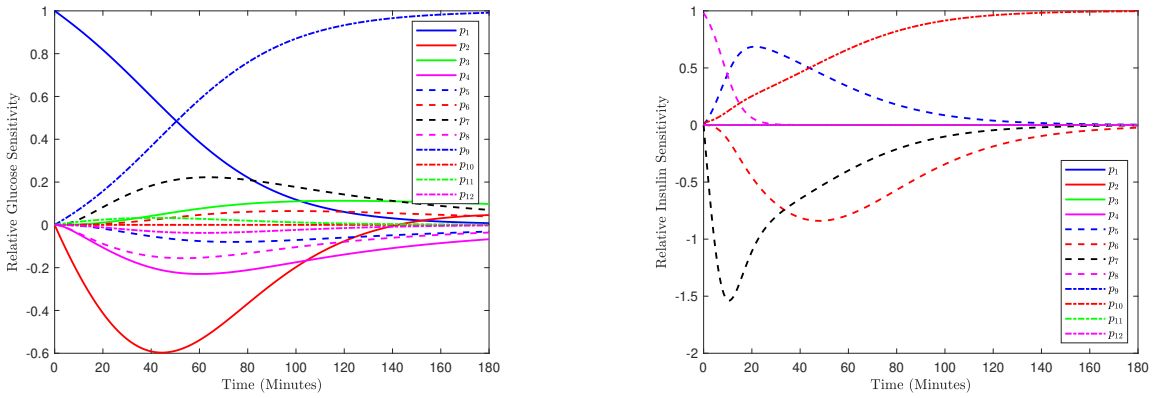

(a) (b)

Figure 4.5: Glucose and insulin sensitivities to parameters, respectively, with a choice of Input Method 3 [1].

Just as the nonsmooth switch appearing in Input Method 1 invites corresponding nonsmoothness in parametric sensitivities (recall Figure 4.2b), the switching nature of Input Method 2 yields similar abrupt changes in behavior in terms of insulin sensitivities. The vertical bars appearing in Figure 4.4 correspond the the times $t = p_5 = 20$ min, where the output of the mid function associated with Input Method 2 switches from being constant to decreasing, and $t = p_6 = 60$ min, where the mid function switches its output to zero. Sharp changes in the parametric sensitivity of insulin concentration I are observed at each switching time. At $t = p_5$ min, a sharp increase is observed with respect to p_5 itself, which is clearly seen in Figure 4.6; meanwhile, insulin sensitivity to the switching time p_6 peaks at (and remains high nearby to) $t = p_6$ min, but is low elsewhere. Since the value of p_6 directly influences the time at which insulin secretion ceases, small perturbations to the parameter become influential as $t = p_6$ min is approached on the time horizon — once the switch is made, however, sensitivity to this parameter decreases rapidly. The third parameter required in the choice of Input Method 2, γ, exhibits its maximum influence at roughly $t = p_5$ min and diminishes over time; insulin sensitivity to other parameters including p_7, p_8, and p_{10} follows a similar trajectory as that seen in the case of Input Method 1. Presumably due the absence of the state variable G in the formulation of Input Method 2, insulin appears to be largely insensitive to the other parameters not explicitly

appearing in the right-hand side rule for $\dot{I}$. On the other hand, glucose sensitivity results are nearly indistinguishable from seen in Input Method 1, with the exception of the sensitivities pertaining to the differing input parameters p_5, p_6, and γ.

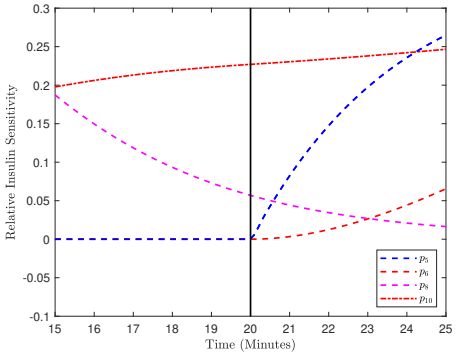

Figure 4.6: A closer view of Figure 4.4b, where the sharp switch in insulin sensitivity to p_5 is more clearly seen [1].

In Input Method 3, where the L-sensitivity functions recover the classical sensitivity functions due to the absence of any nonsmoothness, glucose sensitivities are again nearly indistinguishable from those seen in Input Methods 1 and 2 (apart from those relating to the input parameters p_5 and p_6 in this case). The insulin sensitivities are a bit more unique, though qualitative behavior similar to Input Method 1 can still be seen in, e.g., sensitivity to parameters p_7 and p_{10} — though nuances like the brief plateau of sensitivity to p_7 and the clearly sigmoidal sensitivity to p_{10} present when using Input Method 1 (Figure 4.2b) are absent in Figure 4.5b. For a similar presumed reason as Input Method 2, parameters absent from the right-hand side rule for $\dot{I}$ such as $p_1 \to p_4$ are not influential to insulin concentration when using Input Method 3.

In Table 4.4, we highlight differences in parameter sensitivities arising in state variables G and I due to the different choices 3 input methods considered (recalling their formulation from Table 4.3). This is done with respect to the input parameters p_5, p_6, and γ according to three different metrics: the maximum magnitude, average magnitude, and variance of observed relative sensitivity.

Input Method	p_i	$\max \lvert \widehat{S}_G^{p_i} \rvert$	$\text{avg}\left(\widehat{S}_G^{p_i}\right)$	$\text{var}\left(\widehat{S}_G^{p_i}\right)$	$\max \lvert \widehat{S}_I^{p_i} \rvert$	$\text{avg}\left(\widehat{S}_I^{p_i}\right)$	$\text{var}\left(\widehat{S}_I^{p_i}\right)$
1	p_5	0.078	-0.046	0.001	0.752	0.148	0.071
	p_6	0.148	0.086	0.003	5.245	-0.523	1.071
2	p_5	0.020	-0.011	0.000	0.339	0.062	0.013
	p_6	0.056	-0.031	0.000	3.187	0.283	0.409
	γ	0.085	-0.051	0.000	0.737	0.181	0.075
3	p_5	0.080	-0.051	0.000	0.686	0.217	0.053
	p_6	0.065	0.042	0.000	0.840	-0.367	0.084

Table 4.4: Sensitivity metrics for glucose and insulin concentrations with respect to model input parameters: the absolute maximum of relative sensitivity over time horizon, the average relative sensitivity over time horizon, and the absolute variance of relative sensitivity over time horizon [1].

Several overall observations can be made. First, the sensitivity of G with respect to the parameter studied is more uniform than those corresponding to insulin sensitivity I, as seen through the differences in variance. This is presumably contributed to by the presence of the relevant parameters in the right-hand side rule for $\dot{I}$, and absence elsewhere. Furthermore, notice that across each row, the average sensitivity of G to any given parameter is always opposite in sign to the average sensitivity of I to the same parameter, independent of the input method chosen. This can be understood via the opposing nature of glucose-insulin interactions within the body in general.

In Input Method 1, recall that p_5 represents the rate of pancreatic secretion (when active) and p_6 represents the threshold glucose concentration above which insulin secretion is triggered. An increase in the reference value of p_5 would therefore simulate an introduction of more insulin to the bloodstream, and as a result, the average sensitivity of insulin concentration I to this parameter is positive. On the other hand, average glucose sensitivity to the same parameter is negative due to the aforementioned fact that higher insulin levels induce greater glucose uptake (and hence a reduction in the reference solution G over the time horizon). On the other hand, an increase in the reference value of p_6 would raise the threshold glucose concentration required to initialize insulin secretion in the first,

making it more difficult to trigger the release of insulin. This effect is shown to be more influential than the effect of p_5: here, for example, a 1% increase in the reference value of p_6 would produce an approximate average decrease of 0.523% in the reference solution I itself, while a similar increase in p_5 would cause a respective increase in I of only 0.148%.

Incidentally, the metrics associated with Input Method 3 tell a similar qualitative story as in Input Method 1. Parameter p_5 here now represents the initial rate of insulin infusion from an external device (e.g., an insulin pump), and $p_6 > 0$ is an exponential decay parameter describing the steepness of the decrease in infusion over time. Overall, an increase in p_5 would cause a clear increase in the state variable I, while increasing p_6 (resulting in a steeper infusion decrease) would result in a corresponding decrease in I. For these reasons, the sensitivities of I to both parameters in Input Method 3 here are opposite in sign, with the decay parameter p_6 being more influential both at its peak and on average when compared to p_5.

In Input Method 2, a decreasing nonsmooth sigmoidal function is used to model the rate of insulin infusion, with parameters p_5 and p_6 representing the times at which the nonsmooth mid function changes output and parameter γ representing the initial (constant) rate of infusion. An increase in any of these parameters would seem to cause a respective increase in insulin concentration I: by increasing p_5 or p_6, the switching times which the decrease or cessation of insulin secretion would be delayed, meaning that more insulin would be secreted overall. Similarly, by increasing the initial (constant) infusion rate γ, an obvious increase in I would result. Table 4.4 reinforces these ideas quantitatively, with the average insulin sensitivity to each parameter being positive. Of the three parameters, p_6 is shown to be the most influential at its maximum and on average. At the fixed time marking the peak of this sensitivity, a 1% increase in the reference value of p_6 corresponds to a predicted 3.187% increase in the value of the reference solution; from Figure 4.4b, it is clear that said peak sensitivity occurs at $t = p_6 = 60$ min.

4.4 Discussion

The lexicographic sensitivity approach taken in this chapter provides accurate results without the introduction of inherent numerical error, though separate efforts to characterize the sensitivity of the minimal model to its parameters have previously been made. For example, without the knowledge of the lexicographic sensitivity functions, Munir [37] recently performed a "generalized sensitivity analysis" of the minimal model (4.1) using the standard model input (4.2) with the goal of specifically approximating the sensitivity data presented in Section 4.2. This analysis was done by first replacing the max function with the smoothing approximation $\max(0, x) \approx \frac{1}{2}(x + \sqrt{x^2 + \epsilon})$ for some user-defined $\epsilon > 0$, and proceeded by simply implementing the resulting classical sensitivity functions 2.4. The relative accuracy of this approach is not guaranteed in general, especially since it is typically difficult to know how many times points of nondifferentiability may be visited in a simulation *a priori*; therefore, the cumulative numerical error introduced by even small choices of ϵ may be significant. Indeed, there is not even a guarantee of the convergence of the resulting sensitivity functions to those produced by the flexible lexicographic approach (which avoids such issues entirely). Due in part to issues of this nature, Munir deserted this approach later in [37] in favor of a stochastic "generalized sensitivity" approach.

Though the minimal model is relatively simple in nature, it provides a reasonable approximation of biological glucose-insulin interactions; the sensitivity information provided here is therefore potentially relevant in biological applications. In particular, Input Methods 2 and 3 were both successful in replicating the dynamics of glucose concentration from a normal, healthy response (i.e., in Input Method 1), implying that the data supplied in this chapter may be useful in design considerations for, e.g., external insulin pumps for diabetics.

Since several of the parameters appearing in the model can be easily adjusted physically (e.g., p_1 and input parameters p_5, p_6, and γ associated with Input Methods 2 and 3), dynamic optimal control is a future direction of research within the model. In fact, the

sensitivity information given in this chapter can be provided to open-loop nonsmooth optimizers with this goal in mind [31]. A similar direction of interest is nonsmooth dynamic optimization within the model of type 1 diabetes put forth by Hovorka et al. [26] in order to compare the accuracy of previous attempts to optimize the model's input.

CHAPTER 5
QUANTIFYING PARAMETRIC SENSITIVITIES OF A NONSMOOTH MODEL OF RIOT SPREAD

The contents, figures, and tables appearing in this chapter are based on [2]. Following a similar approach as the previous chapter, we now explore the ramifications of lexicographic sensitivity theory when applied to a novel mathematical model describing the spread of riots on a municipal scale.

5.1 Model background

Riots, often a symptom of larger issues causing widespread civil discontent, have long been influential and metamorphic factors in many aspects of history. This is no less true in the modern day, with recent examples of high-profile riots often attracting international attention and social movement. In 2019, for example, the introduction of an extradition bill in Hong Kong set off protests which eventually involved nearly 1 in every 4 residents of the territory [27]; international coverage of the events sparked larger conversations about political change and police brutality (see, e.g., [50]). In January of 2021, another example of such activity was seen as American rioters breached the United States Capitol building in response to the results of the 2020 presidential election, contributing to the deaths of 5 people and causing a number of arrests relating to the riots [46]. In this thesis, the 2005 French riots are of particular interest, which were triggered by the deaths of two minority youths in the municipality of Clichy-sous-Bois outside of Paris and transpired in a violent three-week backlash against police brutality.

Incidents of police harassment and abuse were frequently reported in Clichy-sous-Bois, with a particular emphasis on events which subjected the municipality's youth population to heightened scrutiny. The municipality is among the poorest suburbs of Paris, and low employment rates led to a large number of youths unoccupied with work or school. It was

not uncommon for police to detain and question loitering youth for upwards of several hours without any evidence of wrongdoing — a habit which eventually led to these youth simply fleeing to avoid harassment and interrogation whenever police were noticed in the area [18]. This led to tension between the police and youths which came to a head on October 27, 2005, as police were dispatched to investigate a possible break-in at a construction site and saw a group of about ten teenage boys nearby, who were later revealed to be returning home after a game of soccer. The teenagers fled upon seeing the police and officers pursued, with three of of the teens ultimately scaling a wall in order to hide in a nearby power substation. Within several minutes, power outages occurred across the city as the boys were electrocuted inside. Two of the young men died, and one survived with severe injuries [18].

Despite some discrepancies between different accounts of officers' actions, the deaths invited intense scrutiny into the habits of police in the area and the behaviors which led youth to immediately flee in general. This culminated with the general public rallying behind renewed calls for ending police harassment and brutality, but also spawned riots which broke out shortly after the boys' death and spread throughout the country for the next three weeks. In the end, nearly 3000 rioters were arrested, 9000 cars were destroyed or burned, 125 police or firefighters were injured, and nearly $300 million dollars worth of property damage had been done [43].

Daily police reports described the spread and extent of the riots across the country at a level of detail rarely seen in large-scale riots and allowed impressive progress in attempts to model their spread. In [12], authors amassed the collection of police reports for the relevant timeframe and simplified their contents, measuring the approximate number of rioters and "rioting events" (i.e., individual instances of criminal activities such as arson or assault). This data collection did not discriminate, however, between events transpiring as a direct result of the riots and unrelated events. For this reason, a constant level of "background" criminal activity was assumed among the data.

Riots themselves can be conceived as a form of "social contagion," in which behavior of a group of individuals affects the behavior of nearby susceptible individuals; for this reason, the authors of [12] then fit their data to a generalized modeling framework for social contagions originally formulated by Berestycki et al. in [10]. This framework is built on a conventional SIR (Susceptible-Infected-Recovered) framework for epidemic spread [13] and emphasizes four main concepts which specifically influence dynamics in a social setting: that activity is initialized by an (exogenous) shock or triggering event, that endogenous factors can cause self-reinforcement and growth, that social discontent can accelerate the occurrence of both triggering events and self-reinforcement, and that riot spread between "sites" is influenced by their spatial proximity. Different variations were considered in the context of the 2005 French riots in order to describe the spread at different levels of granularity: between cities (the "municipality scale") and between larger administrative regions (the "département scale").

While the model at hand is similar in nature to that of an SIR epidemic model, there is one key difference at hand. When describing the spread of disease, the probability that a susceptible individual becomes infected (typically) varies proportionally with the fraction of the total population already infected in their community; however, the probability that a susceptible individual (i.e., member of a reference population) joins a riot is instead simply proportional to the current number of rioters (regardless of the proportion of the population engaged in the activity). Furthermore, nonsmoothness is introduced (in the municipal-scale variation of this model) in an effort to describe a so-called "bandwagon effect," which proposes that susceptible individuals are unlikely to join a riot when existing activity is low and that this likelihood grows exponentially once the riot grows beyond a certain threshold. However, this nonsmoothness again invalidates any classical efforts to describe model sensitivity to parameters. In an effort to describe identify key factors to the spread of riots at the most granular possible level, we proceed with a lexicographic sensitivity analysis of this municipal-scale model proposed in [12].

5.2 Model formulation

Within the model, there are two state variables associated with each site involved in the riot. For the i^{th} site, σ_i represents a reservoir of all potential rioting events and is proportional to the number of susceptible individuals present at the site; similarly, λ_i represents the level of rioting activity, and is proportional to the present number of rioters. Under the assumptions that rioters leave the riot at a constant rate and never rejoin once doing so, Bonnasse-Gahot et al. propose the following model for the spread of riots between n total sites at the municipal scale [12]:

$$\begin{aligned} \dot{\sigma}_i &= -\Psi_i(\Lambda_i(\boldsymbol{\lambda}))\sigma_i, \qquad \sigma_i(0) = \varepsilon_0 N_i, \\ \dot{\lambda}_i &= \Psi_i(\Lambda_i(\boldsymbol{\lambda}))\sigma_i - \omega_i\lambda_i, \quad \lambda_i(0) = \begin{cases} 0, & \text{if } i \neq i^0, \\ \lambda^*, & \text{if } i = i^0. \end{cases} \end{aligned} \tag{5.1}$$

In this formulation, each σ_i (i.e., the maximum number of events that may possibly occur at site i) is initialized at a value proportional to the site's reference population, N_i. Here, in the spirit of [12], the reference population is taken as the number of 16-24 year old males without a diploma, the demographic which typically comprises the majority of rioters (see, e.g., [24]). Site i^0 is assumed to be the site where the exogenous "shock" or triggering event occurs, leading to the initial level of rioting activity to be nonzero at site i^0 (i.e., $\lambda^* > 0$) and 0 elsewhere. Parameter ω_i is the aforementioned constant rate at which rioters leave an active riot, and is meant to incorporate a variety of different reasons why individuals choose to leave including, e.g., arrest, fear, and fatigue. The function $\Lambda_i(\boldsymbol{\lambda})$ is meant to represent the "global activity" observed from the perspective of site i; roughly, the authors of [12] suggest interpreting this as the average sentiment of concern that a member of a site's susceptible population holds with respect to rioting events occurring among all sites. This concern may be raised or lowered through, e.g., person-to-person interactions and media coverage of rioting events, with a stronger influence assumed by

events or coverage happening nearby to an individual. It is modeled by the expression

$$\Lambda_i = \sum_{j=1}^{n} W_{ij}\lambda_j, \tag{5.2}$$

with weights W_{ij}, representative of the relative influence of site j on site i, being modeled by the "power decay law"

$$W_{ij} = \begin{cases} (1 + \text{dist}(i,j)/d_0)^{-\delta}, & \text{if } i \neq j \\ 1 & \text{if } i = j. \end{cases} \tag{5.3}$$

Here, $\text{dist}(i,j)$ is the distance between sites i and j in kilometers, parameter d_0 is the "characteristic distance" beyond which geographic influence decreases exponentially, and parameter δ describes the non-local effect of sites (as a result of, e.g., media coverage). This power decay law primarily favors geographic proximity as a medium for riot spread, but also accounts for indirect or long-distance effects from distant sites.

The authors of [12] considered several different formulations for the so-called "activation function" Ψ_i, which represents the likelihood of a susceptible individual to join a riot and is a function of the global activity or "level of concern" seen from site i, within several constraints. First, $\Psi_i(\Lambda_i) = 0$ when $\Lambda_i = 0$ — that is, there should be no propensity for an individual to riot when no rioting activity is present. Secondly, $\Psi_i(\Lambda_i)$ should approach some $\Lambda_i^* < 1$ monotonically from below as Λ_i approaches infinity, suggesting that the likelihood for a susceptible individual to join a riot saturates for large riots. The best of the considered options was identified using the Akaike Information Criterion (AIC; see [44]) after employing maximum likelihood estimation to optimize parameter values in each case, and is given as the nonsmooth sigmoidal function

$$\Psi_i = \eta_i \max(0, 1 - \exp(-\gamma_i(\Lambda_i - \Lambda_i^c))), \tag{5.4}$$

with parameter η_i describing a general level of rioting susceptibility within the site, Λ_i^c representing the threshold on global activity seen from site i above which rioting activity grows exponentially, and γ_i representing the steepness of the activity function after the

Parameters		
p_i	*Description*	p_i^0
ω	rate of removal/recovery from rioting activity	0.26
η	susceptibility parameter and saturating value	0.63
γ	sharpness of threshold effect in rioting activation	1.27
Λ^c	rioting activation threshold	0.06
d_0	power law decay parameter	0.008
δ	power law decay parameter	0.67
ξ_0	initial value proportionality constant	0.00656
λ^*	initial rioting activity caused by exogeneous shock	5.5

Table 5.1: Site-independent parameters used in (5.1), with reference values from [12] [2].

threshold is reached. In this formulation, the global activity term Λ_i builds without physical consequence until it reaches the threshold parameter Λ_i^c, after which the bandwagon effect is initiated and rioting begins. For simplicity, we assume independence of parameters between sites (e.g., $\eta_i = \eta$ for all $i \in \{1, 2, \ldots, n\}$, etc.), resulting in 8 model parameters in total. A summary of all parameters present in the model can be found in Table 5.1.

In order to visualize the form of a typical system, suppose we investigate the simple case where there are two potential rioting sites ("Site 1" and "Site 2") and that rioting initializes in Site 1. Assuming site-independent parameters, the model (5.1) would incorporate $2 \times 2 = 4$ total state variables and take the following form:

$$\begin{aligned}
\dot{\sigma}_1 &= -\eta \max(0, 1 - \exp(-\gamma((W_{1,1}\lambda_1 + W_{1,2}\lambda_2) - \Lambda^c)))\sigma_1, && \sigma_1(0) = \varepsilon_0 N_1, \\
\dot{\lambda}_1 &= \eta \max(0, 1 - \exp(-\gamma((W_{1,1}\lambda_1 + W_{1,2}\lambda_2) - \Lambda^c)))\sigma_1 - \omega\lambda_1, && \lambda_1(0) = \lambda^*, \\
\dot{\sigma}_2 &= -\eta \max(0, 1 - \exp(-\gamma((W_{2,1}\lambda_1 + W_{2,2}\lambda_2) - \Lambda^c)))\sigma_2, && \sigma_2(0) = \varepsilon_0 N_2, \\
\dot{\lambda}_2 &= \eta \max(0, 1 - \exp(-\gamma((W_{2,1}\lambda_1 + W_{2,2}\lambda_2) - \Lambda^c)))\sigma_2 - \omega\lambda_2, && \lambda_1(0) = 0.
\end{aligned}$$

Within our simulations, reference populations N_i (i.e., the number of 16-24 year old males without a diploma) were calculated using 2007 data from the Institut National de la Statistique et des Études Économiques (INSEE), which is France's national statistics

bureau. Relevant distances between sites were calculated between the geographic centroids of each municipality using QGIS [41] in conjunction with data supplied by the collaborators at OpenStreetMap ([39]; map data copyrighted by OpenStreetMap contributors and available from `www.openstreetmap.org`), as they were in [12]. Based on the geographic and population data collected here, we proceed with $n = 1287$ total sites within the Île-de-France region in which the initial rioting site Clichy-sous-Bois is situated; furthermore, we select $t = t_0 = 0$ to represent October 27, 2005 and $t = t_f = 44$ days later (i.e., December 10, 2005) in order to capture the full riot dynamics.

Among the 1287 sites present in our analysis, we highlight the 12 most active sites within the Île-de-France region in order to characterize the general behavior of the model at hand. The INSEE assigns each municipality in France a unique 5-digit administrative identification code which we adopt in our analysis; in particular, the highlighted sites are Clichy-sous-Bois (the initial site; INSEE 93014), Meaux (77284), Mantes-la-Jolie (78361), Grigny (91286), Nanterre (92050), Aulnay-sous-Bois (93005), Bobigny (93008), Saint-Denis (93066), Sevran (93071), Stains (93072), Champigny-sur-Marne (94017), and Argenteuil (95018). The geographic location of these 12 sites can be found in Figure 5.5a later in this chapter, with Clichy-sous-Bois appearing just north of center. Simulations of the state variables for these sites are found in Figure 5.1 alongside simulations of the global activity function Λ_i in each site. These follow largely intuitive behavior. Each state variable σ_i (reservoir of events at site i) is a monotonically decreasing function due to the removal of potential rioting events in each site's reservoir over time, while each λ_i (rioting activity at site i) behaves in a wavelike fashion and suggests that the riots largely die out within 3 weeks. Examination of each Λ_i suggests that the global activity seen from each site follows similar wavelike behavior — recall, however, that the nonsmooth activation function Ψ_i switches output as Λ_i crosses the threshold described by parameter Λ^c. Our analysis suggests that this switch, indicating the start of the bandwagon effect, occurs within a day

of the triggering event even in sites beyond Clichy-sous-Bois; between 3 and 4 weeks later, the switch is thrown once more as the bandwagon effect then subsides in each site.

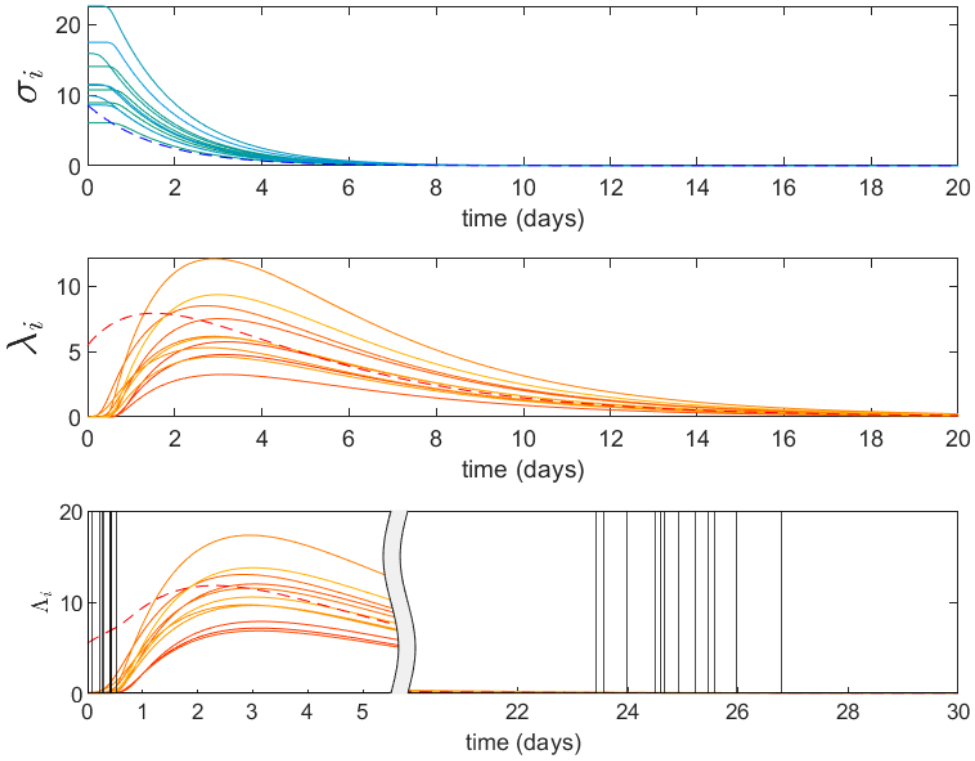

Figure 5.1: Simulations of (5.1) with the dynamics of the initial rioting site Clichy-sous-Bois denoted by dashed lines. Vertical lines appearing in the results of Λ_i represent the times at which each of the 12 highlighted sites have their respective activation functions ψ_i (5.4) turned on as threshold parameter Λ^c is crossed [2].

5.3 Lexicographic sensitivity analysis

Recalling our original goal of characterizing the sensitivity of the spread of these riots to the parameters outlined in the section so far, we now proceed with a sensitivity analysis of the model at hand. The nonsmoothness present in the activation function Ψ_i associated with each site invalidates classical sensitivity theory, but we note that the PC^1 right-hand side functions associated with Equation 5.1 make this model well-suited for the lexicographic approach.

Theorem 5.1 (Lexicographic Sensitivity System of the Rioting Model)**.** *Given some reference parameter* $\boldsymbol{p}^* \in \mathbb{R}^8$*, assume that the corresponding reference solution* $(\boldsymbol{\sigma}^*, \boldsymbol{\lambda}^*)$ *exists on the time horizon* $[t_0, t_f] = [0, 44]$*. Suppose* $\boldsymbol{M} \in \mathbb{R}^{8\times 8}$ *is a full row rank directions matrix with the form*

$$\boldsymbol{M} = \begin{bmatrix} \boldsymbol{M}_{\omega} \\ \boldsymbol{M}_{\eta} \\ \boldsymbol{M}_{\gamma} \\ \boldsymbol{M}_{\Lambda^c} \\ \boldsymbol{M}_{d_0} \\ \boldsymbol{M}_{\delta} \\ \boldsymbol{M}_{\varepsilon} \\ \boldsymbol{M}_{\lambda^*} \end{bmatrix}.$$

Then the corresponding lexicographic (forward-parametric) sensitivity functions at site i *are given by*

$$\begin{bmatrix} \boldsymbol{S}_{\sigma_i}(t) \\ \boldsymbol{S}_{\lambda_i}(t) \end{bmatrix} = \begin{bmatrix} \boldsymbol{X}_{\sigma_i}(t)\boldsymbol{M}^{-1} \\ \boldsymbol{X}_{\lambda_i}(t)\boldsymbol{M}^{-1} \end{bmatrix} = \begin{bmatrix} [\sigma_i(t;\cdot)]'(\boldsymbol{p}^*;\boldsymbol{M})\boldsymbol{M}^{-1} \\ [\lambda_i(t;\cdot)]'(\boldsymbol{p}^*;\boldsymbol{M})\boldsymbol{M}^{-1} \end{bmatrix}, \tag{5.5}$$

where the LD-derivatives $(\boldsymbol{X}_{\sigma_i}, \boldsymbol{X}_{\lambda_i})$ *are the unique solution of the LD-sensitivity system*

$$\begin{aligned} \dot{\boldsymbol{X}}_{\sigma_i} &= -[\Psi_i]'\sigma_i - \Psi_i \boldsymbol{X}_{\sigma_i}, \\ \dot{\boldsymbol{X}}_{\lambda_i} &= [\Psi_i]'\sigma_i + \Psi_i \boldsymbol{X}_{\sigma_i} - \lambda_i \boldsymbol{M}_{\omega} - \omega \boldsymbol{X}_{\lambda_i}, \end{aligned} \tag{5.6}$$

on the time horizon $[t_0, t_f] = [0, 44]$ *with initial conditions*

$$\begin{bmatrix} \boldsymbol{X}_{\sigma_i}(0) \\ \boldsymbol{X}_{\lambda_i}(0) \end{bmatrix} = \begin{cases} \begin{bmatrix} N_i \boldsymbol{M}_{\varepsilon} \\ \mathbf{0} \end{bmatrix}, & \text{if } i \neq i^0, \\ \\ \begin{bmatrix} N_i \boldsymbol{M}_{\varepsilon} \\ \boldsymbol{M}_{\lambda^*} \end{bmatrix} & \text{if } i = i^0. \end{cases} \tag{5.7}$$

Furthermore, given

$$\begin{aligned}\Psi_i &= \eta \max(0, v_i),\\ v_i &= 1 - \exp(-\gamma(\Lambda_i - \Lambda^c)),\\ \Lambda_i &= \sum_{j=1}^{n} W_{ij}\lambda_j,\end{aligned}$$

we find that

$$\begin{aligned}[\Psi_i]' &= max(0, v_i)\boldsymbol{M}_\eta + \eta \boldsymbol{slmax}(\mathbf{0}, [v_i \quad v_i']),\\ [v_i]' &= (1 - v_i)\left((\Lambda_i - \Lambda^c)\boldsymbol{M}_\gamma - \gamma \boldsymbol{M}_{\Lambda^c}\right) + (1 - v_i)\left(\gamma \Lambda_i'\right),\\ [\Lambda_i]' &= \left(\sum_{j=1}^{n} \begin{bmatrix} \dfrac{\partial W_{ij}}{\partial d_0} & \dfrac{\partial W_{ij}}{\partial \delta} \end{bmatrix} \lambda_j\right) \begin{bmatrix} \boldsymbol{M}_{d_0} \\ \boldsymbol{M}_\delta \end{bmatrix} + \left(\sum_j W_{ij} \boldsymbol{X}_{\lambda_j}\right),\end{aligned}$$

with each function being evaluated at the reference parameter

$\boldsymbol{p}^* = (\omega^*, \eta^*, \gamma^*, \Lambda^{c*}, d_0^*, \delta^*, \varepsilon^*, \lambda^{**}) \in \mathbb{R}^8$.

Proof. Recall that for the i^{th} site, the right-hand side function of (5.1) is given by

$$\boldsymbol{f}(\boldsymbol{p}, \sigma_i, \lambda_i) = \begin{bmatrix} f_1(\boldsymbol{p}, \boldsymbol{\sigma}, \boldsymbol{\lambda}) \\ f_2(\boldsymbol{p}, \boldsymbol{\sigma}, \boldsymbol{\lambda}) \end{bmatrix} = \begin{bmatrix} -\Psi_i \sigma_i \\ \Psi_i \sigma_i - \omega \lambda_i \end{bmatrix}. \tag{5.8}$$

Given any full row rank directions matrix $\mathbf{M} \in \mathbb{R}^{8\times 8}$, we aim to find the LD-derivative of the right-hand side function $\boldsymbol{f}$ from (5.8) since the LD-sensitivity system (3.8) is given by

$$\begin{bmatrix} \dot{\mathbf{X}}_{\sigma_i}(t) \\ \dot{\mathbf{X}}_{\lambda_i}(t) \end{bmatrix} = \boldsymbol{f}' \left(\begin{bmatrix} \boldsymbol{p}^* \\ \boldsymbol{\sigma}(t) \\ \boldsymbol{\lambda}(t) \end{bmatrix} ; \begin{bmatrix} \mathbf{M} \\ \mathbf{X}_{\boldsymbol{\sigma}}(t) \\ \mathbf{X}_{\boldsymbol{\lambda}}(t) \end{bmatrix} \right). \tag{5.9}$$

Proposition 3.9 dictates that the LD-derivatives appearing in Equation (5.9) may be calculated component-wise. By the LD-derivative product rule also appearing in

Proposition 3.9, we find that

$$
\begin{aligned}
&f_1'(\boldsymbol{p}^*, \boldsymbol{\sigma}, \boldsymbol{\lambda}; (\mathbf{M}, \mathbf{X}_{\sigma_i}(t), \mathbf{X}_{\lambda_i}(t))) \\
&= \frac{\partial f_1}{\partial \boldsymbol{p}}\mathbf{M} + \frac{\partial f_1}{\partial \boldsymbol{\sigma}}\mathbf{X}_{\boldsymbol{\sigma}}(t) + \frac{\partial f_1}{\partial \boldsymbol{\lambda}}\mathbf{X}_{\boldsymbol{\sigma}}(t) \\
&= -\left(\frac{\partial \Psi_i}{\partial \boldsymbol{p}}\sigma_i + \Psi_i\frac{\partial \sigma_i}{\partial \boldsymbol{p}}\right)\mathbf{M} - \left(\frac{\partial \Psi_i}{\partial \boldsymbol{\sigma}}\sigma_i + \Psi_i\frac{\partial \sigma_i}{\partial \boldsymbol{\sigma}}\right)\mathbf{X}_{\boldsymbol{\sigma}}(t) - \left(\frac{\partial \Psi_i}{\partial \boldsymbol{\lambda}}\sigma_i + \Psi_i\frac{\partial \sigma_i}{\partial \boldsymbol{\lambda}}\right)\mathbf{X}_{\boldsymbol{\lambda}}(t) \\
&= -\left(\frac{\partial \Psi_i}{\partial \boldsymbol{p}}\sigma_i\mathbf{M} + \frac{\partial \Psi_i}{\partial \boldsymbol{\sigma}}\sigma_i\mathbf{X}_{\boldsymbol{\sigma}}(t) + \frac{\partial \Psi_i}{\partial \boldsymbol{\lambda}}\sigma_i\mathbf{X}_{\boldsymbol{\lambda}}(t)\right) - \left(\Psi_i\frac{\partial \sigma_i}{\partial \boldsymbol{p}}\mathbf{M} + \Psi_i\frac{\partial \sigma_i}{\partial \boldsymbol{\sigma}}\mathbf{X}_{\boldsymbol{\sigma}}(t) + \Psi_i\frac{\partial \sigma_i}{\partial \boldsymbol{\lambda}}\mathbf{X}_{\boldsymbol{\lambda}}(t)\right) \\
&= -[\Psi_i]'\sigma_i - \Psi_i[\sigma_i]' \\
&= -[\Psi_i]'\sigma_i - \Psi_i\mathbf{X}_{\sigma_i}.
\end{aligned}
$$

Note that f_2 may be expressed as

$$f_2(\boldsymbol{p}, \boldsymbol{\sigma}, \boldsymbol{\lambda}) = -f_1(\boldsymbol{p}, \boldsymbol{\sigma}, \boldsymbol{\lambda}) - \alpha(\boldsymbol{p}, \boldsymbol{\lambda}),$$

where $\alpha(\boldsymbol{p}, \boldsymbol{\lambda}) = \omega\lambda_i$. We can find the LD-derivative α' via the relationship (3.1) since it is C^1 with respect to both parameters and state variables:

$$\alpha'(\boldsymbol{p}^*, \boldsymbol{\lambda}; (\mathbf{M}, \mathbf{X}_{\boldsymbol{\lambda}})) = \lambda_i\mathbf{M}_\omega + \omega^*\mathbf{X}_{\lambda_i}.$$

Thus, we find that

$$
\begin{aligned}
&f_2'(\boldsymbol{p}^*, \boldsymbol{\sigma}, \boldsymbol{\lambda}; (\mathbf{M}, \mathbf{X}_{\sigma_i}(t), \mathbf{X}_{\lambda_i}(t))) \\
&\qquad = -f_1'(\boldsymbol{p}^*, \boldsymbol{\sigma}, \boldsymbol{\lambda}; (\mathbf{M}, \mathbf{X}_{\sigma_i}(t), \mathbf{X}_{\lambda_i}(t))) - \alpha'(\boldsymbol{p}^*, \boldsymbol{\lambda}; (\mathbf{M}, \mathbf{X}_{\boldsymbol{\lambda}})) \\
&\qquad = [\Psi_i]'\sigma_i + \Psi_i\mathbf{X}_{\sigma_i} - \lambda_i\mathbf{M}_\omega - \omega^*\mathbf{X}_{\lambda_i},
\end{aligned}
$$

which gives the form of Equation (5.6) when combined with the form of f_1' above. The initial conditions (5.7) may be found by straightforward partial differentiation since the initial conditions of Equation (5.1) are C^1 and Equation (3.1) applies. Afterwards, the form of Equation (5.5) follows directly from an application of Theorem 3.22.

Now suppose we are given the functions

$$\begin{aligned}\Psi_i(\boldsymbol{p},\boldsymbol{\lambda}) &= \eta\max(0,v_i),\\ v_i(\boldsymbol{p},\boldsymbol{\lambda}) &= 1-\exp(-\gamma(\Lambda_i-\Lambda^c)),\\ \Lambda_i &= \sum_{j=1}^{n} W_{ij}\lambda_j,\end{aligned}$$

where W_{ij} is a C^1 function of the parameters d_0, δ. By the lexicographic product rule, we can compute

$$\begin{aligned}[\Psi_i]'(\boldsymbol{p}^*,\boldsymbol{\lambda};(\mathbf{M},\mathbf{X}_{\boldsymbol{\lambda}})) &= \max(0,v_i)\mathbf{M}_\eta + \eta^*[\max\circ(0,v_i)]'(\boldsymbol{p}^*,\boldsymbol{\lambda};(\mathbf{M},\mathbf{X}_{\boldsymbol{\lambda}}))\\ &= \max(0,v_i)\mathbf{M}_\eta + \eta^*\mathbf{slmax}(\mathbf{0},[v_i \quad v_i']),\end{aligned}$$

where the final equality holds by the LD-derivative rule for the max function found in Proposition (3.12).

Turning our attention to v_i, we again recall the relationship found in (3.1) since this function is C^1 with respect to both parameters and state variables. The main challenge, therefore, simply lies in taking the classical partial derivatives; here we calculate

$$\begin{aligned}&[v_i]'(\boldsymbol{p}^*,\boldsymbol{\lambda};(\mathbf{M},\mathbf{X}_{\boldsymbol{\lambda}}(t)))\\ &\quad= \frac{\partial v_i}{\partial \boldsymbol{p}}\mathbf{M} + \frac{\partial v_i}{\partial \boldsymbol{\lambda}}\mathbf{X}_{\boldsymbol{\lambda}}(t)\\ &\quad= -\exp(-\gamma^*(\Lambda_i-\Lambda^{c*}))\\ &\qquad\left(\begin{bmatrix}0 & 0 & -(\Lambda_i-\Lambda^{c*}) & \gamma^* & -\gamma^*\dfrac{\partial\Lambda_i}{\partial d_0} & -\gamma^*\dfrac{\partial\Lambda_i}{\partial\delta} & 0 & 0\end{bmatrix}\mathbf{M}\right.\\ &\qquad\left.-\gamma^*\begin{bmatrix}\dfrac{\partial\Lambda_i}{\partial\boldsymbol{\lambda}}\end{bmatrix}\mathbf{X}_{\boldsymbol{\lambda}}(t)\right)\\ &\quad= -\exp(-\gamma^*(\Lambda_i-\Lambda^{c*}))\left([0 \quad 0 \quad -(\Lambda_i-\Lambda^{c*}) \quad \gamma^* \quad 0 \quad 0 \quad 0 \quad 0]\,\mathbf{M}\right.\\ &\qquad\left.-\gamma^*\frac{\partial\Lambda_i}{\partial\boldsymbol{p}}\mathbf{M} - \gamma^*\frac{\partial\Lambda_i}{\partial\boldsymbol{\lambda}}\mathbf{X}_{\boldsymbol{\lambda}}(t)\right)\\ &\quad= -\exp(-\gamma^*(\Lambda_i-\Lambda^{c*}))\left([0 \quad 0 \quad -(\Lambda_i-\Lambda^{c*}) \quad \gamma^* \quad 0 \quad 0 \quad 0 \quad 0]\,\mathbf{M} - \gamma^*[\Lambda_i]'\right)\\ &\quad= \exp(-\gamma^*(\Lambda_i-\Lambda^{c*}))\left([0 \quad 0 \quad (\Lambda_i-\Lambda^{c*}) \quad -\gamma^* \quad 0 \quad 0 \quad 0 \quad 0]\,\mathbf{M} + \gamma^*[\Lambda_i]'\right)\end{aligned}$$

$$= \exp(-\gamma^*(\Lambda_i - \Lambda^{c*}))\left((\Lambda_i - \Lambda^{c*})\mathbf{M}_{\gamma^*} - \gamma^*\mathbf{M}_{\Lambda^{c*}} + \gamma^*[\Lambda_i]'\right).$$

The form of $[v_i]'$ presented in the theorem follows directly after noticing that $\exp(-\gamma(\Lambda_i - \Lambda^c)) = (1 - v_i)$. The form of $[\Lambda_i]'$ follows in turn from term-by-term partial differentiation since it is C^1:

$$\begin{aligned}[\Lambda_i]'(\boldsymbol{p}^*, \boldsymbol{\lambda}; (\mathbf{M}, \mathbf{X}_{\boldsymbol{\lambda}})) &= \frac{\partial \Lambda_i}{\partial \boldsymbol{p}}\mathbf{M} + \frac{\partial \Lambda_i}{\partial \boldsymbol{\lambda}}\mathbf{X}_{\boldsymbol{\lambda}}(t) \\ &= \left(\sum_{j=1}^{n} \begin{bmatrix} \dfrac{\partial W_{ij}}{\partial d_0} & \dfrac{\partial W_{ij}}{\partial \delta} \end{bmatrix} \lambda_j\right) \begin{bmatrix} \mathbf{M}_{d_0} \\ \mathbf{M}_{\delta} \end{bmatrix} + \left(\sum_j W_{ij}\mathbf{X}_{\lambda_j}\right).\end{aligned}$$

□

Following a similar path as our previous analysis in Chapter 4, we hard-coded the **slmax** function and implemented the nonsmooth sensitivity system 5.6 alongside initial conditions (5.7) and the riot model itself (5.1) in the ode45 solver of MATLAB on the time horizon $[t_0, t_f] = [0, 44]$. Our simulation included 1287 sites which are each described by a pair of state variables; in addition, the sensitivities of each state variable are described by 8 sensitivity functions (i.e., one for each parameter present in the model). The simulation itself therefore required the simultaneous solving of $(1287 \times 2) + (1287 \times 2 \times 8) = 23,166$ fully coupled equations. This process yielded the numerical solutions of the LD-sensitivity functions ($\mathbf{X}_{\boldsymbol{\sigma}}$,$\mathbf{X}_{\boldsymbol{\lambda}}$); these results are then right-multiplied by $\mathbf{M}^{-1}$ in order to determine the lexicographic forward-parametric sensitivity functions ($\mathbf{S}_{\boldsymbol{\sigma}}$,$\mathbf{S}_{\boldsymbol{\lambda}}$) via Equation (3.6).

Different choices for the directions matrix $\mathbf{M}$ were also explored in the form of seven successive circular right-shifts of the identity matrix, which in turn gave lexicographic preference to each unit coordinate direction in parameter space. Unfortunately, limitations imposed by the runtime of the simulation prevented the analysis of a greater number of options for $\mathbf{M}$, though in each case studied we found that simulation results were identical beyond small numerical discrepancies.

Relative sensitivities are again explored here for the purpose of easier comparison between the effect of parameters — however, due to the tendency of rioting behavior to

return to a basal value of 0 over time, the relative sensitivities in the spirit of Equation (4.10) are unsuitable for this model due to the presence of the state variable in the denominator (i.e., the relative sensitivity functions may tend to infinity). To counter this issue, we scaled the resulting sensitivity functions in the following way:

$$\begin{aligned}\widehat{\mathbf{S}}_{\sigma_i}(t) &= \mathbf{S}_{\sigma_i}(t) \odot \frac{1}{\frac{\sigma_i(t)}{(\boldsymbol{p}^*)^{\mathrm{T}}} + \mathbf{1}};\\ \widehat{\mathbf{S}}_{\lambda_i}(t) &= \mathbf{S}_{\lambda_i}(t) \odot \frac{1}{\frac{\lambda_i(t)}{(\boldsymbol{p}^*)^{\mathrm{T}}} + \mathbf{1}},\end{aligned} \tag{5.10}$$

where the addition of 1 to each state variable avoids infinite behavior resulting from division by said variables tending to zero. (Note that in the absence of this addition, these functions would simplify to a form which mirrors that in Equation (3.6).)

The relative lexicographic sensitivity functions associated with the state variables, activation function Ψ_i, and "global activity" function Λ_i within Clichy-sous-Bois (the initial site of rioting, INSEE 93014) are found in Figure 5.2. Note that at $t = t_0 = 0$, the global activity Λ_i (i.e., Equation (5.2)) as seen from Clichy-sous-Bois must be greater than or equal to λ^* since the term $W_{ii}\lambda_i = \lambda^*$ in this case and $W_{ij}, \lambda_j \geq 0$ in general; furthermore, since λ^* is greater than the threshold parameter Λ^c, we find that the output of the nonsmooth activation function (5.4) is nonzero starting at $t = t_0$ and hence the bandwagon effect is immediately established. The vertical lines appearing on plots in Figure 5.2 represent the time at which the activation function (5.4) switches its output to zero at after approximately 24.69 days of activity.

The sensitivity results found in Figure 5.2 establish several parameters as the most influential within the site. The removal rate from the riot, ω, is the most dominant within the dynamics of riot activity λ_i. The sensitivity function $S^{\omega}_{\lambda_i}$ is (mostly) negative, meaning an increase in the removal rate yields a predicted decrease in rioting activity for fixed time t, as intuition would suggest here. To a lesser extent the riot susceptibility parameter η, which describes the saturating probability that a susceptible member of the population joins a large riot, plays an opposing role in these dynamics: early in the time horizon, $S^{\eta}_{\lambda_i}$ is

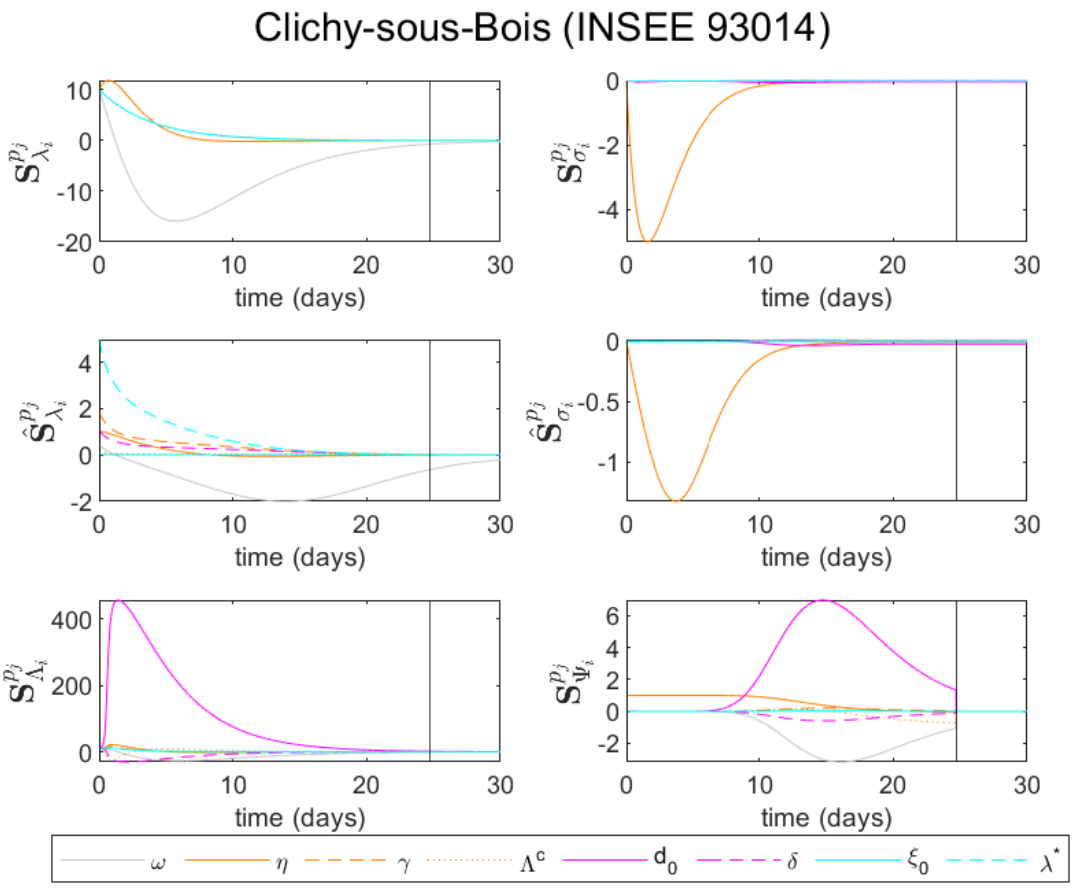

Figure 5.2: Simulations of the lexicographic sensitivity functions ($\mathbf{S}_{\lambda_i}$ and $\mathbf{S}_{\sigma_i}$) and relative lexicographic sensitivity functions ($\widehat{\mathbf{S}}_{\lambda_i}$ and $\widehat{\mathbf{S}}_{\sigma_i}$) for initial rioting site Clichy-sous-Bois. Sensitivity functions for the "global activity" function Λ_i and activation function Ψ_i are also given. Vertical lines correspond to time $t = 24.69$ days at which the activation function Ψ_i reverts to an output of 0 [2].

large and positive, indicating that an increase in this parameter would grow the riot itself quickly. Meanwhile, η seems to also be the most influential parameter on the reservoir of events σ_i. Here, however, the negative sensitivity function $S^{\eta}_{\sigma_i}$ suggests that an increase in population susceptibility would result in a sharp decrease in the number of rioting events within the reservoir (indeed, due to the increase in riot size discussed above). The relative sensitivity functions convey a largely similar story, while also manifesting the relative importance of the initial value parameter λ^* for early times in the horizon; the influence of this parameter diminishes over time, as expected. Notably, sharp changes in sensitivity are observed in the activation function Ψ_i as its output changes to zero, with the L-derivative

approach capturing this sharp behavior as the threshold is crossed. Further analysis establishes the characteristic distance d_0 as influential within the global activity function Λ_i and within Ψ_i, though this large influence is apparently not translated to the larger scope of the state variables σ_i, λ_i themselves.

Figure 5.3 communicates analogous results for the municipality of Saint-Denis (INSEE 93066), which hosts the largest reference population (i.e., 16-24 year old males without a diploma) of any individual municipality in the Île-de-France region and is located directly outside of Paris (only approximately 15 km/9.3 mi from the initial rioting site Clichy-sous-Bois). We first note that the influential parameters within Clichy-sous-Bois, η and ω, play largely similar roles here (note their similar qualitative behaviors between Figures 5.2 and 5.3 despite the change in scale). It is notable, however, that the effects of the parameters d_0 and δ — the parameters appearing in the weightings W_{ij} (5.3) within the global activity function Λ_i — are magnified here to a large extent. This behavior is representative of the other most active sites, with weightings only playing a large relative role outside of the initial site itself.

In order to gain a more well-rounded view into the sensitivities of the riot dynamics throughout the country, we chose three more sites with unique qualities (in addition to initial site Chichy-sous-Bois and most populous site Saint-Denis) for direct comparison: Tartre-Gaudran (INSEE 78606, which hosts the smallest reference population of only approximately 1 person), Livry-Gargan (INSEE 93046, which borders Clichy-sous-Bois), and Fontaine-Fourches (INSEE 77187, which is situated farthest from Clichy-sous-Bois). The rioting activity λ_i for each site on the time horizon $[t_0, t_f] = [0, 14]$ is shown in Figure 5.4 alongside the respective relative sensitivities $\mathbf{S}_{\lambda_i}$, while the geographic location of each participating site can be observed in Figure 5.5b.

Rioting activity reaches its height in the populous municipality of Saint-Denis, while rioting activity is almost completely negligible in the distant site of Fontaine-Fourches and the largely uninhabited site of Tartre-Gaudran. The scale of their respective sensitivities

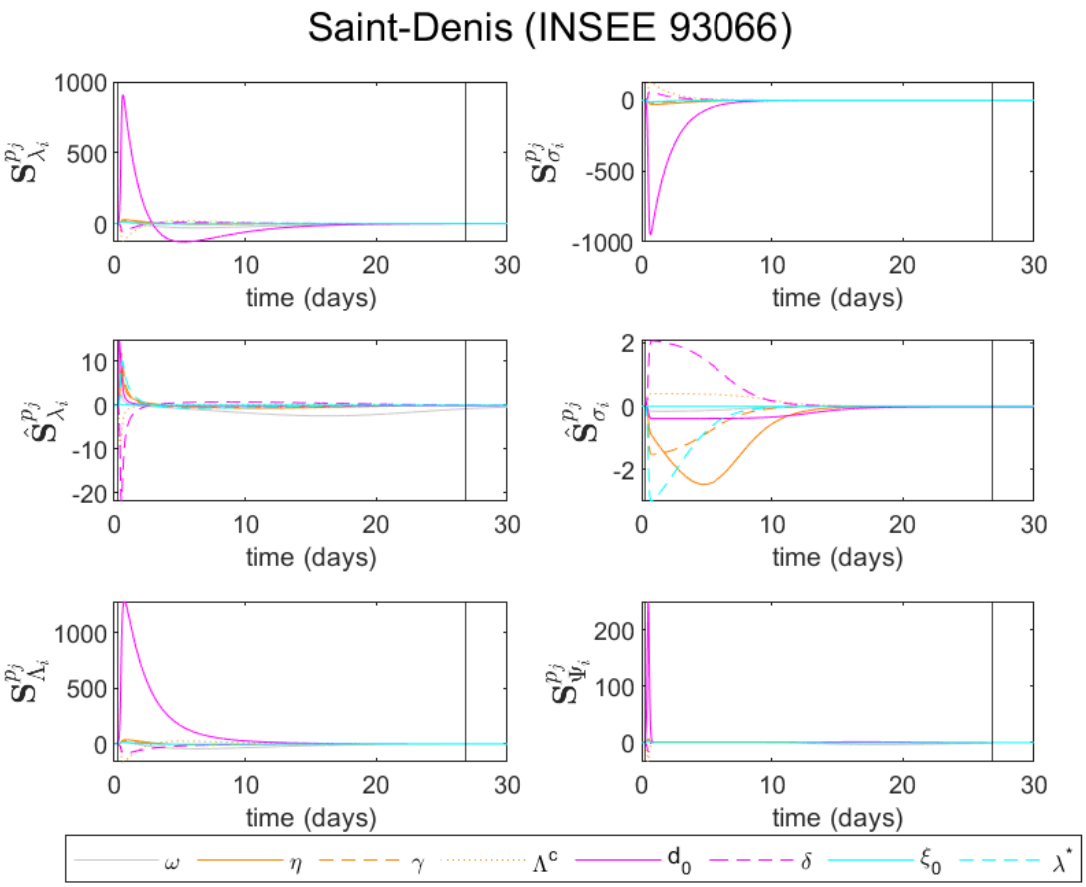

Figure 5.3: Lexicographic sensitivity functions and relative lexicographic sensitivity functions for the populous site of Saint-Denis [2].

reflects this, with Saint-Denis possessing the largest observed magnitude of sensitivity to any parameter by a large margin. The sensitivities observed in the site of Livry-Gargan closely mirror the qualitative behaviors exhibited in Saint-Denis and is typical of other active sites as well; the sensitivities observed in Clichy-sous-Bois, on the other hand, remain unique due to the effects of the initial triggering event.

With the goal of again expanding the scope of our analysis in order to visualize the influence of parameters across all 1287 sites present in the model, we now consider the metric

$$\|\widehat{S}_{\lambda_i}^{p_j}\|_1 = \int_{t_0}^{t_f} |\widehat{S}_{\lambda_i}^{p_j}(t)|dt,$$

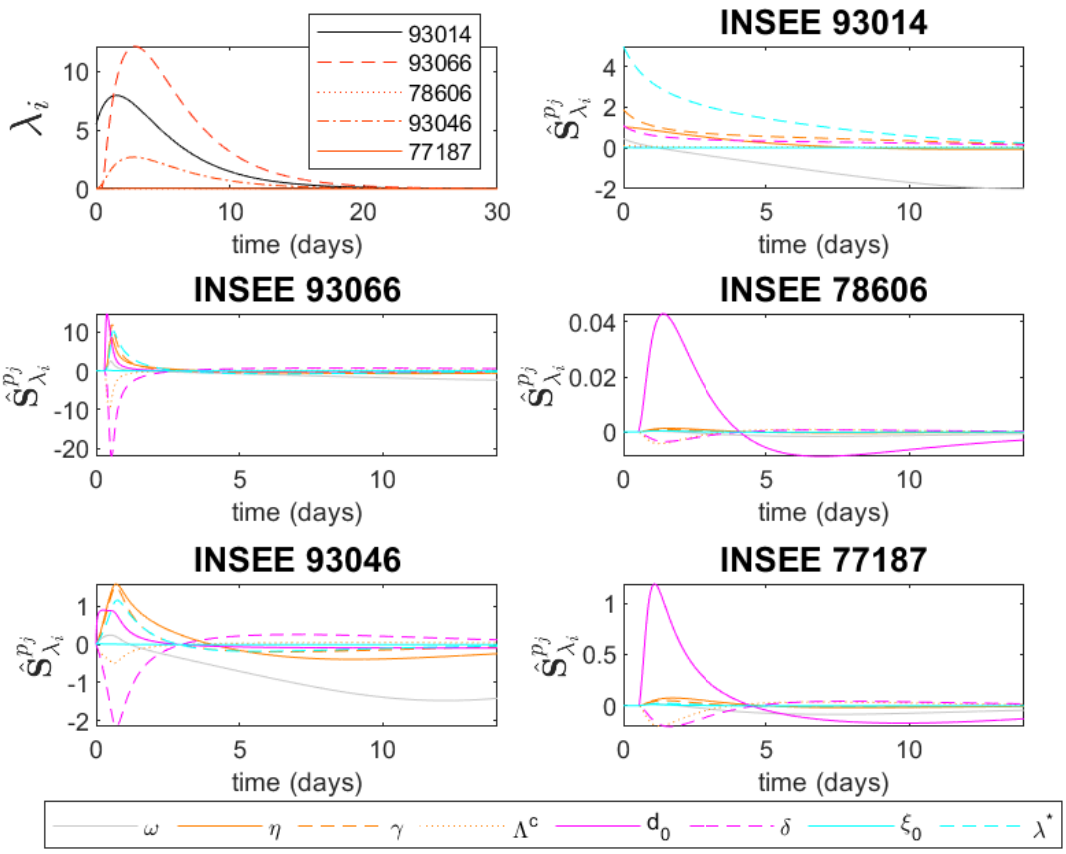

Figure 5.4: Riot activity and relative riot lexicographic sensitivity functions for the 5 distinct sites [2].

which allows the characterization of the total overall (relative) influence of parameter p_j to the rioting activity appearing within site i over the time horizon $[t_0, t_f] = [0, 44]$. This metric was calculated in each site with respect to the four key parameters highlighted so far: ω, η, d_0, and δ. Results were then provided to a routine employing the Mapping toolbox of MATLAB in conjunction with geographic data from the collaborators at OpenStreetMap (Map data copyrighted OpenStreetMap contributors and available from `https://www.openstreetmap.org`) in order to generate the heat maps presented in Figures 5.5c to 5.5f. Within these figures, lightly-shaded municipalities displayed low overall sensitivity to the parameter at hand, while heavily-shaded municipalities experienced high levels of overall sensitivity. Noting that Clichy-sous-Bois is located north-of-center within the region and just northeast of Paris, it is reasonable that the

largest sensitivity metrics $\|\widehat{S}_{\lambda_i}^{p_j}\|_1$ depicted here are predominantly concentrated in this area for each parameter studied due to large reference populations N_i and direct proximity to the initial riots. The maximum overall sensitivity in any site is observed with respect to ω, though the relative absence of any heavily-shaded municipalities outside the Paris area in Figure 5.5b indicates that inter-municipal relative sensitivity to ω is highly variable across the region. In contrast, region-wide sensitivity to d_0 (for example) is more uniform, but the maximum overall sensitivity observed with respect to this parameter clearly falls short of that exhibited by ω (noting the differences in scale between Figures 5.5c and 5.5e).

We proceed by attempting to quantify the apparent contrasts between the scale and variance of region-wide sensitivity to different parameters. To do this, we average the metrics $\widehat{S}_{\lambda_i}^{p_j}$ across the region with respect to each parameter via

$$\mu_j = \frac{1}{n}\sum_{i=1}^{n} \|\widehat{S}_{\lambda_i}^{p_j}\|_1. \tag{5.11}$$

The region-wide standard deviation of $\widehat{S}_{\lambda_i}^{p_j}$ with respect to each parameter p_j is calculated via a similar method and is expressed as SD_j. The results of these calculations are given in Figure 5.6.

Ultimately, this analysis solidifies ω as the most influential parameter on average to rioting activity across the region, though it also highlights the high standard deviation experienced between municipalities. Clichy-sous-Bois, for example, experiences high relative sensitivity to ω (recall Figure 5.2), though SD_ω remains high due to the emergence of other more locally influential parameters such as d_0 in other sites (recall, e.g., Figure 5.3). On average, the distance parameters d_0 and δ are the second and third most important parameters, respectively, though each also exhibit high standard deviation across the region as well. Moderate region-wide is enjoyed by the parameters η, γ, Λ^c, and λ^*, while parameter ε_0 is insignificant at large.

Perhaps most surprising among these results is the relative unimportance of the threshold parameter Λ^c. Recall the results of Chapter 4.2, in which we formulated the basic

(a) 12 most active municipalities.

(b) 5 distinct municipalities.

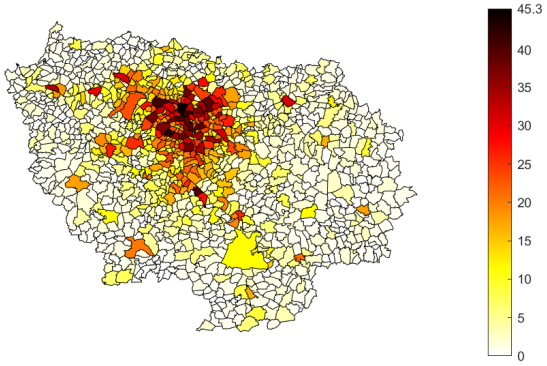

(c) $\|\widehat{S}^{p_j}_{\lambda_i}\|_1$ for $p_j = \omega$.

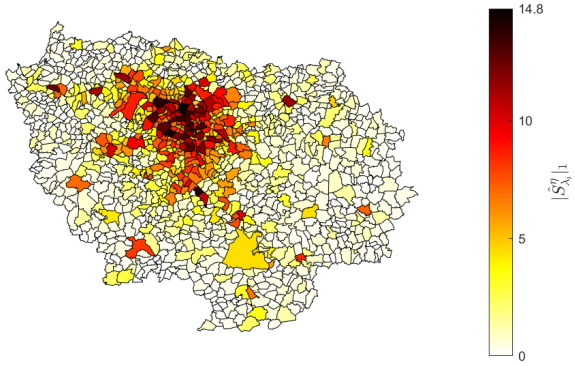

(d) $\|\widehat{S}^{p_j}_{\lambda_i}\|_1$ for $p_j = \eta$.

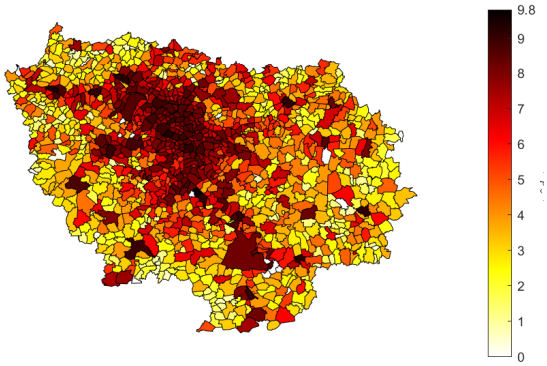

(e) $\|\widehat{S}^{p_j}_{\lambda_i}\|_1$ for $p_j = d_0$.

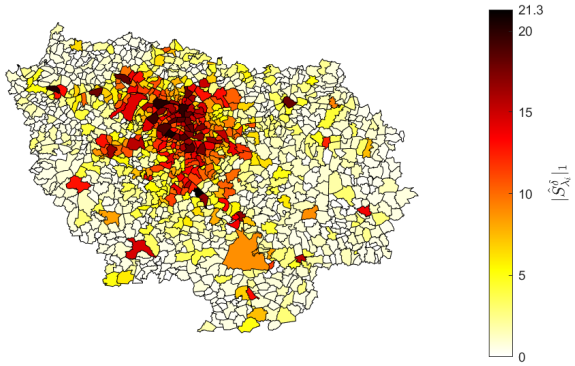

(f) $\|\widehat{S}^{p_j}_{\lambda_i}\|_1$ for $p_j = \delta$.

Figure 5.5: Heat maps of $\|\widehat{S}^{p_j}_{\lambda_i}\|_1$ across Île-de-France [2].

variation of the minimal model of glucose-insulin kinetics. The threshold parameter p_6 describing the blood-glucose concentration at which insulin began to be secreted was shown to be highly influential in, e.g., Figure 4.2b. In the present model, Λ^c behaves in a similar

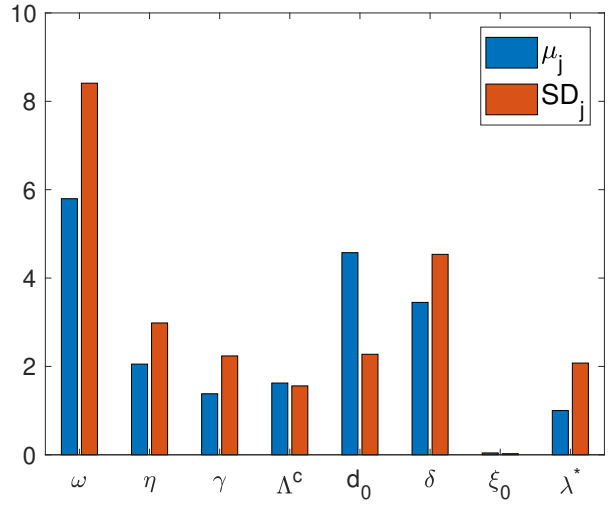

Figure 5.6: Parameter influence measures across Île-de-France [2].

way, now describing the threshold global activity which mobilizes the bandwagon effect (and hence growth of a site's rioting activity). Since the crossing of this threshold influences the very spread of the riot itself, it is surprising that it is not more important overall (in the spirit of, e.g., the minimal model's p_6 discussed above). This becomes more clear upon closer analysis of the initial state of Λ_i across all sites, as it turns out that the particular reference values outlined in Table 5.1 induce a total of 22 different sites (including Clichy-sous-Bois itself) to satisfy the inequality $\Lambda_i > \Lambda^c$ at $t_0 = 0$. Thus, the bandwagon effect is immediately in effect in these sites, with small perturbations in Λ^c likely not preventing this widespread initial riot growth. Hence, the predicted influence of Λ^c as a whole is relatively small on average.

5.4 Discussion

The work of Bonnasse-Gahot et al. [12] proposing a model capable of replicating riot dynamics is a milestone in the study of social contagions, and was supported by a compilation of a comprehensive dataset allowing model verification against the 2005 French riots. Part of the model's utility comes in the ability to replicate riot dynamics at multiple scales or levels of granularity (e.g., between cities or between larger regions) — a feature

which is expanded on in [12] with few adjustments to the model (5.1). In [2], the paper which forms the foundation of the present chapter, we considered multiple levels of granularity in the model and even performed a non-local sensitivity analysis at the municipality scale using parameter values sampled from a Latin Hypercube Sampling scheme — in essence, allowing us to perform a full-scale lexicographic sensitivity analysis with many qualitatively different choices of reference parameters and then compare the resulting model behavior. In each case, the parameters ω, η, d_0, and δ were routinely the most influential, with the rankings of relative importance largely following a similar behavior as that discussed within the local analysis of the municipality-scale model in the preceding section. With this in mind, we suggest that our results here are not limited to the 2005 French riots on which [12] is based, and that our analysis may have more general implications.

Since the removal rate ω seems to be the most influential parameter in general, it should be the primary focus in any efforts to curtail the growth or spread of rioting behavior (via, e.g., focused political action in the area). Efforts to adjust other influential parameters such as the susceptibility parameter η should also be considered, though the reference value of η in particular will likely change from riot to riot based on levels of social tension associated with, e.g., the triggering event, making certain subsets of the population as a whole more or less likely to riot in response. Efforts to make adjustments could be made via, e.g., media coverage or political action which appeases a significant portion of the reference population, with potential issues arising if such efforts are made by autocratic governments or against peaceful protests. Parameters such as the distance parameters d_0 and δ seem less malleable in general, meaning that while influential, it is unclear how real-world adjustments could be made. Similar difficulties may be seen in attempts to adjust other parameters such as γ and ε_0, which suffer from overly abstract physical interpretation. The heat maps found in Figure 5.5 also confirm the intuitive idea that any efforts which are made in reducing riot spread should be focused in heavily populated areas

and those nearby to the initial site of rioting, since parametric sensitivities are shown to be highest in these areas.

One clear direction of future research involves the introduction of site-dependent parameters to the model — for example, demographic or geographic considerations may cause parameters such as ω, η, γ, or Λ^c to vary between sites (as alluded to in the formulation of the model in Equation (5.1)). The challenge associated with this task is primarily computational: for each new parameter introduced to the model, 1287 more sensitivity equations are introduced to describe the sensitivity of each σ_i and λ_i present. In a full-scale model, assuming site-dependent ω_i, η_i, γ_i, and Λ_i^c, the LD-sensitivity system associated with Equation (5.1) would be comprised of roughly 13.3 million fully-coupled ordinary differential equations, making numerical solutions nearly impossible to furnish due to computational limitations. More focused study in the topic of which parameters are most likely to vary between municipalities may provide insight into which parameters warrant a smaller-scale site-dependent sensitivity analysis. Another area of interest is the analysis of rioting behavior in different countries or environments to see if similar results are furnished.

CHAPTER 6
CONCLUSION

In this thesis, we were motivated by the shortcomings of classical sensitivity theory when applied in the context of mathematical models which incorporate switching behavior. Such behavior typically results in the introduction of points of nondifferentiability within the model at hand, invalidating classical derivative-based efforts to characterize parametric sensitivities. Recent developments in nonsmooth analysis, however, have been shown to be useful in efforts to extend sensitivity theory into the nonsmooth case.

We first discussed classical sensitivity theory, but noted it may fail when participating ODEs are not C^1; therefore, we introduced the Clarke Jacobian as an attractive generalized derivative object which satisfies a number of useful calculus properties, but then showed that it suffers from difficulties in computation in general. Closely related objects referred to as lexicographic (L-)derivatives were then introduced and it was highlighted that they to lie in or near the set-valued Clarke Jacobian, with the result of Proposition 3.5 implying that L-derivatives are computationally relevant objects which can stand in for Clarke Jacobian elements in dedicated numerical methods employing them. The existence of lexicographic directional (LD-)derivatives enable the automatable calculation of L-derivatives within this setting, however, circumnavigating the typical difficulties in Clarke Jacobian calculation. After exploring the process of calculating LD- and L-derivatives in general, we discussed how LD-derivatives can be employed in lexicographic sensitivity theory which is analogous to classical theory but applicable to a much larger class of (nonsmooth) ODE systems.

Using the established lexicographic sensitivity theory, we then explored a pair of models exhibiting nonsmoothness: a classic model of glucose-insulin kinetics and a recently-developed municipal-scale model describing the spread of riots. In the variation of the former meant to model a healthy individual, nonsmoothness arises from an effort to model pancreatic behavior as a biochemical threshold is crossed and insulin secretion

abruptly turns on and off. We presented the parametric sensitivities for this case which have previously only been estimated using a smooth approximation to evade the nonsmoothness inherently present in the model; by considering the case of a diabetic subject as well, we also produced novel results regarding parametric sensitivities in two distinct cases where insulin infusion is performed by an external device as opposed to the pancreas. One of these considerations was nonsmooth (but PC^1) in nature, warranting the use of lexicographic sensitivity theory and allowing the automatable and accurate calculation of the lexicographic sensitivity functions. Within our analysis of the nonsmooth model of riot spread, we noted that the nonsmoothness arising from an effort to model the sudden change in likelihood for a person to join a riot as the riot grows beyond a threshold size again invalidates classical theory. By employing lexicographic sensitivity theory here as well, we furnished the first known parametric sensitivity information associated with the model.

Beyond the future directions for research associated with the minimal and riot models themselves in Sections 4.4 and 5.4 respectively, there are also several future directions for lexicographic theory as a whole. In general, the approach of using an LD-derivative (which can be found using its sharp calculus rules) to calculate a corresponding L-derivative via the relationship in Theorem 3.7 is systematic in producing a single element of the lexicographic subdifferential. Recall that in both Chapters 4 and 5, however, many different choices of directions matrix $\mathbf{M}$ were employed in the search for different resulting lexicographic sensitivity functions (i.e., L-derivatives of ODE solutions) since the lexicographic subdifferential may be a non-singleton set at points of nondifferentiability. Despite the many choices studied, we found the same L-derivatives in each case, though this need not hold in general. The ability to calculate more than one element of the lexicographic subdifferential is therefore of interest and it is hoped that future study, perhaps regarding a systematic approach to the choice of directions matrix $\mathbf{M}$, will guarantee different resulting L-derivatives (and hence lexicographic sensitivity functions in

future relevant applications). Another area of interest involves the explicit development of a nonsmooth dynamic optimization algorithm in the spirit of [31] for the models explored in this thesis or other relevant examples. One pertinent such example involves the insulin infusion term u appearing in the Hovorka model of glucose-insulin kinetics [26]. This input was a previous candidate for dynamic optimization in [26], and so results arising from a lexicographic approach could be compared to (or improve on) existing results. We also note that lexicographic sensitivity theory has great potential within the analysis of other many other nonsmooth models in mathematical biology, such as those describing sharp behavioral changes in predator-prey dynamics or the spread of disease, and hope that the approach outlined and employed within this thesis will serve as a foundation for future studies.

REFERENCES

[1] Matthew Ackley and Peter Stechlinski. Lexicographic derivatives of nonsmooth glucose-insulin kinetics under normal and artificial pancreatic responses. *Applied Mathematics and Computation*, 395:125876, 2021.

[2] Matthew Ackley and Peter Stechlinski. Determining key parameters in riots using lexicographic directional differentiation. *SIAM Journal on Applied Mathematics*, In Production.

[3] American Diabetes Association et al. Classification and diagnosis of diabetes: Standards of medical care in diabetes—2019. *Diabetes Care*, 42(Supplement 1):S13–S28, 2019.

[4] Kim E Andersen and Malene Højbjerre. A population-based bayesian approach to the minimal model of glucose and insulin homeostasis. *Statistics in Medicine*, 24(15):2381–2400, 2005.

[5] American Diabetes Association. Hyperglycemia (high blood glucose). 2021.

[6] American Diabetes Association. Hypoglycemia (low blood sugar). 2021.

[7] American Diabetes Association. Statistics about diabetes. 2021.

[8] Paul I Barton, Kamil A Khan, Peter Stechlinski, and Harry AJ Watson. Computationally relevant generalized derivatives: theory, evaluation and applications. *Optimization Methods and Software*, 33(4-6):1030–1072, 2018.

[9] Yazdan Batmani. Blood glucose concentration control for type 1 diabetic patients: a non-linear suboptimal approach. *IET Systems Biology*, 11(4):119–125, 2017.

[10] Henri Berestycki, Jean-Pierre Nadal, and Nancy Rodríguez. A model of riots dynamics: shocks, diffusion and thresholds. *Networks and Heterogeneous Media*, 10(3):1–34, 2015.

[11] Richard N Bergman, Y Ziya Ider, Charles R Bowden, and Claudio Cobelli. Quantitative estimation of insulin sensitivity. *American Journal of Physiology-Endocrinology And Metabolism*, 236(6):E667, 1979.

[12] Laurent Bonnasse-Gahot, Henri Berestycki, Marie-Aude Depuiset, Mirta B Gordon, Sebastian Roché, Nancy Rodríguez, and Jean-Pierre Nadal. Epidemiological modelling of the 2005 French riots: a spreading wave and the role of contagion. *Scientific Reports*, 8(1):107, 2018.

[13] Fred Brauer, Carlos Castillo-Chavez, and Carlos Castillo-Chavez. *Mathematical Models in Population Biology and Epidemiology*, volume 2. Springer, 2012.

[14] Frederick Chee and Tyrone Fernando. *Closed-Loop Control of Blood Glucose*. Springer, 2007.

[15] Gita Cherian. A guide to the principles of animal nutrition. *Oregon State University*, 2020.

[16] Frank H Clarke. *Optimization and Nonsmooth Analysis*, volume 5. SIAM, 1990.

[17] Frank H Clarke. Nonsmooth analysis in systems and control theory, 2009.

[18] Thomas Crampton. Behind the furor, the last moments of two youths. *The New York Times*, November 2005.

[19] Andrea De Gaetano and Ovide Arino. Mathematical modelling of the intravenous glucose tolerance test. *Journal of Mathematical Biology*, 40(2):136–168, 2000.

[20] Abraham J Domb, Joseph Kost, and David Wiseman. *Handbook of Biodegradable Polymers*, volume 7. CRC press, 1998.

[21] Francisco Facchinei, Andreas Fischer, and Markus Herrich. An LP-Newton method: nonsmooth equations, KKT systems, and nonisolated solutions. *Mathematical Programming*, 146:1–36, 2014.

[22] Michael E Fisher. A semiclosed-loop algorithm for the control of blood glucose levels in diabetics. *IEEE Transactions on Biomedical Engineering*, 38(1):57–61, 1991.

[23] Andreas Griewank and Andrea Walther. *Evaluating Derivatives: Principles and Techniques of Algorithmic Differentiation*, volume 105. SIAM, 2008.

[24] Michael Gross. Why do people riot? *Current Biology*, 21:R673–R676, 2011.

[25] Philip Hartman. Ordinary differential equations (Corrected reprint of the 1982 Edition). *SIAM*, 38, 2002.

[26] Roman Hovorka, Valentina Canonico, Ludovic J Chassin, Ulrich Haueter, Massimo Massi-Benedetti, Marco Orsini Federici, Thomas R Pieber, Helga C Schaller, Lukas Schaupp, Thomas Vering, et al. Nonlinear model predictive control of glucose concentration in subjects with type 1 diabetes. *Physiological Measurement*, 25(4):905, 2004.

[27] Ramy Inocenio. Some 1.7 million take part in 11th week of Hong Kong protests. *CBS News*, August 2019.

[28] Hassan K Khalil. *Nonlinear Systems*. Upper Saddle River, 2002.

[29] Kamil A Khan. Branch-locking AD techniques for nonsmooth composite functions and nonsmooth implicit functions. *Optimization Methods and Software*, 33(4-6):1127–1155, 2018.

[30] Kamil A Khan and Paul I Barton. Generalized derivatives for solutions of parametric ordinary differential equations with non-differentiable right-hand sides. *Journal of Optimization Theory and Applications*, 163(2):355–386, 2014.

[31] Kamil A Khan and Paul I Barton. Generalized gradient elements for nonsmooth optimal control problems. In *53rd IEEE Conference on Decision and Control*, pages 1887–1892, 2014.

[32] Kamil A Khan and Paul I Barton. A vector forward mode of automatic differentiation for generalized derivative evaluation. *Optimization Methods and Software*, 30(6):1185–1212, 2015.

[33] Claude Lemaréchal, J J Strodiot, and A Bihain. On a bundle algorithm for nonsmooth optimization. In O L Mangasarian, R R Meyer, and S M Robinson, editors, *Nonlinear Programming 4*. Academic Press, New York, 1981.

[34] Eugene L Lozner, Alexander W Winkler, FHL Taylor, and John P Peters. The intravenous glucose tolerance test. *The Journal of Clinical Investigation*, 20(5):507–515, 1941.

[35] Ladislav Lukšan and Jan Vlček. A bundle-Newton method for nonsmooth unconstrained minimization. *Mathematical Programming*, 83:373–391, 1998.

[36] Max D Morris. Factorial sampling plans for preliminary computational experiments. *Technometrics*, 33(2):161–174, 1991.

[37] Mohammad Munir. Generalized sensitivity analysis of the minimal model of the intravenous glucose tolerance test. *Mathematical Biosciences*, 300:14–26, 2018.

[38] Yu Nesterov. Lexicographic differentiation of nonsmooth functions. *Mathematical Programming*, 104(2-3):669–700, 2005.

[39] OpenStreetMap Contibutors. OpenStreetMap, https://www.openstreetmap.org.

[40] Lawrence Perko. *Differential Equations and Dynamical Systems*, volume 7. Springer Science & Business Media, 2013.

[41] QGIS Development Team. *QGIS Geographic Information System*. QGIS Association, 2020.

[42] Liqun Qi and Jie Sun. A nonsmooth version of Newton's method. *Mathematical Programming*, 58:353–367, 1993.

[43] Peter Sahlins. Civil unrest in the French suburbs, November 2005. *Social Science Research Council*, October 2006.

[44] Yosiyuki Sakamoto, Makio Ishiguro, and Genshiro Kitagawa. Akaike information criterion statistics. *Dordrecht, The Netherlands: D. Reidel*, 81(10.5555):26853, 1986.

[45] Stefan Scholtes. *Introduction to Piecewise Differentiable Equations*. Springer Science & Business Media, 2012.

[46] Nicole Sganga. Ex-national security officials call for commission to investigate capitol attack. *CBS News*, April 2021.

[47] Peter Stechlinski, Kamil A Khan, and Paul I Barton. Generalized sensitivity analysis of nonlinear programs. *SIAM Journal on Optimization*, 28(1):272–301, 2018.

[48] GM Steil, Bud Clark, Sami Kanderian, and K Rebrin. Modeling insulin action for development of a closed-loop artificial pancreas. *Diabetes Technology & Therapeutics*, 7(1):94–108, 2005.

[49] Gianna Toffolo, Richard N Bergman, Diane T Finegood, Charles R Bowden, and Claudio Cobelli. Quantitative estimation of beta cell sensitivity to glucose in the intact organism: a minimal model of insulin kinetics in the dog. *Diabetes*, 29(12):979–990, 1980.

[50] Jin Wu, KK Rebecca Lai, and Alan Yuhas. Six Months of Hong Kong Protests. How Did We Get Here? *The New York Times*, November 2019.

BIOGRAPHY OF THE AUTHOR

Matthew Ackley was born in Norfolk, Virginia, and moved to the Mid-Coast region of Maine in 2011. After graduating from Camden Hills Regional High School in 2016, Matthew attended the University of Maine, where he was engaged in both research and volunteer work while maintaining memberships in the honors societies of Phi Kappa Phi and Pi Mu Epsilon. In 2019, he earned the degree of Bachelor of Arts in Mathematics.

Matthew is a co-author of the articles "Lexicographic derivatives of nonsmooth glucose-insulin kinetics under normal and artificial pancreatic responses", published in Applied Mathematics and Computation, and "Determining key parameters in riots using lexicographic directional differentiation", published in the SIAM Journal on Applied Mathematics. He is a candidate for the Master of Arts degree in Mathematics from the University of Maine in May 2021.